NATIONAL AERONAUTICS AND SPACE ADMINISTRATION

Technical Report 32-1460

Volume III

Mariner Mars 1969 Final Project Report

Scientific Investigations

J. A. Stallkamp
A. G. Herriman
and the
Mariner Mars 1969 Experimenters

JET PROPULSION LABORATORY
CALIFORNIA INSTITUTE OF TECHNOLOGY
PASADENA, CALIFORNIA

September 15, 1971

NATIONAL AERONAUTICS AND SPACE ADMINISTRATION

Technical Report 32-1460

Volume III

Mariner Mars 1969 Final Project Report

Scientific Investigations

J. A. Stallkamp
A. G. Herriman
and the
Mariner Mars 1969 Experimenters

JET PROPULSION LABORATORY
CALIFORNIA INSTITUTE OF TECHNOLOGY
PASADENA, CALIFORNIA

September 15, 1971

Prepared Under Contract No. NAS 7-100
National Aeronautics and Space Administration

Preface

The work described in this report was performed by the technical divisions of the Jet Propulsion Laboratory, under the cognizance of the *Mariner* Mars 1969 Project.

This is Volume III of the three volumes that constitute the final report of the *Mariner* Mars 1969 Project. The three volumes correspond in chronological order to the three principal activities of the project.

The preparation and preflight phase for the dual spacecraft mission, *Mariner VI* and *Mariner VII*, from December 1965 through March 1969, is described in Volume I. The project management, planning, and mission analysis are presented in Part 1; the development, design, and testing of spacecraft system and subsystems are detailed in Part 2; and the launch and earth-based systems are covered in Part 3.

The conduct of the flight phase of the mission from February–March 1969 to October 1969 is presented in Volume II. A summary of the events of the entire flight phase and the flight path report are given in Part 1; the launch phase is discussed in Part 2; and Part 3 covers the space flight phase, including details of spacecraft system and subsystem performance.

Postflight scientific analysis of the mission scientific data is given in Volume III. The project scientist's report is provided in Part 1 and some experimenters' interpretations are included in Part 2.

A comprehensive report of the tracking and data system support to the mission will be provided in a separate report.

Contents

Part 1. Scientific Mission

Tables

Figure

Contents (contd)

Part 2. Scientific Results

Journal Reprints

Abstract

This is the third of three volumes of the *Mariner* Mars Final Project Report. It describes the scientific program and lists the initial publications of the investigator teams. Volume I describes preoperational activities, including planning, development and design, manufacture, and testing. Volume II describes mission performance during the launch and space-flight phases.

The scientific mission of the *Mariner VI* and *VII* project consisted of the design of the six selected experiments, the construction of four instruments and their incorporation into the spacecraft, the selection of flyby dates and aiming points for the spacecraft and pointing strategy for the instruments, and the acquisition, return, and analysis of data. Thanks to the excellent performance of the many engineering subsystems, including several that were first of their kind, enhanced options were carried out that materially increased the amount of scientific data returned. Initial reports have been published; more will follow as the interpretation of the data continues.

Part 1. Scientific Mission

I. Mission Inception

The *Mariner* Mars 1969 mission came into being in December 1965, along with the *Mariner* Venus 67 mission, following the reprogramming of the much larger *Voyager* mission. The two *Mariner* missions were geared to resources–time schedules. The Venus flight was to use hardware left over from the *Mariner* Mars 1964 mission, with modifications for its inward, toward-the-sun, flight. The *Mariner* flights to Mars in 1969 would use completely new hardware, patterned after the *Mariner* 1964 equipment but capable of a much expanded scientific mission.

The scientific objective of *Mariner* Mars 1969 was to conduct exploratory flyby missions as a basis for future experiments, particularly those related to the search for extraterrestrial life. It was not the objective to determine the existence or absence of biological activity on Mars, past or present. The intent was to look closely at the planet and its environment in the spectrum from ultraviolet to radio waves. Analyses and interpretations of the data obtained would greatly expand our knowledge of this environment, with which life forms would have to cope.

The invitation for scientific experiments was issued by NASA Headquarters on January 14, 1966, with a submission date of March 14, 1966. Since the *Voyager* 1971 proposal solicitation had been carried out in the last months of 1965, *Voyager* proposals modified to conform with *Mariner* constraints were accepted. Selection was to be made by May 15, 1966, so that the general scientific requirements could be included in the system design to be completed by July 1. A total of 37 proposals were received. Of these, 20 involved measurements only at Mars encounter, 10 involved interplanetary measurements, and the remainder involved both. During the early stages of the selection, it was decided by OSSA, NASA Headquarters, that no interplanetary investigations would be carried out. All resources would be used to obtain information about Mars in support of future, more sophisticated missions. Six experiments were selected. Four of them, infrared spectroscopy, surface temperature (infrared radiometry), ultraviolet spectroscopy, and visual imaging (television), would have on-board instruments; the remaining two, S-band occultation and celestial mechanics, would obtain their data from the radio tracking signals. The detailed objectives of each experiment are given in the next section; Table 1 lists the experiments

Table 1. *Mariner* Mars 1969 science experiments and investigators

Experiment	Investigator	Affiliation	Part of spectrum utilized	Possible information obtainable
Television	R. B. Leighton[a] B. C. Murray R. P. Sharp N. H. Horowitz A. G. Herriman A. Young M. E. Davies C. Leovy B. A. Smith	CIT CIT CIT CIT JPL JPL Rand Corp. University of Washington New Mexico State University	Nonfiltered: 4500—6700 Å Red band: 5400—6700 Å Green band: 4900—5600 Å Blue band: 4500—5000 Å	Surface feature characteristics and variations. At least one complete far-encounter survey covering a full rotation of Mars at higher than earth-based resolution. Overlapping, alternating red, green, and blue filtered pictures during near encounter. At closest approach of 3000 km altitude, geometrical spacing of ≈1 km between adjacent picture elements for wide-angle camera and ≈0.1 km spacing for narrow-angle camera
Infrared spectrometer	G. C. Pimentel[a] K. C. Herr	UCB UCB	1.9—14.3 μ	Atmospheric species, e g., methane, ethylene, acetylene, methanol, N_2O, NO, NO_2, NH_3, CO, C_3O_2, O_3, H_2O_2, CO_2, H_2O, SO_2, H_2S
Ultraviolet spectrometer	C. A. Barth[a] F. C. Wilshusen K. Gause K. K. Kelley R. Ruehle J. B. Pearce E. F. Mackey W. G. Fastie	University of Colorado University of Colorado University of Colorado University of Colorado University of Colorado University of Colorado Packard-Bell Electronics Corp. Johns Hopkins University	1100—4300 Å	Atmospheric species, e.g., H, O, N, N_2^+, CO, N_2, NO, CN, O_3
Infrared radiometer	G. Neugebauer[a] G. Munch S. C. Chase	CIT CIT Santa Barbara Research Center, Hughes Aircraft Co.	8—12 μ 18—25 μ	Measurement of thermal flux radiated from the surface (temperature equivalent 145 to 310°K)
S-band occultation	A. J. Kliore[a] G. Fjeldbo S. I. Rasool	JPL Stanford University Goddard Institute of Space Studies	13 cm	Surface pressure and scale height of atmosphere, planet radius
Celestial mechanics	J. D. Anderson[a] W. L. Martin	JPL JPL		Refinement of measurement of the mass of Mars and the astronomical unit

[a]Principal investigator.

and the principal investigators and co-investigators and their affiliations.

In addition to the primary scientific objective, a second mission objective was to develop and demonstrate technology needed for succeeding missions. In several instances these engineering objectives were in fact a part of the scientific requirements for the primary mission, e.g., the two-degree-of-freedom scan platform and more accurate before-encounter orbit determination. In other cases the advanced capability of several engineering subsystems was used to increase significantly the scientific return of the mission. This is further discussed in Section V.

The mission provided for two flights in order to increase the absolute chance for at least one successful flyby past Mars and return of scientific data. For the scientists, the requirement was to maximize the scientific return in the event of two successful flights. A wide range of options could be entertained by the scientists. One of the items requiring immediate attention was whether to send both spacecraft to the same place but separated in arrival time in order to look for temporal changes or send them to different places to get different kinds of data. The latter plan was chosen. A primary scientific reason for this was that data was desired from both the warm equatorial regions and the polar cap region, and both types of data could not be obtained satisfactorily from a single spacecraft. This fundamental decision was made early in the project by the principal investigators. The final selection of arrival dates and aiming and slewing strategies was a continuously evolving process up to the encounters.

II. Experiment Objectives

Objectives of the individual science experiments provided for the accomplishment of the *Mariner* 1969 primary mission objective. This objective was to conduct flyby missions in order to make exploratory investigations of Mars which would set the basis for future experiments, particularly those related to the search for extraterrestrial life. The secondary objective was to develop technology needed for succeeding Mars missions. The science experiments attained the primary objective, and the spacecraft engineering performance in support of the science experiments attained the secondary objective.

A. Ultraviolet Spectrometer Investigation

The objectives of the UVS experiment were:

(1) To detect the presence of atoms, ions, and molecules in the upper atmosphere of Mars. The atmospheric species that were the prime objectives of the experiment were:

Atoms: hydrogen, 1216 A
oxygen, 1304 Å
nitrogen, 1200 Å

Ions: molecular nitrogen, 3914 Å
carbon monoxide, 4264 Å

Molecules: nitrogen, 1354 Å, 3371 Å
nitric oxide, 2150 Å
carbon monoxide, 2160 Å
cyanogen, 3876 Å

The wavelengths listed are nominal wavelengths where the species were sought. The spectral lines of other potential atmospheric species, such as argon 1049 Å, krypton 1325 Å, and zenon 1470 Å, lie in this spectral range. From present knowledge of the solar spectrum, there is not sufficient energy to excite these lines.

(2) To measure the scale height of each of these constituents. The altitude ranges where the species were sought and the nominal scale heights are as follows:

Constituent	Height range, km	Scale height, km
Atoms:		
hydrogen	250–30,000	1000
oxygen	250– 1000	70
nitrogen	100– 200	70
Ions:		
molecular nitrogen	250– 400	70
carbon monoxide	250– 400	70
Molecules:		
nitrogen	100– 200	24
nitric oxide	100– 200	24
carbon monoxide	100– 200	24
cyanogen	100– 200	24

(3) To measure the Rayleigh scattering from the lower atmosphere and the ultraviolet reflectivity of the planetary surface. The presence of molecules that absorb in the ultraviolet, such as ozone, would be detected and measured.

B. Visual Imaging Investigation (Television)

The objectives of the TV experiment were:

(1) To determine the general physiography over much of the planet Mars at a resolution significantly better than that obtainable from earth and to topographically categorize the basic light and dark areas and perhaps learn more about seasonal variations.

(2) To further explore geographically this unknown planetary surface for additional clues as to its origin.

(3) To obtain sufficient coverage at a suitable resolution to distinguish, on the basis of crater morphology and other criteria, between an episodic and a continuous history.

C. Infrared Spectrometer Investigation

The objectives of the IRS experiment were:

(1) To acquire data relevant to ascertaining the possibility of the presence of life (current and past)

on Mars. The chemical considerations of importance to assist in supplying the answer to this question include:

(a) The presence of an oxidizing or a reducing atmosphere.

(b) The presence of polyatomic molecules that suggest biochemical processes, affect the ambient surface temperature, and limit ultraviolet light flux at the surface.

(c) The compositional variations of atmospheric constituents relative to geographical locale.

(2) To provide information concerning surface composition, gas temperature, surface albedo, surface temperature, and atmospheric photochemistry.

D. Surface Temperature Investigation (Infrared Radiometer)

The objectives of the IRR experiment were:

(1) To measure the infrared radiation emitted from the area of Mars scanned by the television system to obtain a temperature mapping which could be correlated with topological or cloud features observed visually.

(2) To obtain a surface cooling curve in a scan roughly perpendicular to the terminator to obtain data relative to the nature of the surface.

(3) To obtain temperature measurements of the dark side surface, which is inaccessible from the earth.

(4) To obtain absolute temperature measurements of the south polar cap in order to differentiate between CO_2 and H_2O caps.

E. S-Band Occultation Investigation

The primary objectives of the S-band experiment were:

(1) To obtain measurements leading to an improved determination of the pressure and density in the atmosphere of Mars at the surface and their variation with altitude. Measurements at four locations on the surface of Mars, separated in latitude, are necessary to observe possible latitudinal variations.

(2) To obtain measurements leading to an improved determination of the electron density profile of the ionosphere of Mars at four locations above the planet's surface.

A secondary objective was to obtain precise measurements of the radius of Mars at four points on its surface, thus yielding information on physical measurements of the figure of the planet.

F. Celestial Mechanics Investigation

The objectives of the CM experiment were:

(1) To obtain certain parameters which are of significance to the fields of celestial mechanics and astrodynamics. In particular, it was desired to obtain from the radio tracking data the mass of Mars, the mass of the moon, the astronomical unit, and other parameters which would be used in the construction of improved ephemerides of the earth and Mars.

(2) To detect general relativistic effects on the spacecraft.

III. The Scientific Instruments

Of the six science experiments, two did not require that instruments be carried on board the spacecraft. The celestial mechanics and the occultation investigations required the transmission and reception of the S-band radio signals from earth to the spacecraft and return. The other four investigations required instruments mounted on a movable scan platform. They were supplied power and control functions from the spacecraft and generated data which was telemetered or stored and ultimately telemetered to earth. In the following paragraphs brief descriptions of the on-board instruments are given that are oriented here primarily toward scientific measurement capability. Engineering and performance data is given in Volumes I and II and in publications by the principal investigators and their co-workers.

A. Ultraviolet Spectrometer

The UVS was a mechanically scanned grating spectrometer, with a grating spacing of 2160 rulings/mm. It was a two-channel device, with a G-type photomultiplier tube responding in the 1100 to 1900 Å region and an N-type tube sensitive from about 1600 to 4350 Å. The

tubes were read out sequentially and continuously, each scanning its part of the spectrum, during a 3-s time period. Nominal dispersion from the grating was 20 Å per mm in first order onto exit slits 1 mm wide, giving effective instrument resolution of 20 Å in first order.

The field of view of the slit was 0.229×2.29 deg at a nominal planetary range of 6000 km. The atmospheric coverage was 24 km in width and 240 km in length. During the limb crossings, the slit projection was aligned with the limb of Mars while the spacecraft motion carried the field of view down through the atmosphere in a direction perpendicular to the long dimension of the slit. Hence, at the spacecraft velocity of about 8 km/s relative to Mars, one slit width of motion occurred during the 3 s time for the scanning of a spectrum. Under ideal conditions an altitude resolution of 24 km would be obtained.

To provide for efficient recording of the data, it was necessary that data taking by all the experiments in near-encounter begin simultaneously. However, the UVS was designed primarily for use in the atmosphere above the limb, while the television and the radiometer were designed primarily to view the disk of the planet. The UVS slit field of view was therefore offset to trail the TV/IRR optic axes by 11 deg. The UVS would start taking data well above 1000 km altitude, at the time the TV and IRR were crossing the limb.

Because of the extreme difference in intensity of light coming from the atmosphere and the disk in wavelengths seen by the N channel, two photosensors, one beyond each end of the slit, were provided to switch the N channel sensitivity to a lower value at the limb crossing. This prevented saturation of the signal so that ozone might be detected and Rayleigh scattering from the lower atmosphere and the degree of UV penetration to the surface could be measured. The sensitivity of the photosensors was adjusted to permit the gain to switch back to the high value at terminator crossing to again permit upper atmospheric measurements. It was not necessary to switch the gain of the G while the surface was being viewed.

B. Television Cameras

The TV experiment used two cameras in order to obtain both high resolution and broad coverage. For camera B, the optics were a modified Schmidt-Cassegrain system of 504 mm focal length. The field of view was 1.1 by 1.4 deg, with a rectangular format on the vidicon faceplate of 9.6 by 12.3 mm. Using the same vidicon format with a 50-mm lens, camera A had a field of view 11 by 14 deg. The two cameras operated alternately at 42.24-s intervals. The range to the planet was such that camera A frames overlapped from one to the next and the camera B frames were nested within the overlap regions. Camera A had a four-window rotary shutter fitted with color filters. The filter sequence was blue–green–red–green, providing comparisons of the spectral reflectivity characteristics of the Martian surface in the camera A overlap regions. Camera B had only a single broadband filter to eliminate blue wavelengths since Mars is known to exhibit very low contrast in blue light.

Except for optics and shutters the cameras were identical; both used vidicons and shared the same video data processing circuitry. The vidicon format was scanned by 704 lines; each line was sampled 934 times to form picture elements (pixels). Two data channels were provided for on-board processing and storage of the video data. In order to maximize the data return, an analog recording scheme was devised. Since *Mariner IV* experience had shown Mars to be a very low contrast object on a small scale, the analog data was contrast-enhanced by means of cubing circuitry. To avoid saturation by the cubing process at large radiance transitions, such as at the limb and at the polar cap edge, the signal was first processed by an automatic gain control. Hence, in the analog channel, overall photometric accuracy was sacrificed to maximize the capability to discriminate small-scale radiance differences on the low-contrast surface. To supply some photometrically accurate data, a channel was provided to process and record sampled digitized data. Over most of the area of each picture, every seventh pixel of each television line was digitized to eight-bit accuracy. After deletion of the two most significant bits of each pixel to further compress the data, the digitized data was recorded on the digital tape recorder. The missing bits were later inserted during image processing.

The very complex on-board video data processing left much work to be done after receipt of the data on the ground. "Raw" pictures from the analog channel were available immediately after Mars encounter, but much work is required to be done by the Image Processing Laboratory to produce noise-removed, geometrically corrected, and photometrically corrected Mars pictures.

C. Infrared Spectrometer

The IRS spectral range of 1.9 to 14.3 μ was covered by a two-channel instrument using variable-wedge interference filters and cooled detectors. Energy from Mars

was collected by a 25.4-cm Dall-Kirkham telescope and passed through a beam splitter to provide separate signals for the two channels. Two circular interference filters, one in each of the light paths, were mechanically rotated; the scan period was 10 s for a full spectra. In this time two spectral bands, one from 1.9 to 6.0 μ and the other from 4.0 to 14.3 μ, were obtained. For in-flight calibrations, calibration disks were provided with polystyrene and opaque segments, alternatively interjected into the field of view at every sixth spectrum. The polystyrene windows provided wavelength calibration, and the opaque segment gave temperature calibration.

Separate blackened tuning fork choppers modulated the radiation in each channel at approximately 500 Hz. The tuning fork in channel 1 (the long-wavelength channel) provided a cold reference at about 165°K, which was maintained by radiative cooling. The channel 2 tuning fork provided a temperature reference at the ambient temperature of the main instrument case of about 235°K.

Channel 2 used a lead selenide detector cooled to about 165°K by radiative cooling. Channel 2 operated on sunlight reflected from the planet. Channel 1 operated on energy emitted from the planet and therefore was useful on the night side of the planet as well as the sun-illuminated side. Channel 1 used a mercury-doped germanium detector cooled to about 20°K by a two-stage Joule-Thompson cryostat using gaseous nitrogen and hydrogen. Channel 1 failed on *Mariner VI* but operated successfully on *Mariner VII*.

The slit apertures for the two channels were arranged so that their projected fields of view were arranged end-to-end and generally perpendicular to the sweep direction, with only a small amount of overlap. Each slit subtended approximately 0.06 by 2.1 deg, with 0.3-deg end-to-end overlap. Hence the overall field of view was about 0.06 by 3.9 deg; at Mars distance during closest approach the slit swath on the surface was about 220 km wide, or about 120 km per channel. The pointing direction of the IRS trailed that of the television cameras by 4 deg so that, as data recording was initiated, the IRS view would sweep down through the lower atmosphere before reaching the surface.

D. Infrared Radiometer

The IRR was designed to measure the infrared energy emitted from the surface of Mars for the determination of surface temperature. Two channels were provided to cover a dynamic range of 120 to 330°K since the temperatures encountered at Mars were expected to vary widely over the diverse regions viewed. Channel 1 used a passband from 8.2 to 12.4 μ; channel 2 used a passband from 18 to 25 μ. Both passbands were defined by interference filters to exclude the effects of atmospheric absorption. Channel 1 was most suitable for the higher temperatures expected in the equatorial zone, while channel 2 would respond at the peaks of black-body radiation curves corresponding to Mars polar cap temperatures. With this scheme the relative sensitivity of the instrument was better than 0.5°K over the entire range. Absolute accuracy of temperature determination was subject to systematic effects. The most important of these was the sensitivity of the instrument to radiation from outside the primary field of view, equivalent to "wings." Also, since the instrument measures energy rather than temperature directly, the temperature calculation depends on the assumed surface emissivity. However, it was felt that the temperature values obtained are good to within a few degrees Kelvin.

The instrument used two bimetallic thermopile detectors, one for each channel, each behind a separate 2.5-cm telescope. Input energy was reflected into the lenses by a rotatable plane mirror capable of being stepped to three different positions. During each 63-s operational cycle, the instrument spent a total of 56.7 s viewing Mars. The remainder of the interval was used looking at "hot" and "cold" reference sources to provide calibration sources for absolute radiometric measurements. The "cold" source was empty space viewed at right angles to the direction toward Mars. The "hot" source within the instrument was a plate whose temperature was monitored by a thermistor.

The radiometers were boresighted with the high-resolution television cameras to permit correlation of information from the two experiments. This also permitted radiometric coverage of Mars from both spacecraft throughout their approach phases.

IV. Science Mission Design

Optimization of the missions to achieve the best scientific return was a many-variable problem the solution to which evolved continuously from mission inception until the *Mariner VII* encounter. The process is described in three phases:

(1) The establishment of the configuration of the science instruments on the spacecraft based on the initial mission profiles available early in the hardware development period.

(2) The development of standard science mission profiles, including aim point selection and instrument scan platform operational sequences. Since it was a requirement that the mission could be controlled by internal commands from the Central Computer and Sequencer (CC&S), programmed before launch, this second phase ended with preparation of the CC&S launch tapes.

(3) The determination, from flight engineering telemetry and tracking data, of steps to be taken via ground commands to obtain incremental improvements in the science return.

Science mission planning was the task of satisfying experimental requirements to the highest degree possible, within both the spacecraft and operations constraints and conflicts in requirements among the experiments. Most of the constraints were known in general terms early in the planning, but many were refined during design interactions. The following section gives a listing of various constraints, experiment requirements, and experimenter ideas that were considered in science mission planning. General spacecraft and operations constraints are listed here as engineering constraints. The reader is referred to Volume I for more details in this area. The purpose here is to give general background information relative to the scientific experiments.

A. Engineering Constraints

1. Planetary quarantine. This constraint is imposed by international agreement to minimize the probability of contaminating the planet with terrestrial microorganisms. Since the *Mariner* 1969 spacecraft were not sterilized, it was necessary to assure that the trajectories were such that the probability of impacting Mars was very low. The Mariner 1969 allocated probability was 6×10^{-5}.

2. Sun and Canopus occultation. Since in the normal mode of operation the spacecraft depended on the sun and the star Canopus for attitude control, trajectories which would cause occultation of either by the body of the planet were not permitted.

3. Goldstone constraint. To maximize the ease and reliability of commanding the spacecraft and later to make possible the use of the high-rate telemetry channel, it was required that both encounters take place during times when the spacecraft were in view from the Goldstone tracking station in Southern California.

4. Data storage and telemetry rate constraints. The amount of scientific data that could be returned was limited by the capacity of the spacecraft tape recorders and the telemetry data rate. At first, the rate was 270 bits/s, but the use of block coding was ultimately authorized and used, permitting digital and analog playback at 16.2 kbits/s. This increased the total data return, particularly from the far-encounter phase of the mission.

5. Scan platform constraints. The stepping rate of the platform limited the magnitude of pointing direction change that could be accomplished during the time between successive television exposures. The minimum possible platform cone angle (angle between pointing direction and roll axis vector toward the sun) was 101 deg, which placed an upper limit on the phase angles for viewing the planet.

6. CC&S constraints. Although the CC&S was very versatile, demands on its services placed limits on the number of platform slews that could be performed during near-encounter.

7. FEPS constraints. Earlier than three days before encounter the Mars disk was too small to assure that the far-encounter planet sensor (FEPS) signal would be above threshold. Later than 4 to 6 hours before encounter, the disk more than filled the FEPS field of view, and it was uncertain whether the FEPS would accurately track the planet.

B. Science Requirements

Science requirements were formally documented prior to the flights in JPL Planning Document 91 (*Mission Plan and Requirements*, February 1969). In its final form the list was the result of much study and analysis by the experiment teams; few of the requirements had to be compromised during the actual missions.

1. Ultraviolet spectroscopy. Requirements for UVS were:

(1) Data recording shall begin at a minimum altitude of 1000 km above the bright limb.

(2) The slit alignment shall be within 3 deg of the local horizontal plane at 100 km altitude above the lighted limb with 90% confidence.

(3) The scan trace tangency point at limb crossing shall be within 30 deg of the subsolar point.

2. Photographic imaging (television). Requirements for TV were:

(1) The far-encounter pictures shall be sufficient in number and so spaced that coverage of all Martian longitudes is obtained at the highest feasible resolution.

(2) The wide-angle TV pictures shall overlap sufficiently so that each narrow-angle picture falls within the region of overlap and color reconstitution is possible.

(3) At least one wide-angle picture of the lighted limb shall be obtained for each spacecraft.

(4) At least two wide-angle pictures and one narrow-angle picture shall be taken of the southern polar cap on at least one of the two flybys. No more than three wide-angle and two narrow-angle pictures of the southern polar cap shall be taken. (This was later modified for *Mariner VII* when pictures from *Mariner VI* were obtained.)

(5) At least 24 pictures shall be taken on the lighted side of Mars for each spacecraft.

3. Infrared spectroscopy. Requirements for IRS were:

(1) The far-encounter television sequence must be terminated early enough so that the IRS experiment is not significantly degraded because of radiative heating of the IRS instrument by other portions of the spacecraft viewed by the radiative cooling plate.

(2) Data recording shall begin at a minimum altitude of 400 km above the lighted limb surface.

(3) A minimum of 6 min of dark-side data shall be obtained.

(4) A near-equatorial scan shall be made by at least one of the two flybys.

4. Surface temperature (infrared radiometry). Requirements for IRR were:

(1) Optic axes shall be boresighted with the TV cameras to within ±0.3 deg.

(2) The scan shall cross the southern polar cap on at least one of the two flybys.

(3) The scan shall not cross the terminator while viewing the polar cap.

(4) No platform slew shall be made during the time when the IRR scan is within ±10 deg longitude from the terminator.

(5) At least 6 min of dark-side data shall be obtained.

5. S-band occultation. Requirements for S-band were:

(1) Each spacecraft shall pass behind Mars as seen from earth.

(2) Radio beam tangent points at occultation entrance and exit shall be widely separated in absolute value of latitude.

(3) The DSS antenna elevation angles shall exceed 15 deg during occultation data gathering periods.

6. Celestial mechanics (CM). Requirements for CM were that a sufficient amount of control over the tracking data quality and quantity and the indigenous nongravitational spacecraft accelerations be applied to realize at least a factor of 3 improvement in the accuracy of determination of the mass of Mars and to gain information on the AU and the ephemerides of earth and Mars.

C. Instrumental Constraints

In addition to scientific requirements for the investigations, there were instrumental constraints that had to be satisfied.

1. Ultraviolet spectroscopy. If the near-encounter strategy requires the collection of primary limb atmospheric data by the UVS after viewing the planet, at least 30 s must be allowed for the N tube in channel 2 to recover from the excessive dark current induced by viewing the bright planet. In terms of altitude, this means the view axis of the UVS must be brought back to not less than 600 km above the limb.

2. Photographic imaging (television). Since the TV cameras are shuttered alternately every 42.24 s by mechanical shutters, the cameras should be subjected to no more than 72 h of cumulative running time during the mission. If a failure-mode operation must be adopted during encounter, thermal imbalance between the camera B optics and the camera B head should be avoided, since out-of-focus pictures might result. Science power turn-on should be so timed as to insure, within the limits

of the encounter uncertainties, that a particular color filter will be in place on the A camera for the shuttering of the first near-encounter picture. The color of the filter desired depends on the color response of the vidicon and will therefore depend on the unit being flown.

3. Infrared spectroscopy. The detector in one channel of the IRS will be cooled by radiative cooling. It is therefore necessary that the radiator plate have an unobstructed view of deep space for a sufficient length of time prior to near-encounter to reach the designed operating temperature for the detector.

The second IRS detector will be cooled by cryostatic cooling, using Jules-Thompson expansion of N_2 and H_2 gases. The blowdown of the compressed gases should start at E — 35 min and continue through the encounter sequence.

Because excessive risk is involved in operating the IRS scan motor for extended periods, the IRS motor start command has been divorced from the science power turn-on and coupled with the blowdown command for the IRS cooldown, and thus will occur at E — 35 min.

Because of the general cooling requirements of the IRS, the cruise heater should be turned off and the electronics on no later than E — 48 h. (The electronics provide a lesser heat load than the cruise heater in this instrument.)

4. S-band occultation. For this experiment, the spacecraft radio may be considered the science instrument. It is important that no major power changes such as turning on gyros or switching the traveling wave radio output tube from low to high power be made after approximately E — 10 h. Even minor power changes should be avoided where possible after the start of near-encounter. A change in temperature of the crystal determining the radio carrier frequency, if not stabilized by the time of occultation exit, will jeopardize the reacquisition of the radio signal and hence the S-band occultation results.

D. Experimenters' Requests

The mission would have been severely overconstrained if all the secondary experimenters' requests had been firm requirements. The several items summarized here did have influence on the mission design.

1. Ultraviolet spectroscopy. The area scanned by the UVS on the surface of Mars was to be included in the wide-angle TV coverage and was to include, if possible, the areas photographed by the high-resolution TV. Data was to be returned from the UVS to look for night glow during the time it scanned off the dark limb of Mars to an altitude of several hundred kilometers. If possible, the UV slit projection was to be tangent to the dark limb at that time.

2. Photographic imaging (television). Although it was required that there be 24 pictures taken on the illuminated side of the planet, assuming the first to be centered on the limb and the last to be centered on the terminator, it was desirable that as many pictures as possible be taken on the illuminated side.

It was desirable that the first picture of each near-encounter pass be a wide-angle picture. No high-resolution pictures were to be taken off the limb.

Overlapping wide-angle pictures of the limb from each spacecraft were desired. (More precisely, it was the lower atmosphere above the limb that was of interest, since the actual limb line would not be the same for two subsequent photographs.) Except for the limb photographs, pictures taken at highly oblique view angles were to be avoided since the ground resolution of such pictures would be degraded.

Some stereo coverage, obtained by covering the same area with two different platform pointing angles, was desirable. However, a large amount of such stereo coverage was not desired as this would have diminished the total area covered at kilometer resolution.

Wide-angle camera coverage was to be selected to include a maximum of the known types of Martian surface features.

3. Infrared spectroscopy. One minute of data was to be returned after the IRS slit projection had passed the dark limb to provide calibration data. It was desired that this time be in addition to the 6-min dark-side viewing time. Surface tracks of the slit projection from subsequent platform positions on a given spacecraft were not to overlap; that is, IRS "stereo" was considered undesirable. It was considered preferable to cover a different area instead.

The IRS track was to cover a maximum of known types of Martian surface features. The IRS track was to cover the same areas covered by the high-resolution TV and the IRR track.

Near-equatorial areas were preferred to the more southerly areas, since the long-wavelength channel depended on the thermal radiation from the planet. This was considered particularly important on the dark side of Mars. Oblique views of the surface of the planet were to be minimized so that the best possible resolution could be achieved.

4. Infrared radiometer. In addition to obtaining data from the polar cap, IRR investigators wanted to obtain data several degrees off the edge of the cap and then to cross the edge of the cap. It was desired that the tracks across the terminator be continuous for at least 10 and preferably 15 deg on each side of the terminator.

5. S-band occultation. S-band investigators preferred that occultations occur at such times as viewing from both DSS 14 and DSS 41 could be achieved. The spacecraft were to pass as close to the planet as possible so as to minimize the distances between them and the occulting limbs.

6. Celestial mechanics. Celestial mechanics investigators requested that closest approach distances be minimal. Trajectories having lower velocities with respect to Mars were preferred.

E. Scan Platform Configuration

A major difference between this mission and the previous Mars mission, *Mariner* 1964, was the use of a large scan platform with two degrees of freedom. The *Mariner IV* platform could be rotated only in clock angle (i.e., about the roll axis, the spacecraft's direction to the sun).

In addition to clock angle rotation, the *Mariner* 1969 platform could be moved in cone angle (the angle between the platform look direction and the roll axis).

It was not clear at first that all the science instruments should be mounted on the second gimbal of the scan platform and thus be movable in two degrees of freedom. The important requirement that the UVS slit achieve tangency with the Martian limb seemed to impose a severe restriction on the freedom of coverage of the other instruments. Also, it seemed that the minimum cone angle limit of the platform would not permit UVS viewing of the limb at the most favorable range. Two alternatives were proposed and discarded. The first involved mounting the UVS on the side of the spacecraft toward the sun. This would have caused intolerable stray light problems as well as temperature control difficulties. Secondly, it was possible to mount the UVS on the clock gimbal but exclude it from cone angle motion. This would have complicated construction of the platform and worsened the already difficult instrument crowding problem. It was finally decided to mount all the science instruments on the platform. Relative pointing directions of the instruments were chosen to best carry out the objectives of all experiments. Some compromises were required.

The two TV cameras were boresighted to place the high-resolution coverage in the overlap areas formed by the wide-angle camera coverage. This pattern was achieved since exposures of the high-resolution and wide-angle camera alternated.

The IRR was boresighted with the TV cameras so that IRR coverage within the high-resolution TV coverage was assured.

The IRS pointing direction was offset −4 deg in cone angle so that, when the TV axes crossed the limb and data recording began, the IRS would look at a region at least 400 km above the limb. To assure IRS coverage of the areas on the planet covered by the high-resolution TV and the IRR, the IRS pointing direction was offset +0.95 deg perpendicular to the cone offset.

The UVS pointing direction was offset −11 deg in cone angle so that, when data recording began, the UVS would look at an altitude of at least 1000 km. To obtain the best possible overlap with the coverage of the other instruments on the surface, the UVS was offset 4.8 deg in the perpendicular direction. This was later changed to 3.0 deg because the aim points were moved northward from the original nominal aim points.

V. Encounter

The basic elements of the encounter sequence were determined by the requirements of the experimenters given in the previous section. For the 1969 flights, the solar system geometry provided a lighted-side approach about 25 deg from the actual sun line. Television pictures of the entire planet would be taken in a far-encounter phase. Both spacecraft would pass the planet on the evening side. One spacecraft would pass over or near the edge of the south polar cap and the other over equatorial regions; closest approach would be near the evening terminator. During the near-encounter phase, data taking would start about 20 min before closest approach with the instruments pointing forward and making an angle of about 45 deg from sunlight direction. The actual start

of data recording would be when the TV and IRR instruments crossed the lighted limb of the planet; the UVS and IRS instruments would be looking through the atmosphere as desired by their investigators. While the lighted side was being viewed, the instrument printing directions would be changed several times in discrete steps between TV pictures, ending with the instruments pointing almost perpendicular to sunlight direction. The motion of the spacecraft would then take the instrument views over the terminator, the dark side, and dark limb of the planet. The spacecraft would then go behind Mars relative to the earth to carry out the S-band occultation experiment. The planned coverage of the planet is shown in Fig. 1.

A major task was the incorporation of the 64-m-diam Mars antenna into the encounter sequence. This antenna is located at Goldstone, California, and is part of the world-wide Deep Space Network (DSN). Because there was only one such large antenna, it was not permissible to design a mission that required its availability to accomplish primary objectives. On the other hand, it was fully intended to use it and benefit from its higher performance. The mission sequence was required to be a two-fold plan. One part was a conservative, automatic sequence that did not require the large antenna; the other was an enhanced, optional sequence that did.

In the conservative, automatic sequence the real-time science data stream would be sent to earth at the rate of 66⅔ bits/s from the time of science power turn-on, through encounter, and until its interruption by occultation. (The contents of the three science data streams are given in the next section.) The two other science data streams would go to magnetic tape recorders. These tape recorders could hold about 25 min of data each. The digital tape recorder would operate only during the near-encounter phase. About 75% of its time would be used while the instruments were viewing the lighted side of the planet and 25% while viewing the dark side. The analog tape recorder would contain only television data and hence would not be needed on the dark side. It would use 25% of its tape to record 8 pictures during far-encounter and the remaining 75% during the light side portion of the near-encounter. Only one tape load of data for each recorder would be obtained. After encounter the digital recorder would be played back and the data transmitted to earth at a rate of 270 bits/s. This was a 60 to 1 reduction from the recording rate of 16,200 bits/s, and thus it would take about a day for the playback of the full digital recorder. After two playbacks of the digital data and verification of its successful recovery at earth, the transfer of the analog data to the digital recorder would take place. In seven cycles the analog recorder would play back its data at one-seventh its record speed. Each of these analog data blocks would be digitized sequentially and placed on the digital tape recorder in about 25 min at the 16,200-bits/s record rate of the latter. Then each data block would be played back from the digital recorder at the slow 270-bits/s rate for transmission to earth.

The entire process of recovering the analog data once would take about 8 days; two recoveries of analog data would be made at the minimum. This basic sequence was automatic because it could be started and performed by planet sensor devices and on-board logic. This feature has been used on all *Mariner* spacecraft; the sequence is placed in the spacecraft before launch. Thus if a nominal midcourse maneuver is performed, a nominal mission can be carried out without further command communication from earth. Of course this would be a failure mode, but useful scientific data might well be recovered. In earlier *Mariners* the sequence logic was "hard wired" and could not be modified during flight. In the *Mariner* 1969 spacecraft, the CC&S was a special-purpose computer that could be reprogrammed in flight to do all sorts of different and, for science, marvelous things. It was this capability that permitted the enhanced optional mission sequences that were actually carried out.

The enhanced optional sequences required the use of the large Mars station antenna. When the spacecraft was in view of Goldstone, a high-rate block-coded telemetry mode would be used that would match the 16,200-bits/s digital data generation rate. This telemetry option, like the programmable CC&S, was new technology and part of the engineering objectives of the mission. The required telemetry equipment was prepared on an accelerated basis from the R&D stage.

In addition to antenna availability, several spacecraft subsystems including power, temperature control, and radio had to be operating at or above nominal levels. Such evaluations could be made only as the spacecraft approached their encounters with Mars. In addition to the transmission of the high-rate digital data stream in real-time, the television data from the playback of the analog recorder could also be transmitted in real-time. Thus the contents of this recorder could be received in about 3 h instead of 1 week. Time did not permit an analog-to-digital recorder transfer and digital playback until after encounter in the conservative mission. Analog data could be telemetered to earth even as late as the first part of encounter day pass of the Goldstone antenna in the enhanced mission. The analog tape could then be

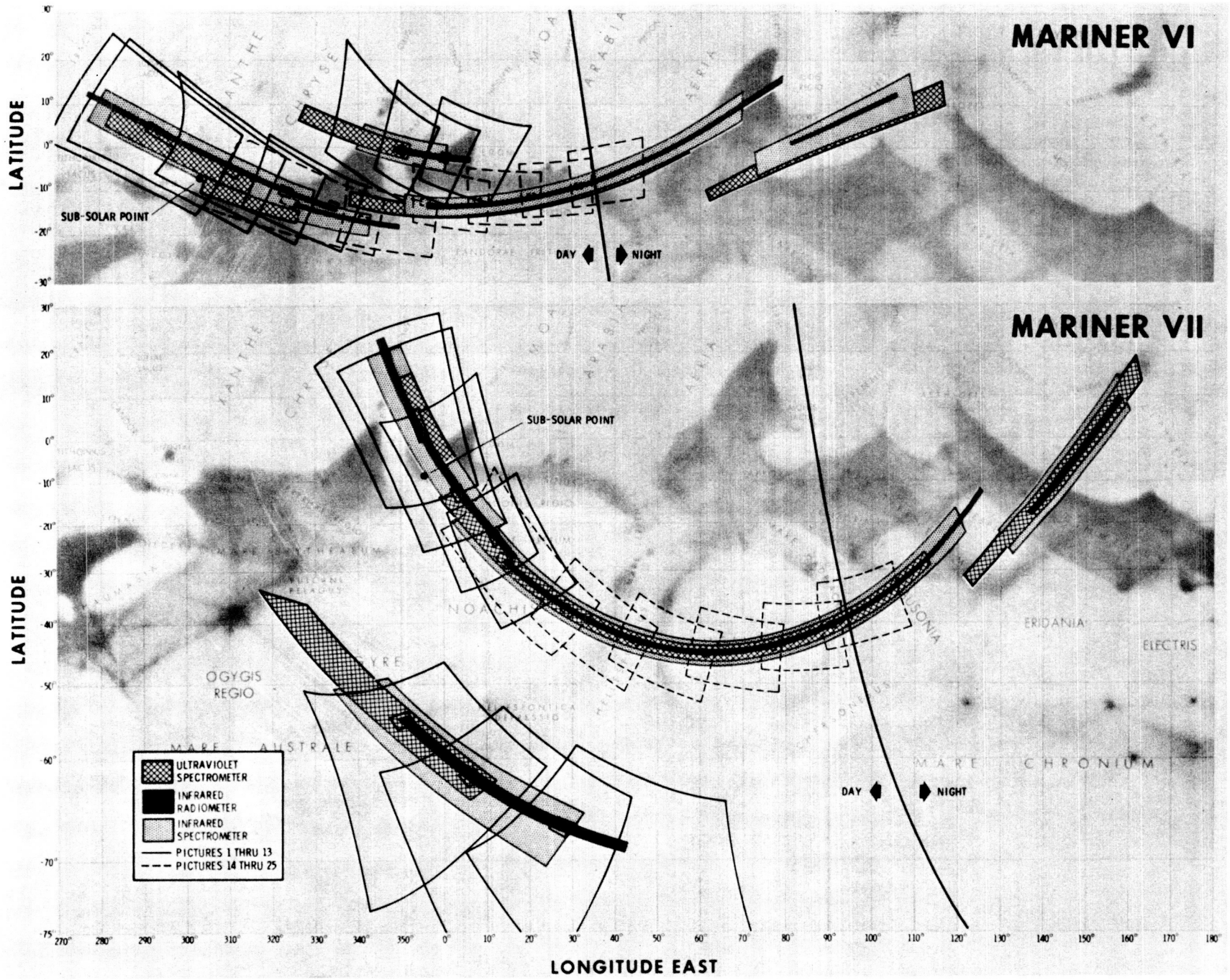

Fig. 1. *Mariner* Mars 1969 scientific planetary scans

erased and be ready for near-encounter. Thus full tape loads of 35 far-encounter pictures could be taken during each of several 24-h periods before encounter. Since the digital data going only to the digital recorder in the basic mission could now be received in real-time, the 25-min recorder time limit for near-encounter data would be removed. Spectrometer and digital television data would be received starting hours before actual encounter and would continue after encounter until the entrance into occultation, when communication from the spacecraft would be temporarily interrupted.

Since the decision to use the high-rate system could not be made until near the Mars encounter, the enhanced encounter sequences had to be optional and not automatic. The sequences themselves were stored in the versatile CC&S along with the conservative, automatic sequence. In order to exercise the option of an enhanced sequence, a command had to be received at the spacecraft. Furthermore, the enhanced sequences were divided into sequential parts. Continuation to the next part required another command; if it was not received, the CC&S would restore the conservative sequence. Provision was made to check the operation of the high-rate telemetry system several days before encounter. On the basis of these tests and the continuing general and specific conditions of the spacecraft subsystems, the decisions to use the enhanced sequences would be made.

Proper operation of the scan platform during the near-encounter phase was critical to the scientific success of the mission. Four slews were used in both encounters; the five pointing directions were chosen to satisfy the scientific requirements of the experiments. The most critical pointing requirement was at the third (*Mariner VI*) and second (*Mariner VII*) positions, at which the second, and shorter-range, limb crossing of the UVS would take place. The platform had two degrees of motion, clock (azimuth angle) and cone (polar angle). Each was controlled by servo systems that caused the platform to follow reference potentiometers. These potentiometers were moved in discrete steps of about one degree; the platform followed, and the actual platform position was measured with another set of potentiometers. In the near-encounter sequence the initial position was adjusted by stepping the reference potentiometers by ground command. This was a relatively straightforward and rapid process. The platform moved to its new position, and this position was verified in the next cycle of engineering telemetry.

After this initial setting, subsequent positions of the platform were controlled by the CC&S. For each slew, it issued a number of step commands to the reference potentiometers; it was thus a delta-type operation rather than a go-to-a-specified-position type. Changing a pointing direction usually meant changing one or more quantitative commands in the CC&S memory if other pointing directions were to be maintained. The verification that the new numbers of slew steps were properly encoded was a relatively long process. As a consequence of these operational circumstances, a rigorously defined procedure for updating the platform near-encounter pointing directions was followed. The cycle was first to obtain a better estimate of precisely where the spacecraft was going to pass the planet from the most recent trajectory data, apply the requirements of the scientists, determine the new numbers, and then change the CC&S memory. The problem was that aiming point precision did not increase rapidly until the spacecraft was within a few hours of the planet. The established procedure was that the last information for the CC&S slews was required at 4 h before encounter. A final adjustment of the initial platform position was permitted as late as 1.5 h. Thus, based on the slews stored in the CC&S, an initial platform position could be selected at that late time to give the desired critical pointing direction for the second UVS limb crossing. A small change in the other, less critical, pointing requirements would be accepted.

The *Mariner VI* encounter was carried out as planned. The enhanced sequences were used, thus increasing the amount of scientific data returned. Science power was turned on at about —49 h.* The exact time was based on the TV color filter sequence desired at near-encounter. Proper operation of the instruments and scan platform was verified. The platform was moved to its far-encounter position and servo-controlled there by the far-encounter planet sensor. Starting at about —47.6 h, 33 pictures were taken at equal intervals of about 37 min, ending at about —28 h. These pictures were played back to earth via the high-rate telemetry system, and high-rate digital data was obtained. The platform was moved to the near-encounter position and back to far-encounter to verify its continuing proper operation.

The next option, a second set of 17 far-encounter pictures taken between about —22 and —7 h, was carried out. The platform was then returned to the near-encounter position so that the IRS radiation plate would be looking entirely into deep space for maximum radiative cooling. The second set of pictures was played back. A portion of the low-rate real-time science data was obtained to verify the detailed operation and sequencing of the instruments. The telemetry was switched again to

*In the following sequence of events, time is measured relative to closest approach.

the high-rate digital mode to await planet encounter. Ultraviolet spectroscopy data was obtained at all times the digital high-rate telemetry mode was on. At the —4-h point, a decision was made to adjust a platform pointing direction so that the IRS instrument view would not straddle the light-dark transition area at the south edge of Sabaeus Sinus. At about —35 min, the cryogenic cooldown of the IRS was started by the triggering of a planet sensor, and the only flaw in the *Mariner VI* encounter occurred: the cooldown failed to activate. As a result only the 1.9- to 6-μ-wavelength channel operated; no data was obtained in the 4- to 14.3-μ channel. The near-encounter slewing and TV picture recording proceeded as planned. Radiometer and spectrometer and digital television data continued to be received in real-time until entry into occultation. Closest approach occurred at 5:19:7, August 1, 1969, GMT.

The *Mariner VII* encounter was different from original plans in many respects. Five days before encounter, coincidentally at the time of *Mariner VI* encounter, radio contact with *Mariner VII* was lost for a period of hours. When contact was reestablished by rolling the spacecraft back to its proper orientation, the tracking and telemetry data indicated a serious anomaly, which was immediately termed "the happening." The trajectory had been definitely altered by a small but operationally significant amount. Furthermore, the tracking data taken over the next days showed the trajectory to be still changing under the action of a small force. A dozen telemetry channels were not operating, including those that would give the position of the scan platform. Severe electrical transients had occurred, with unknown consequences to various subsystems.

In addition to these problems, the scientists now wished to alter the near-encounter slewing strategy. The far-encounter pictures of the south polar cap taken by *Mariner VI* had shown interesting and exciting features; the scientists wanted to get more data and take more pictures of the cap. Return of the dark-side radiometer and spectrometer data would then have to be by the high-rate telemetry system; the digital recorder would have run out of tape if the entire sequence were started earlier in order to get the additional pictures and other scientific data on the lighted side.

Two days later, still three days before encounter, the project manager made the decision to go ahead with the enhanced optional plans in spite of the "happening." Science power had not yet been turned on; it could not be known if any of the instruments had been damaged until this was done. A plan to work around the loss of the platform position reading potentiometers had been formulated. The high-rate telemetry system had worked extremely well on *Mariner VI;* return to the basic, automatic sequence could occur if trouble developed on *Mariner VII.* The additional optional choice between 33 near-encounter pictures and the originally planned 25 would be programmed into the CC&S to meet the scientific request for more pictures of the south polar cap. The performance of the radiative cooling of the IRS on *Mariner VI* indicated that return to the near-encounter position could be delayed until 5 h before near-encounter; valuable far-encounter pictures at closer range could thus be obtained.

At about —70 h, science power was turned on and the *Mariner VII* encounter sequence began. Proper instrument performance was verified and the task of platform position determination began. The platform was stepped to the far-encounter position under control of the reference potentiometers. This was not a normal operation; ordinarily control of the platform would have been switched to a far-encounter planet sensor. From trajectory data, planet position relative to the spacecraft in clock and cone angles was known. Thus when the planet was seen in the television picture, the pointing directions of the platform were known with the platform still controlled by the near-encounter reference potentiometers. (These pictures were returned to JPL, most providently in real-time, by the same equipment used for the commercial TV release described at the end of this section.) The platform was then stepped back to a typical near-encounter position and the number of steps was counted. A calibration of the reference potentiometers had been made as part of the prelaunch testing; it was not as accurate as the data that would have been obtained from the position reading potentiometers, but would have to suffice. (It was suspected that the electrical transients during the "happening" had stepped the reference potentiometers an unknown amount, and this stepping to and from far-encounter was needed to reestablish a reference position for them.) Platform control was then transferred to the far-encounter sensor, and the first far-encounter optional sequence was initiated by ground command.

Three sets of far-encounter pictures were taken; 34 from —67.5 to —54 h, 34 from —47 to —29 h, and 25 from —24 to —5 h. The data was played back between the picture sequences, and other high-rate digital data and scan platform operation verification data was obtained in the same way as has been described for *Mariner VI.* The platform was returned to the near-encounter position at —5 h and preparations made for near-encounter. The

high-rate telemetry channel had worked without fault, and it was elected to do the further enhanced, 33-picture near-encounter sequence. Cooldown of the IRS was initiated, and this time was successful; all channels of all scientific instruments worked during the near-encounter of *Mariner VII*. Platform pointing and slewing parameters had been adjusted according to the scientists' wishes. The *Mariner VII* encounter was tremendously successful in spite of the many difficulties. Closest approach occurred at 5:00:48, August 6, 1969, GMT.

Several weeks before encounter, when the situation with regard to use of the high-rate system looked very favorable, it was decided to attempt a real-time presentation of the analog far-encounter pictures to the world. The data received at Goldstone was recorded on magnetic tape there as the primary record and, in addition, was sent via a commercial communications channel to JPL in Pasadena. There, while an additional tape recording was made, the data flowed in real-time into a computer and video-scan device for decoding and visual display. The television experiment principal investigator and his co-investigators participated in a nationally released television commentary program. The released Mars television pictures did come in real-time from Mars. However, since they came from the analog recorder, it was not a "live" show, but corresponded more to the slow-speed video replay used widely in the televising of sporting events. No attempt was made to show digital pictures in real-time, since they required extensive processing before they could be interpreted as pictures. However, the near-encounter spectrometer data that was received strictly in real-time at JPL from Mars was recorded and then processed into spectra. Thousands of these preliminary IRS and UVS spectra were delivered in plotted form to the principal investigators within 6 h of the taking of the data at Mars.

VI. Science Data Formats and Data Handling

Some detailed information about the science data formats and data handling techniques is necessary to complete the description of the *Mariner VI* and *VII* scientific missions. For two experiments, S-band occultation and celestial mechanics, the data originated on the ground at the DSN stations. In general terms, this data consisted of spacecraft-to-earth range and doppler data along the communication path. During occultation, this path passed through the atmosphere of Mars and produced the data for the S-band experiment. Both entrance and exit occultation data were obtained. The celestial mechanics experiment used all the tracking data obtained during the entire mission. For example, a space mission that leaves the region of earth–moon can provide data for measurement of the earth–moon mass ratio. For both these experiments the data was processed, recorded, and delivered to the two principal investigators directly without any interaction with the telemetered data from the on-board instruments. This tracking data was also used by the Flight Path Analysis Group in Mission Operations for the determination of the trajectory path to Mars, the midcourse maneuver required, and the prediction and documentation of the flyby trajectory past Mars.

For the on-board instruments, the characteristics of the science data formats, the data recording, and the telemetry modes were determined by the requirements of the experiments and the capabilities of spacecraft subsystems and the ground receiving equipment of the DSN. The *Mariner IV* spacecraft had used a data rate of 8⅓ bits/s from an 8-W transmitter to the 26-m-diam antennas of the DSN. The *Mariner VI* and *VII* spacecraft used a 20-W transmitter and larger spacecraft antennas than *Mariner IV*. Also, the range to Mars at encounter was much shorter. As a result, primary data rates of several hundred bits/s were possible at the time of encounter. This primary mode would use 26-m-diam ground antennas; two such antennas at each of several DSN stations around the world would be committed to the primary mission. In the actual mission the large Mars station antenna was used. However, a mission had to be designed that would require only the smaller antennas if the larger was not available.

The spectrometers and television instruments produced data at many thousands of bits/s so that tape recording was mandatory. The IRS data rate was 1333⅓ bits/s with 10 bits/word; the UVS rate was 3200 bits/s with 8 bits/word. The only slow data rate instrument was the IRR, at about 8 bits/s with 10 bits/word. These instruments produced digital words at their interfaces with the Data Automation System (DAS). These digital bits were transmitted directly or stored in digital form on the digital tape recorder. The television instrument generated both analog and digital data. With the large volume of television data desired by the experimenters, all-digital recording was not possible. The experimenters traded the exact precision of digital data recording required by the other experiments for the much larger number of data points (picture elements or pixels) that could be recorded in analog form on the same length of magnetic tape. To provide a definitive, quantitatively accurate framework to reference this analog data, every seventh picture element was digitized to 8 bits. After the first 2 most significant bits were discarded, these

6-bit television words were recorded on the digital tape recorder. It was confidently felt that the missing digital bits could be supplied from knowledge of the brightness of large areas of Mars. It was also known from *Mariner IV* pictures that the surface of Mars had quite low contrast. Automatic gain control and nonlinear cubic enhancement were applied to the analog signal before analog recording in order to increase the amount of scientifically useful information per bit of television data.

The three science data streams operated continuously when science power was on; various portions of the data were transmitted to earth in real-time or recorded on an analog and digital recorder. The real-time data stream operated at 66⅔ bits/s. It contained identification, timing, science sequence status, and instrument engineering data. The IRR science data and the UVS far-encounter Lyman alpha science data were also in this stream. In the conservative sequence, this would be the only science data returned in real-time; portions of the other data streams would go to tape recorders for subsequent transmission after encounter.

The television analog data stream contained television data only. The television camera output modulated an 18.9-kHz carrier wave. The time for full scan line was 60 ms; the line when ultimately digitized as part of the analog playback operation would consist of 1134 digital words of 6 bits each. The first 200 digital words were used for line count, other timing and identification information, and digital data from the preceding television line. Scan retrace in the camera was accomplished during this time. The remaining 934 digital words were the active picture elements (pixels). Each TV picture consisted of 704 of these lines and required 42.24 s to be transferred from the vidicon to the analog tape recorder. This data could go only to the analog recorder. When it was replayed at a rate of one-seventh the record speed and the analog data digitized, the resulting digital data stream had a rate of 16,200 bits/s. In the conservative sequence mission, this data would go to the digital recorder for subsequent transmission at an even lower rate. In the optional sequence missions actually carried out, this data was transmitted in real-time to earth.

The high-rate digital data stream contained the IRS and UVS data, the real-time data stream (IRR data, etc.), the necessary identification data, and the digital picture data from every seventh pixel. A frame contained 972 bits and was the same length as the TV line (60 ms). The synchronization was provided by the DAS, which controlled all science data taking and handling on the spacecraft. A frame of high-rate digital data contained two-thirds television data and one-third all other data, encoded in sequential blocks of 324 bits of TV, 162 bits of other, 324 bits of TV, and 162 bits of other. The spectrometers operated at constant scan rates of 3 s/spectrum for the UVS and 10 s/spectrum for the IRS. The data from these instruments was generated in digital form and at constant rates at the DAS/instrument interfaces. It was stored in small buffers in the DAS for insertion into the data frame in the 162-bit blocks. The digital, every-seventh-pixel TV data passed through the DAS without time buffering. As a consequence of the overall mechanization, this digital TV data would be available only for the first 40% and the last 40% of the active television line. The times of the center part of the active line and the retrace portion of the total line were used for the other data. In the conservative sequence mission, this digital data would go to the digital tape recorder for transmission at 270 bits/s after encounter and occultation. In the actual missions, this data was also transmitted in real-time. In fact, in the near-encounter portion of the missions, this was done for several hours before, during, and after the operation of the tape recorder and provided additional dark space calibrations and spectral data for the UVS and IRS experiments. Also, this data stream was sent to earth in real-time during parts of the far-encounter sequence, providing full UVS spectra of interplanetary space instead of individual Lyman-alpha data points.

Performance of all spacecraft and ground data handling elements was excellent including (and in particular) during the high rate telemetry mode. Primary recordings were made at the Mars antenna site while the data was additionally transmitted to the Space Flight Operations Facility (SFOF) at JPL. There, additional recordings were made and some real-time display of the TV pictures was provided. From these SFOF recordings, preliminary master data record type tapes were made for the high-rate digital data; the UVS and IRS data was extracted and spectral plots made. Tapes of TV digital, every-seventh-pixel, and full-picture analog data were made available to the Image Processing Laboratory for the start of the detailed picture reconstruction. These first data packages were so complete and free of dropouts that analysis and processing steps could be started by the principal investigators and their teams immediately. After the encounters, digital tape recorder playback was started. This high-rate digital near-encounter data was redundant to data received in real-time. In a change from original plans, these digital playbacks were interrupted when the Mars antenna could receive telemetry. At these times, the analog tape recorders were replayed

Table 2. Science data from on-board instruments

Type of data	Amount of data	
	Mariner VI	*Mariner VII*
Far-encounter pictures	50	93
Near-encounter pictures	25	35
UVS spectra	540	780
IRS spectra	168	205
IRR data points	1600	2000

directly in the high-speed telemetry mode; two full playbacks could be made during a view period. Six such playbacks of TV analog data were made for *Mariner VI* and four for *Mariner VII* on succeeding days. Because of the inherent errors in an analog recording and playback process, the additional playbacks were desired for averaging purposes in the picture reconstruction. Thus, in a few days instead of the originally planned 2½ weeks, all the near-encounter data was returned. After the two digital playbacks were completed, the analog-to-digital transfer and digital replays were started. These activities actually served only as subsystem performance checks. The science data had been returned via the high-rate mode with no loss of data in the process. After the last playback of *Mariner VII* and the primary tapes had been received from the Mars antenna station, the production of the master data records was undertaken. The data was time-tagged and assembled into complete frames and pictures. This task was completed in October 1969.

The total amount of primary planetary science data received from the on-board instruments is summarized in Table 2. The picture counts are exact; the other numbers are approximate. Some off-planet calibration data is included in the UVS, IRS, and IRR data points. In addition to this planetary data, about 30,000 far-encounter UVS spectra were received with the instrument pointed into interplanetary space. If all the bits generated by all the instruments are counted (including the many far-encounter digital pictures, only some of which contain planetary data), the total bits exceed one billion for the two spacecraft. Of this total, about 320 million for *Mariner VI* and 540 million for *Mariner VII* were planetary science data.

VII. Postencounter and Relativity Experiment

By August 10, 1969, the postencounter playback sequences were completed. Some modifications in the original plans were made since most of the science data was received in the fast high-rate telemetry mode. A battery test cycle was then performed on *Mariner VII*. It was determined that its battery was open-circuited. It is believed that this failure occurred during the "happening" several days before encounter. Fortunately, no battery power was needed during encounter.

With the primary Mars mission data taken and in hand, the experimenters were permitted additional experiments oriented to interplanetary space. Attempts were made to photograph stars with the TV cameras. No definitive results were obtained. The UVS instrument was pointed in a series of directions and a survey conducted; some data has been published by the principal investigator. Also, it was desired to look at a comet with the UVS. No results were obtained. The spacecraft gradually passed out of range of the high-rate telemetry system, making UVS spectra essentially impossible to receive.

With the completion of the primary Mars mission, planning for the relativity experiment was begun. In May 1970, the communication paths from earth to the *Mariner VI* and *VII* spacecraft would pass close enough to the sun so that its massive gravity would influence the propagation of the beams. The orbits of the spacecraft were carefully determined over months preceding and following this time. Departure from the expected time of transit of ranging signals would be determined, and thus a direct experimental measurement of this relativistic effect made. The experimental data was successfully acquired and supported the Einstein form of relativity. The principal investigators were Dr. John Anderson of JPL and Dr. Duane Muhleman of Caltech.

In a last scientific measurement in December 1970, the UVS and the IRR instruments looked at the plumes from midcourse motor burns. With the depletion of gases used for attitude control, the spacecraft were nearing the end of their sun-oriented, roll-stabilized lives. Only one of two possible midcourse maneuvers had been used in the flight to Mars. The second firings were performed as engineering experiments. The UVS principal investigator has issued a report.

Part 2. Scientific Results

I. Initial Press Conferences

Press conferences were held at the Jet Propulsion Laboratory in Pasadena, California, about 60 hours after each encounter for the purpose of announcing the preliminary results of the scientific investigations. The encounters had occurred at about 10:00 p.m., PDT, and the first sets of data were delivered to the principal investigators between then and the following morning. The experimenter teams had two days and nights to examine the data and formulate initial interpretations.

At the start of the *Mariner VI* conference, held August 2, 1969, the moderator, Dr. John E. Naugle, NASA Associate Administrator, emphasized the preliminary nature of the results to be heard and placed the *Mariner* 1969 mission in perspective with previous and future Mars missions.

The S-band occultation experimenters reported initial results consistent with *Mariner IV* data taken in the 1964 flight. Estimates of the range of surface pressures on Mars were given based on an elevation variation of 12 km from radar data. The surface pressure range was 3 millibars at the high topographic regions and up to 8 millibars at the lower elevations. An electron density higher than obtained in 1964 was reported for the Mars ionosphere.

The ultraviolet spectrometer experimenters reported the presence of atomic hydrogen at very high altitudes, atomic oxygen at intermediate levels, and CO_2, CO, and atomic carbon at lower levels. It was concluded from the initial examination of the data that molecular nitrogen was either not present in the atmosphere or present in only very small quantities. When viewing the surface of the planet, the UVS obtained characteristic scattering spectra. These spectra flicked up and down in intensity, which indicated that the surface atmospheric pressure over the areas being scanned was changing and also that the ultraviolet light was penetrating to the surface.

From the infrared spectrometer experiment it was reported that the long-wavelength channel (4–14μ) did not operate. The data from the other channel showed the presence of CO and CO_2 with indications of atmospheric

water vapor and water ice. The water ice seemed to be in the atmosphere perhaps as a fog. Surface temperature variations were found. There was a weak absorption feature in a region characteristic of methane.

The surface temperature experiment obtained its temperature profile measurements across the equatorial surface of Mars. The data was shown against a theoretical curve assuming a uniform planet and uniform radiation from it. The gross features agreed. It was anticipated the deviations would be interesting when they were further examined in conjunction with the visual features from the television pictures. The cooling curve beyond the terminator was obtained.

Initial interpretations of the visual imaging (television) experiment were made in three areas. The far-encounter pictures were contrasted with earth-based pictures. Features which appear sharp and angular in the earth-based data do not appear sharp in the *Mariner VI* photographs. The boundaries between light and dark areas are diffuse and irregular. The classic canals show as diffused linear features of very low contrast.

In the second area, the near-encounter pictures were reported as being remarkably free of atmospheric effects, both haze and clouds. There was no evidence of the classic blue haze. The bright "W" cloud feature did not show the structure expected of a cloud at the resolution obtained. Some indication of possible haze near the edge of the polar cap was found.

In the third area, detailed surface features, many craters were found, large to small in size, fresh to faint in appearance. These *Mariner VI* pictures seemed to further confirm the feeling first given by the earlier *Mariner IV* photos: Mars is much more like the moon than the earth.

The celestial mechanics experiment yielded initial values for the earth–moon mass ratio and the mass of Mars. The Mars measurement is capable of high accuracy, with uncertainties in the sixth significant figure. Agreement with extended analyses of earlier *Mariner IV* measurements was obtained, and an additional improvement of the complete dynamical map of the solar system, and Mars in particular, would be made.

The *Mariner VII* conference was moderated by Dr. Norman Horowitz, professor of biology at Caltech. In his opening remarks he emphasized the importance of the continuing search for extraterrestial life so long as its existence is not ruled out by conclusive evidence.

Because of a trajectory disturbance, no useful celestial mechanics encounter data was obtained by *Mariner VII* and there was no report from that experiment.

The far-encounter pictures were similar to those of *Mariner VI*, generally mottled in appearance, showing diffuse boundaries between regions and the structured edge of the polar cap. The near-encounter pictures near the polar cap showed a narrow transition zone, about 70 miles wide, between the fully covered polar cap and fully uncovered ground. Ice covered the northern sides of craters in the zone. The interpretation was that they had shallow slopes of only a few degrees. A very significant and startling item was the smoothness of the surface of the very large, bright Hellas area. It was concluded that there is activity in that region that obliterates craters as fast as they are formed.

The major part of the report on the surface temperature experiment was devoted to the polar cap temperature. A primary objective was to distinguish between water ice and solid CO_2. The measurement of $-123°C$ was within a few degrees of that expected from a solid and gaseous CO_2 equilibrium at the surface pressure of Mars. It was concluded that the polar cap was CO_2.

Interpretation of the data from the S-band occultation experiment was hampered by the orbit uncertainty from the trajectory disturbance. Preliminary analysis gave a low pressure of about 3.5 millibars above Hellespontica Depressio, which would indicate the area to be about 6 km higher than an average equal pressure surface. The ionosphere was detected and measured.

The atmospheric data obtained in the ultraviolet spectrometer experiment was essentially the same as obtained by *Mariner VI*. Similarly with *Mariner VI*, preliminary examination showed no molecular nitrogen. New and different data was obtained while the polar cap and boundary regions were being viewed. It was very clearly determined that a large fraction of the ultraviolet light reaches the surface, confirming a very thin atmosphere free of appreciable amounts of dust or haze.

In the *Mariner VII* encounter, both channels of the infrared spectrometer experiment operated. From data over the full-wavelength region of 2–14μ, it could be concluded that the ice fog tentatively reported from *Mariner VI* data was not in the instrument or on the planet surface but was an ice fog in the atmosphere. A very weak indication of water vapor was reported that would require extensive computation for confirmation.

Again using data from several wavelengths, it was concluded that there was solid CO_2 above the polar cap, suspended like a cloud, and that the data was consistent with a water ice polar cap. The final result presented was the detection of gaseous methane and gaseous ammonia over the edge of the southern polar cap. No direct clue as to the origins of these gases could be given.

Following the formal presentations, there was considerable discussion regarding the nature of the polar cap material: whether it is CO_2 ice or water ice. It was acknowledged by the investigators that the question could not be resolved at this time.

II. Experimenters' Reports

It had been decided by the principal investigators that the scientific reporting of their results would be by papers individually published in the open literature. Initial articles were completed as rapidly as the interpretations could be formalized. Final reports covering entire experiments on selected parts were to be prepared later.

Following is a bibliography of articles now published and in press together with reprints of several of the articles. The reprints included herein are indicated by asterisks.

Bibliography

(Asterisks indicate article reprints contained herein)

Visual Imaging (Television)

Cutts, J. A., Soderblom, L. A., Sharp, R. P., Smith, B. A., and Murray, B. C., "The Surface of Mars 3. Light and Dark Markings," *J. Geophys. Res.*, Vol. 76, No. 2, pp. 343–356, 1971.

Cutts, J. A., Danielson, G. E., Jr., and Davies, M. E., "Mercator Photomap of Mars," *J. Geophys. Res.*, Vol. 76, No. 2, pp. 369–372, 1971.

Danielson, G. E., Jr., and Montgomery, D. R., "Calibration of the Mariner Mars 1969 Television Cameras," *J. Geophys. Res.*, Vol. 76, No. 2, pp. 418–431, 1971.

Davies, M. E., and Berg, R. A., "A Preliminary Control Net of Mars," *J. Geophys. Res.*, Vol. 76, No. 2, pp. 373–393, 1971.

Dunne, J. A., Stromberg, W. D., Ruiz, R. M., Collins, S. A., and Thorpe, T. E., "Maximum Discriminability Versions of the Near-Encounter Mariner Pictures," *J. Geophys. Res.*, Vol. 76, No. 2, pp. 438–472, 1971.

*Leighton, R. B., Horowitz, N. H., Murray, B. C., Sharp, R. P., Herriman, A. G., Young, A. T., Smith, B. A., Davies, M. E., and Leovy, C. B., "Mariner 6 Television Pictures: First Report," *Science*, Vol. 165, pp. 684–690, 1969.

*Leighton, R. B., Horowitz, N. H., Murray, B. C., Sharp, R. P., Herriman, A. G., Young, A. T., Smith, B. A., Davies, M. E., and Leovy, C. B., "Mariner 7 Television Pictures: First Report," *Science*, Vol. 165, pp. 787–795, 1969.

*Leighton, R. B., Horowitz, N. H., Murray, B. C., Sharp, R. P., Herriman, A. H., Young, A. T., Smith, B. A., Davies, M. E., and Leovy, C. B., "Mariner 6 and 7 Television Pictures: Preliminary Analysis," *Science*, Vol. 166, pp. 49–67, 1969.

Leighton, R. B., "The Surface of Mars," *Sci. Amer.*, Vol. 222, pp. 26–41, 1970.

Leighton, R. B., and Murray, B. C., "One Year's Processing and Interpretation—An Overview," *J. Geophys. Res.*, Vol. 76, No. 2, pp. 293–296, 1971.

Leovy, C. B., Smith, B. A., Young, A. T., and Leighton, R. B., "Mariner Mars 1969: Atmospheric Results," *J. Geophys. Res.*, Vol. 76, No. 2, pp. 297–312, 1971.

Murray, B. C., Soderblom, L. A., Sharp, R. P., and Cutts, J. A., "The Surface of Mars 1. Cratered Terrains," *J. Geophys. Res.*, Vol. 76, No. 2, pp. 313–330, 1971.

Rindfleisch, T. C., Dunne, J. A., Frieden, H. J., Stromberg, W. D., and Ruiz, R. M., "Digital Processing of the Mariner 6 and 7 Pictures," *J. Geophys. Res.*, Vol. 76, No. 2, pp. 394–417, 1971.

Sharp, R. P., Soderblom, L. A., Murray, B. C., and Cutts, J. A., "The Surface of Mars 2. Uncratered Terrains," *J. Geophys. Res.*, Vol. 76, No. 2, pp. 331–342, 1971.

Sharp, R. P., Murray, B. C., Leighton, R. B., Soderblom, L. A., and Cutts, J. A., "The Surface of Mars 4. South Polar Cap," *J. Geophys. Res.*, Vol. 76, No. 2, pp. 357–368, 1971.

Young, A. T., and Collins, S. A., "Photometric Properties of the Mariner Cameras and of Selected Regions on Mars," *J. Geophys. Res.*, Vol. 76, No. 2, pp. 432–437, 1971.

Bibliography (contd)

Infrared Radiometer

Munch, G., Neugebauer, G., and Chase, S. C., "Mariner 1969: Results of the Infrared Radiometer Experiment," in *Planetary Atmospheres,* Symposium No. 40, Marfa, Texas, October 26–31, 1969. Edited by C. Sagan, T. Owen, and H. Smith. D. Reidel Publishing Co., Dordrecht, Holland.

*Neugebauer, G., Munch, G., Chase, S. C., Jr., Hatzenbeler, H., Miner, E., and Schofield, D., "Mariner 1969: Preliminary Results of the Infrared Radiometer Experiment," *Science,* Vol. 166, pp. 98–99, 1969.

Ultraviolet Spectrometer

Anderson, D. E., Jr., and Hord, C. W., "Mariner 6 and 7 Ultraviolet Spectrometer Experiment: Analysis of Lyman-Alpha Data," *J. Geophys. Res.* (to be published).

*Barth, C. A., Fastie, W. G., Hord, C. W., Pearce, J. B., Kelly, K. K., Stewart, A. I., Thomas, G. E., Anderson, G. P., and Raper, O. F., "Mariner 6: Ultraviolet Spectrum of Mars Upper Atmosphere," *Science,* Vol. 165, pp. 1004–1005, 1969.

Barth, C. A., "Mariner 6 Measurements of the Lyman-Alpha Sky Background," *Astrophys. J. Lett.,* Vol. 161, p. 181, 1970.

Barth, C. A., "Mariner Measurements of Lyman-Alpha Emission from the Galaxy," *Proceedings of the Thirteenth Plenary Meeting of COSPAR,* Leningrad, U.S.S.R., 1970.

Barth, C. A., and Hord, C. W., "Mariner 6 and 7 Ultraviolet Spectrometer Results: Topography and Polar Cap," *Science* (in press).

Barth, C. A., Hord, C. W., Pearce, J. B., Kelly, K. K., Anderson, G. P., and Stewart, A. I., "Mariner 6 and 7 Ultraviolet Spectrometer Experiment: Upper Atmosphere Data," *J. Geophys. Res.,* Vol. 76, No. 10, pp. 2213–2227, 1971.

Dalgarno, A., Degges, T. C., and Stewart, A. I., "Mariner 6: Origin of Mars Ionized Carbon Dioxide Ultraviolet Spectrum," *Science,* Vol. 167, pp. 1490–1491, 1970.

Pang, K., and Hord, C. W., "Mariner 7 Ultraviolet Spectrometer Experiment: Photometric Function and Roughness of Mars Polar Cap Surface," *J. Geophys. Res.* (in press).

Pang, K., and Hord, C. W., "Mariner 7 Ultraviolet Spectrometer Experiment: Topographical Slopes of Mars Polar Cap," (submitted for publication, *J. Geophys. Res.).*

Pearce, J. B., Gause, K. A., Mackey, E. F., Kelly, K. K., Fastie, W. G., and Barth, C. A., "The Mariner 6 and 7 Ultraviolet Spectrometers," *Appl. Opt.,* Vol. 10, No. 4, pp. 805–812, 1971.

Pearce, J. B., Lane, A. L., Kelly, K. K., and Barth, C. A., "Mariner 6 and 7 Ultraviolet Spectrometer: In-flight Measurements of Simulated Jupiter Atmosphere," *Science,* Vol. 172, pp. 941–942, 1971.

Bibliography (contd)

Stewart, A. I., "Mariner 6 and 7 Ultraviolet Spectrometer Experiment: An Interpretation of the Intense CO_2^+, CO, and O Airglow Emissions," *J. Geophys. Res.* (in press).

Thomas, G. E., "Neutral Composition of the Upper Atmosphere of Mars as Determined from the Mariner UV Spectrometer Experiment," *J. Atmos. Sci.* (in press).

Infrared Spectrometer

*Herr, K. C., and Pimentel, G. C., "Infrared Absorptions Near Three Microns Recorded Over the Polar Cap of Mars," *Science*, Vol. 166, pp. 496–499, 1969.

*Herr, K. C., and Pimentel, G. C., "Evidence for Solid Carbon Dioxide in the Upper Atmosphere of Mars," *Science*, Vol. 167, pp. 47–49, 1970.

Herr, K. C., Horn, D., McAfee, J. M., and Pimentel, G. C., "Martian Topography from the Mariner 6 and 7 Infrared Spectra," *Astron. J.*, Vol. 75, p. 883, 1970.

Herr, K. C., Forney, P. B., and Pimentel, G. C., "Mariner Mars 1969 Infrared Spectrometer" (submitted for publication, *Appl. Opt.*).

Horn, D., and Pimentel, G. C., "A 2.5 Kilometer Low Temperature Multiple-Reflection Cell," *Appl. Opt.* (in press).

Pimentel, G. C., "Exploración Espectroscópica Infrarroja de Marte por los Mariner 6 y 7," *Rev. Soc. Quím. México*, Vol. 14, p. 159, 1970.

S-Band Occultation

*Fjeldbo, G., Kliore, A., and Seidel, B., "The Mariner 1969 Occultation Measurements of the Upper Atmosphere of Mars," *Radio Sci.*, Vol. 5, No. 2, pp. 381–386, 1970.

*Kliore, A., Fjeldbo, G., Seidel, B., and Rasool, S., "Mariners 6 and 7: Radio Occultation Measurements of the Atmosphere of Mars," *Science*, Vol. 166, pp. 1393–1397, 1969.

*Kliore, A., Fjeldbo, G., and Seidel, B., "First Results of the Mariner-6 Radio Occultation Measurement of the Lower Atmosphere of Mars," *Radio Sci.*, Vol. 5, No. 2, pp. 373–379, 1970.

Kliore, A., Fjeldbo, G., and Seidel, B., "Summary of Mariner 6 and 7 Radio Occultation Results on the Atmosphere of Mars," Paper m.35, presented at the 13th Plenary Meeting of COSPAR, Leningrad, U.S.S.R., May 20–29, 1970.

Celestial Mechanics

*Anderson, J. D., Efron, L., and Kuen Wong, S., "Martian Mass and Earth–Moon Mass Ratio from Coherent S-Band Tracking of Mariners 6 and 7," *Science*, Vol. 167, pp. 277–279, 1970.

Bibliography (contd)

Anderson, J. D., Esposito, P. B., and Martin, W., "Determination of Astrodynamic Constants and a Test of the General Relativistic Time Delay with S-Band Range and Doppler Data from Mariners 6 and 7," Paper a.6, presented at the 13th Plenary Meeting of COSPAR, Leningrad, U.S.S.R., May 20–29, 1970.

Anderson, J. D., and Esposito, P. B., "Application of Spacecraft Tracking Data to Experimental General Relativity," Paper 70-1317, presented at the AIAA 7th Annual Meeting and Technical Display, Houston, Texas, October 19–22, 1970.

Anderson, J. D., Esposito, P. B., Martin, W., and Muhleman, D. O., "Measurement of General Relativistic Time Delay with Mariner 6 and 7," Paper a.14, presented at the 14th Plenary Meeting of COSPAR, Seattle, Washington, U.S.A., June 17–July 2, 1971.

Anderson, J. D., "Mariner Mars '69 Celestial Mechanics Experiment," in *Planetary Atmospheres*, Symposium No. 40, Marfa, Texas, October 26–31, 1969. Edited by C. Sagan, T. Owen, and H. Smith. D. Reidel Publishing Co., Dordrecht, Holland.

NASA — JPL — Coml., L.A., Calif.

Reprinted from
15 August 1969, Volume 165, pp. 684-690

SCIENCE

Mariner 6 Television Pictures: First Report

Robert B. Leighton, Norman H. Horowitz, Bruce C. Murray, Robert P. Sharp, Alan G. Herriman, Andrew T. Young, Bradford A. Smith, Merton E. Davies and Conway B. Leovy

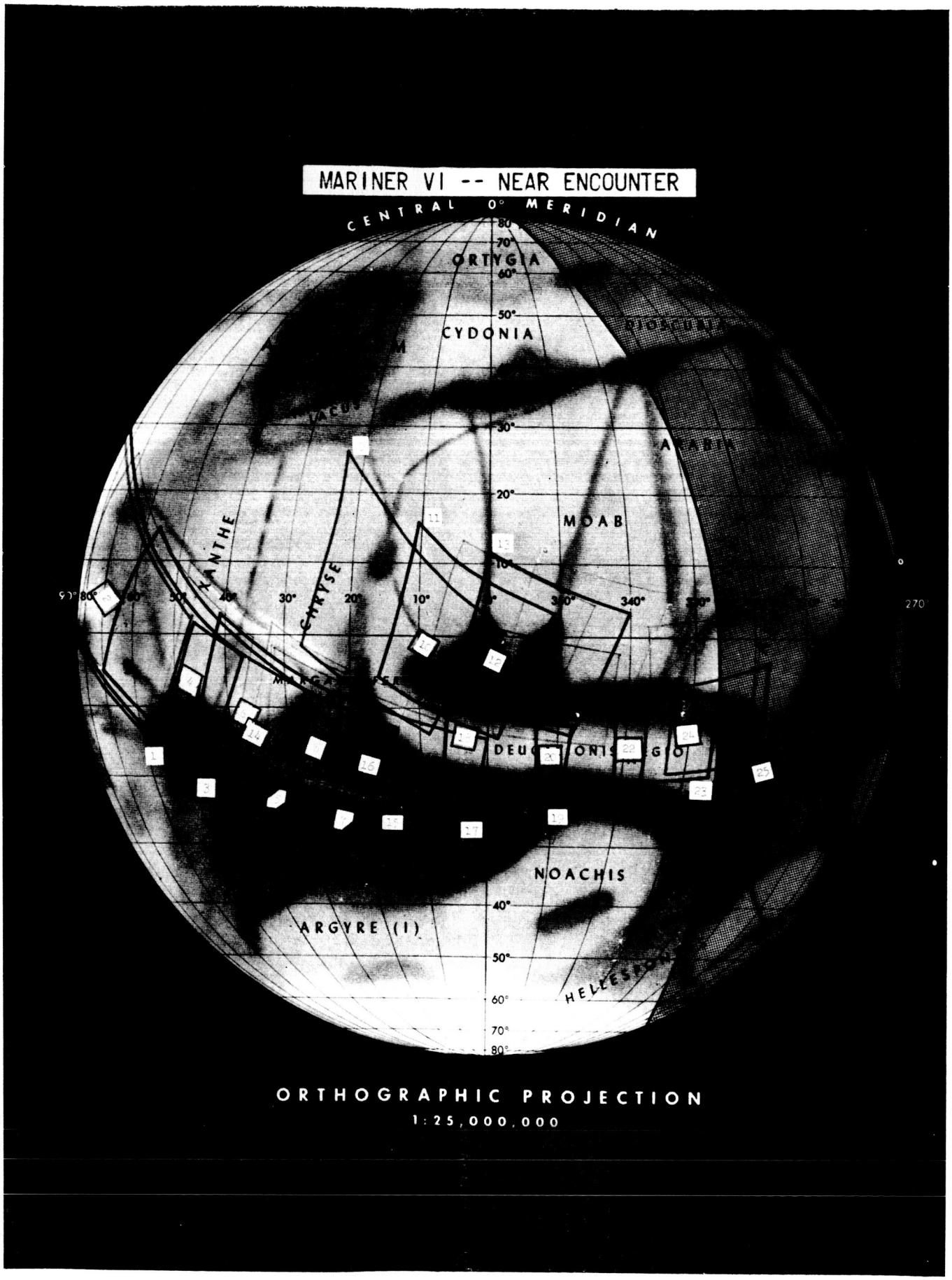

Fig. 1. Approximate locations of Mariner 6 near-encounter pictures. Heavy lines delineate the wide-angle frames. Small rectangles mark the narrow-angle frames.

Mariner 6 Television Pictures: First Report

In July 1965, Mariner 4 flew past Mars and recorded 20 television pictures of the martian surface; the principal television result of that pioneering flight was the discovery that Mars' surface is heavily cratered and resembles the Moon more than it does the Earth (*1*). On 31 July 1969, the more advanced Mariner 6 spacecraft, carrying two television cameras, passed Mars and recorded 75 pictures. A twin spacecraft, Mariner 7, passed Mars on 5 August 1969. This report summarizes the results of a first, qualitative study of the Mariner 6 television pictures, carried out on the uncalibrated data within a few days after receipt on Earth.

The instrumental characteristics of the Mariners 6 and 7 television camera and data systems are outlined in Table 1; those of Mariner 4 are included for comparison.

In order to maximize the return data within limitation of weight, volume, and especially tape recorder capacity, different kinds of picture data were recorded on two tape recorders. A digital tape recorder was used to store the six least significant bits of an eight-bit (256 level) digitally coded signal from every seventh picture element (pixel) of each picture line, and an analog tape recorder was used to store the analog video signal from each pixel. (The two most significant bits of the eight-bit word were averaged over several lines and were transmitted directly to Earth in real time as a component of the engineering telemetry data stream.) Prior to being recorded, in order to enhance the contrast of small-scale features, the analog signal was automatically controlled to an approximately constant average value and was then passed through a circuit having a cube-law response. Both digital and analog signals were later transmitted to Earth as six-bit digitally encoded signals. The digital data had also been earlier transmitted in real time.

An automatic gain control (AGC) and a contrast pre-emphasis introduce certain characteristic artifacts into the analog data, including severe suppression of spatial frequencies lower than about 10 cycles per TV frame width. These effects will eventually be eliminated, but they are represented within the data presented here.

The planetary encounter period is divided into two parts: a "far-encounter" period beginning 54 hours prior to the time of closest approach (E − 54 hours) and a "near-encounter" period bracketing the time of closest approach. During the period E − 48 hours to E − 28 hours, the narrow-angle camera was used to obtain a series of 33 full-disk analog pictures of Mars, with the AGC inhibited. These pictures were transmitted to Earth from E − 28 hours to E − 25 hours, during the period when the signal could be received at the 210-foot diameter (63 m) antenna of the Goldstone, California station of NASA's deep-space net. A second series of 17 far-encounter pictures was recorded from E − 22 hours to E − 7 hours. During an 18-minute interval of the near-encounter period, 25 pictures, alternating between cameras A and B, were recorded.

The near-encounter picture fields, superimposed upon a "map" of Mars, are shown in Fig. 1. The particular regions covered by the pictures were chosen to obtain information about the broadest possible range of classical martian features, such as light areas ("deserts"), dark areas ("maria"), seasonally and secularly variable areas, the polar cap, linear markings ("canals"), cloud or frost areas, and circular "deserts."

The data, when completely analyzed, should increase significantly our understanding of the atmosphere and surface of Mars, provide both global and local maps, and, by inference, contribute to a better understanding of the biological status of the planet.

Both cameras operated normally, and the pictures showed no evidence of veiling glare or haze of the kind seen in the Mariner 4 pictures, thus confirming that the optics of the Mariner 4 camera were most likely contaminated with some unknown scattering material. Hence, the previous conclusion that there was a hazy atmosphere extending to altitudes of 150 km was probably unfounded (*2*). The principal results from preliminary study of the Mariner 6 pictures are: the surface of Mars appears similar to that of the Moon, but there are significant differences; some features seen from Earth are characterized; the "blue haze" hypothesis is disproved; and new phenomena associated with the polar cap are discovered.

Even the earliest versions of picture processing permit a preliminary comparison between certain features observed in the Mariner 6 photographs and those which have been recorded by ground-based observations.

In general, we conclude that the appearance of the maria (large, dark areas) more closely resembles that seen in the better telescopic photographs than that in the hand-drawn renditions of most visual observers. With a few notable exceptions, visual observers have tended to represent the maria with sharp angular outlines, while photographs have shown diffuse, somewhat irregular boundaries. As seen in Figs. 2 to 6 the maria indeed show diffuse, irregular edges with a mottled appearance within.

Telescopic photographs, particularly those taken in blue or green light, often show bright areas referred to as "blue" or "white" clouds. It is a characteristic of these features that they exhibit diurnal and perhaps seasonal variations, becoming more enhanced throughout the martian day to a degree that seems to vary from one apparition to the next. Examples include the Tharsis-Candor "W-cloud" and Nix Olympica. Nix Olympica and parts of the "W-cloud" are clearly seen in the Mariner 6 far-encountered sequence. Nix Olympica has been identified in Fig. 2 as a large white-rimmed crater approximately 500 km in diameter with a bright central spot (see arrow). Figure 2 also shows several bright irregular features in Tempe near the evening (right-hand) limb along the edge of the north polar "haze." Telescopic photographs show

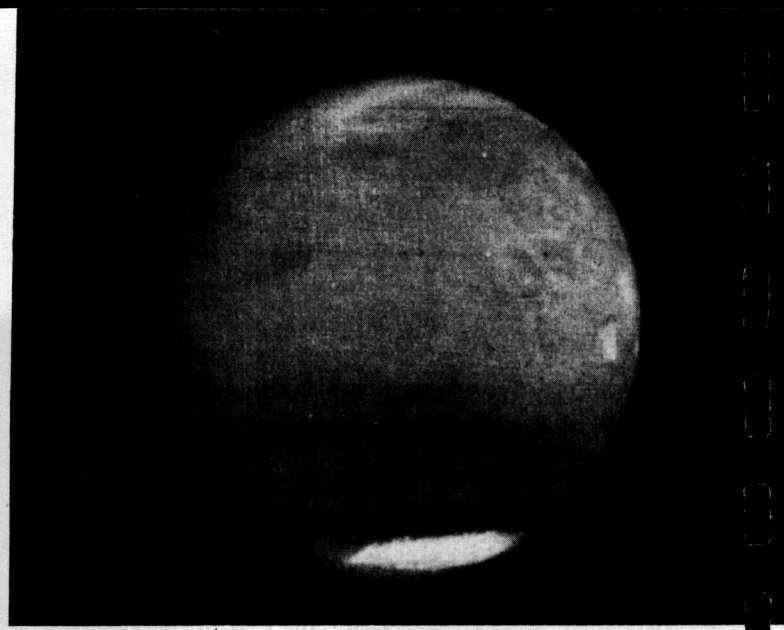

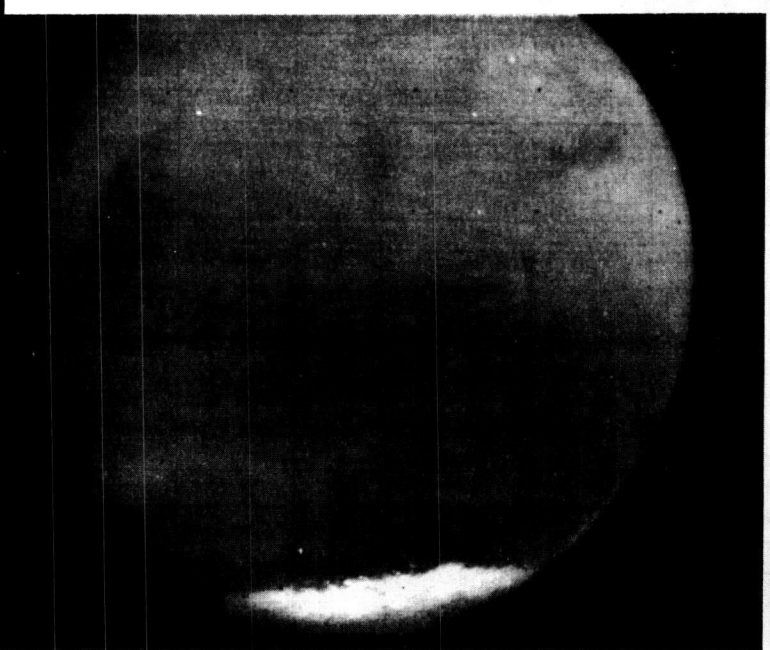

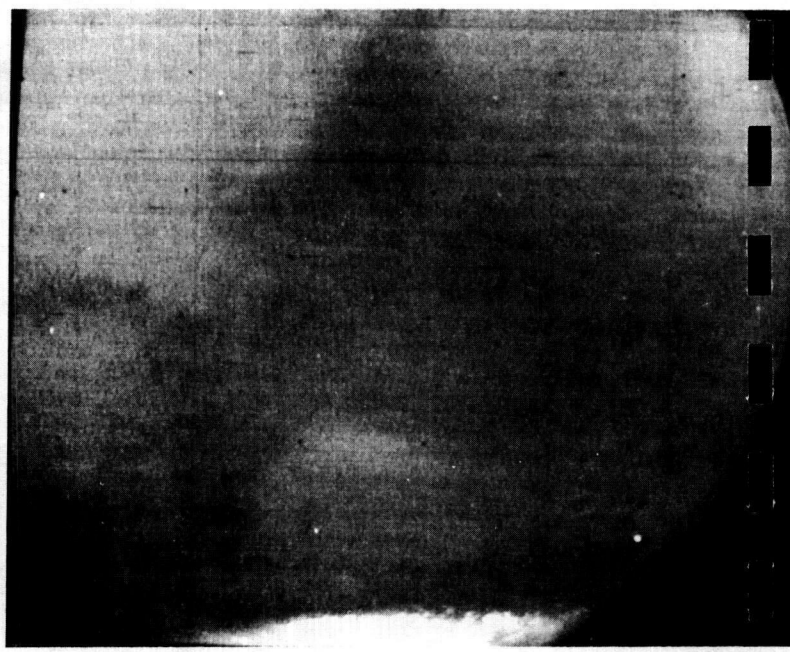

Figs. 2 to 6. The phase angles are 25°. The approximate subspacecraft latitudes are −6°.

Distance to martian surface (km)	Time of picture G.M.T. 7/30/69 (hr : min)	Central meridian east longitude (*3*)	Typical features
	Fig. 2 (top left); far-encounter frame number, 35		
537,000	08 : 36	224.5°	Mare Sirenum, Tharsis
	Fig. 3 (top right); far-encounter frame number, 35		
453,950	11 : 48	177.8°	Mare Sirenum, Mare Cimmerium, Amazonis
	Fig. 4 (center left); far-encounter frame number, 44		
324,900	16 : 46	105.6°	Syrtis Major, Mare Tyrrhenum, Elysium
	Fig. 5 (center right); far-encounter frame number, 47		
252,150	19 : 34	65.0°	Syrtis Major, Hellas
	Fig. 6 (bottom left); far-encounter frame number, 49		
203,600	21 : 26	38.1°	Syrtis Major, Sabaeus Sinus

that the Tempe "cloud" also exhibits diurnal brightening. Figure 3 shows three end points of the "W" near the afternoon limb. The most westerly of these features is a roughly circular region, some 560 km in diameter. It is observed to brighten steadily as it approaches the limb. Near the center of the disk, this particular spot is as dark as, or slightly darker than, its surroundings. This diurnal behavior might be expected from convective clouds of H_2O, but the region exhibits no cloudlike structure during this brightening. Although the best resolution at which it can be seen is only about 35 km, some individual cloud clusters, waves, or streakiness might be seen in convective clouds at this scale. The structureless uniform brightening—seen on both days of far-encounter—and sharply defined, rather angular edges suggest that it is not caused by atmospheric convection but could be due to the photometric function of this area. However, the brightening of this region at the limb and not at the terminator, as observed in ground-based photographs, means that the function would have to violate the reciprocity principle. Furthermore, ground-based photographs show the region to be brighter in the afternoon than in the morning. A number of bright streaks north and west of the "W" are quite possibly responsible for the general brightening of the Tharsis region as seen in telescopic photographs. Although the streaks bear a certain resemblance to the lunar bright-ray system, their true nature is not known at this time.

It is well known that the dark maria are usually not visible on photographs taken in blue light, although occasionally they are visible with rather low contrast during a "blue clearing." To explain the absence of dark features in blue light, some astronomers have invoked the idea of a "blue haze," a layer of suspended particles that absorbs blue light and hides surface features. Mariner 6 near-encounter photographs taken through a blue filter clearly show craters on the martian surface, thus refuting the existence of such an atmospheric blue haze. Photographs taken at the New Mexico State University Observatory only 2 hours before encounter show that no "blue clearing" was in progress at that time. The mechanism responsible for "blue clearing" is still unknown, but it appears that it must be a surface phenomenon as was originally believed.

Figures 4 and 5 reveal two important new characteristics of the south polar cap region. The north edge of the cap is very sharp, but irregular. Several circular areas, resembling craters, appear along the edge: a particularly prominent one, nearly 130 km in diameter, can be clearly seen near the center of the cap edge in Fig. 5. Close inspection near the afternoon limb (right) reveals craterlike structure within the cap region itself. These features rotate with the planet and exhibit no diurnal variations nor any apparent changes between the first and second days of the far-encounter phase, confirming that at least the periphery of the polar cap is on the surface and not in the atmosphere. The second new feature revealed in the cap region in Figs. 2 and 4 is the marked darkening of the cap area near the south limb. As these frames show, it does not rotate with the planet. One possible interpretation of this feature is that it is a thin, varying atmospheric haze. The Mariner 7 photographic (and other instrumental) program has been revised on the basis of these pictures to provide maximum coverage of the south polar cap.

Preliminary study of Mariner 6 near-encounter photographs, like those displayed in Figs. 7 to 10 reinforces the conclusion derived from Mariner 4 that the surface of Mars is more Moon-like than Earth-like. Nonetheless, these Mariner 6 photos also suggest subtle and possibly highly significant differences.

Mars is clearly Moon-like in the abundance, form, arrangement, and sizes of craters. A preliminary count identifies 156 certain craters within the 625,000 km^2 of frame 21 ranging from 3 to 240 km in diameter. The true number is obviously much greater, as narrow-angle frames 20 and 22 covering parts of the same area reveal many more craters down to 300 m in diameter. Various degrees of preservation are seen within this crater population. Preliminary data also suggest a break in the size-distribution curve of craters on at least some parts of Mars which is not recognized in lunar crater populations. These differences would seem to be the result of some weathering and transportational processes that are more effective on Mars than on the Moon.

In detail some martian craters duplicate lunar craters in having slump blocks and terrace as well as radial dry-debris avalanche chutes on steep inner faces. Central peaks, polygonal outlines, blocky ejecta rims, and irregular ejecta sheets are also seen, just as on the Moon. Another Moon-like feature is the irregularly sinuous

Table 1. Nominal instrumental characteristics of Mariners 4, 6, and 7 television camera and data systems.

Item	Mariner 4	Mariners 6 and 7	
		Camera A	Camera B
	Optics		
Aperture (mm)	60	10	200
Focal length (mm)	305	52	508
T-number	8	6.5	3.6, 3.84
Type	Simple Cassegrain	Lens	Equal-radii Schmidt Cass.
Shutter	4-Position rotary	4-Position rotary	2-Blade right-left
Exposure (m sec) ("fast"; "slow")	85;200	90;180	6;12
Filters (eff. wavelength, nm)	R 600 G 540	R 573 G 526 B 469	560
	Picture		
Absolute size (mm)	5.5 × 5.5	9.6 × 12.3	9.6 × 12.3
Angular field (deg)	1.1 × 1.1	11 × 14	1.1 × 1.4
Resolution elements ("pixels")	200 × 200	704 × 935	704 × 935
Frame readout time (sec)	24	42.25	42.25
Picture interval (sec)	48	84.5	84.5
Encoding levels $N = 2^n$	$n = 6$	$n = 8$	$n = 8$
	Tape recorders		
		Digital	Analog
Number	1	1	1
Tracks	4	4	4
Tape length (m)	100	110	110
Stored bits (effective)	5×10^6	1.3×10^7	1.2×10^8
Tape speed (cm sec^{-1})			
Record	32.5	30	30
Playback	0.025	4.3	4.3
	Data transmission rates		
(As used) bit sec^{-1}	8 1/3	16.2×10^3	16.2×10^3
(Backup) bit sec^{-1}		270	270

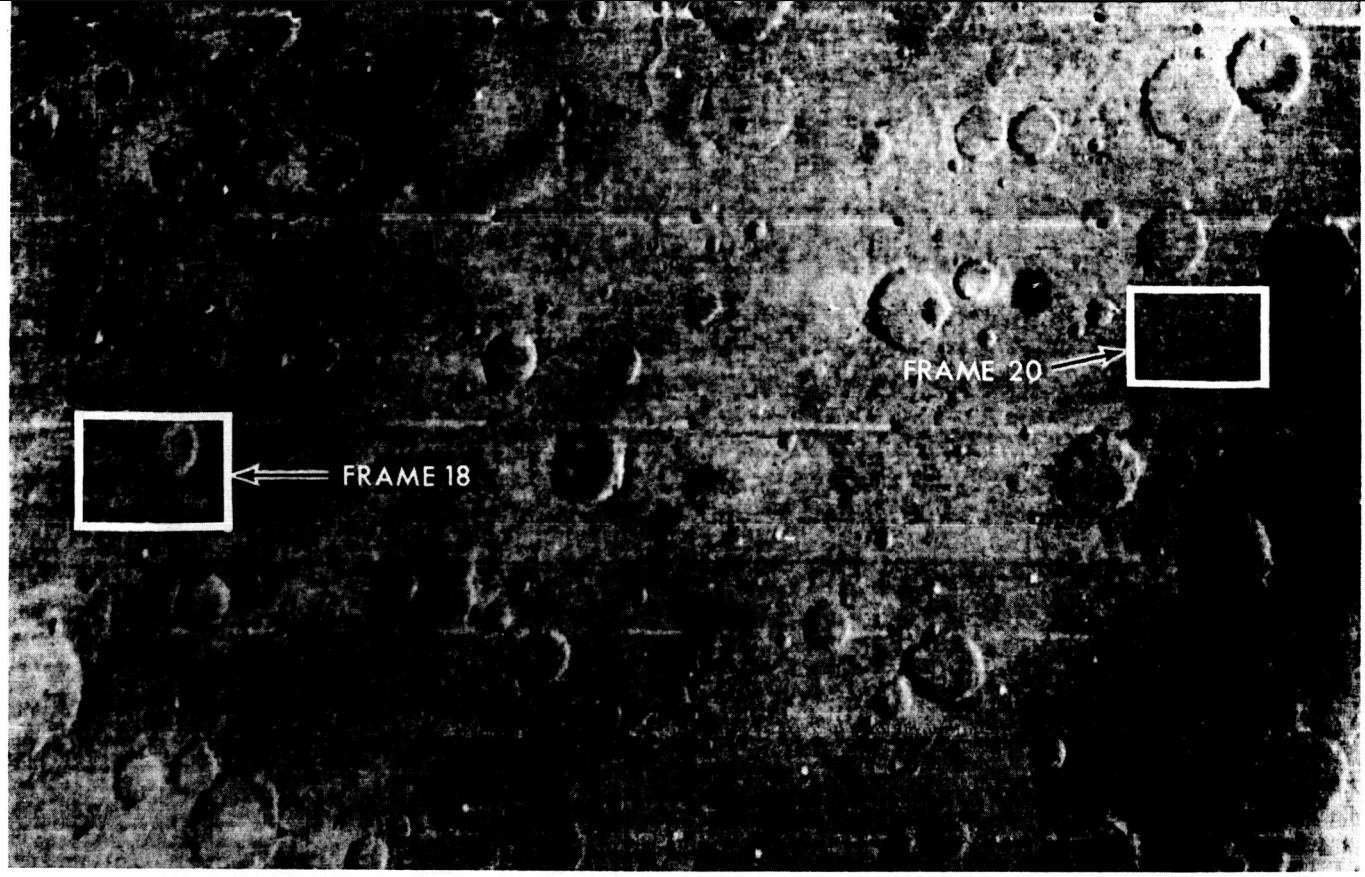

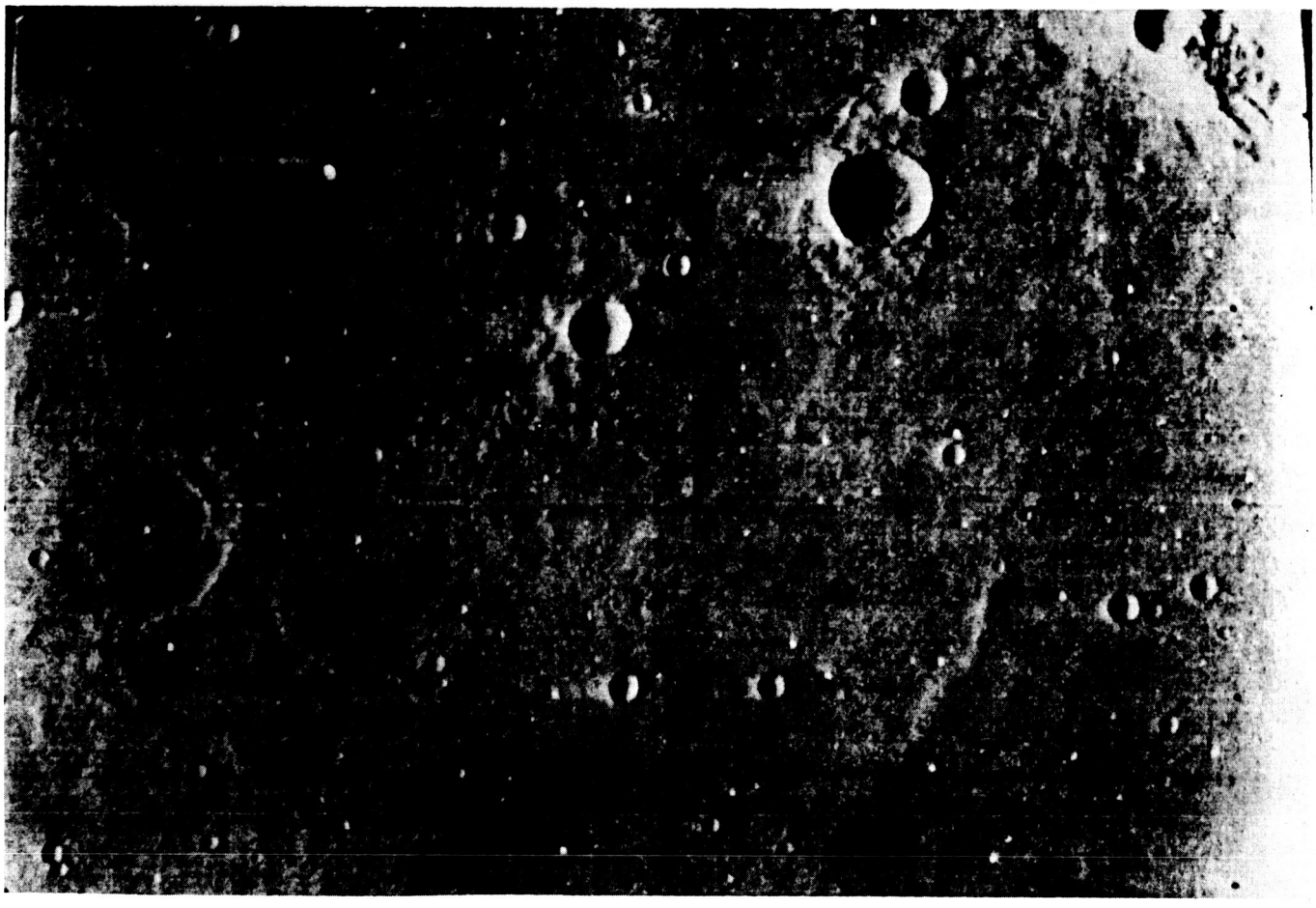

Figs. 7 to 10. Figures 7 and 9 (frames 19 and 21 of the Mariner 6 near-encounter series) are wide-angle photos with overlap on their inner edges and a resolution of about 3 km. Figures 8 and 10 (frames 20 and 22, respectively) cover the small areas shown in Figs. 7 and 9 with a resolution of about 300 m. All photos are within the bright area Deucalionis Regio south of Sabaeus Sinus in the eastern part of the Mariner 6 near-encounter path, approaching the evening terminator. North is at the top.

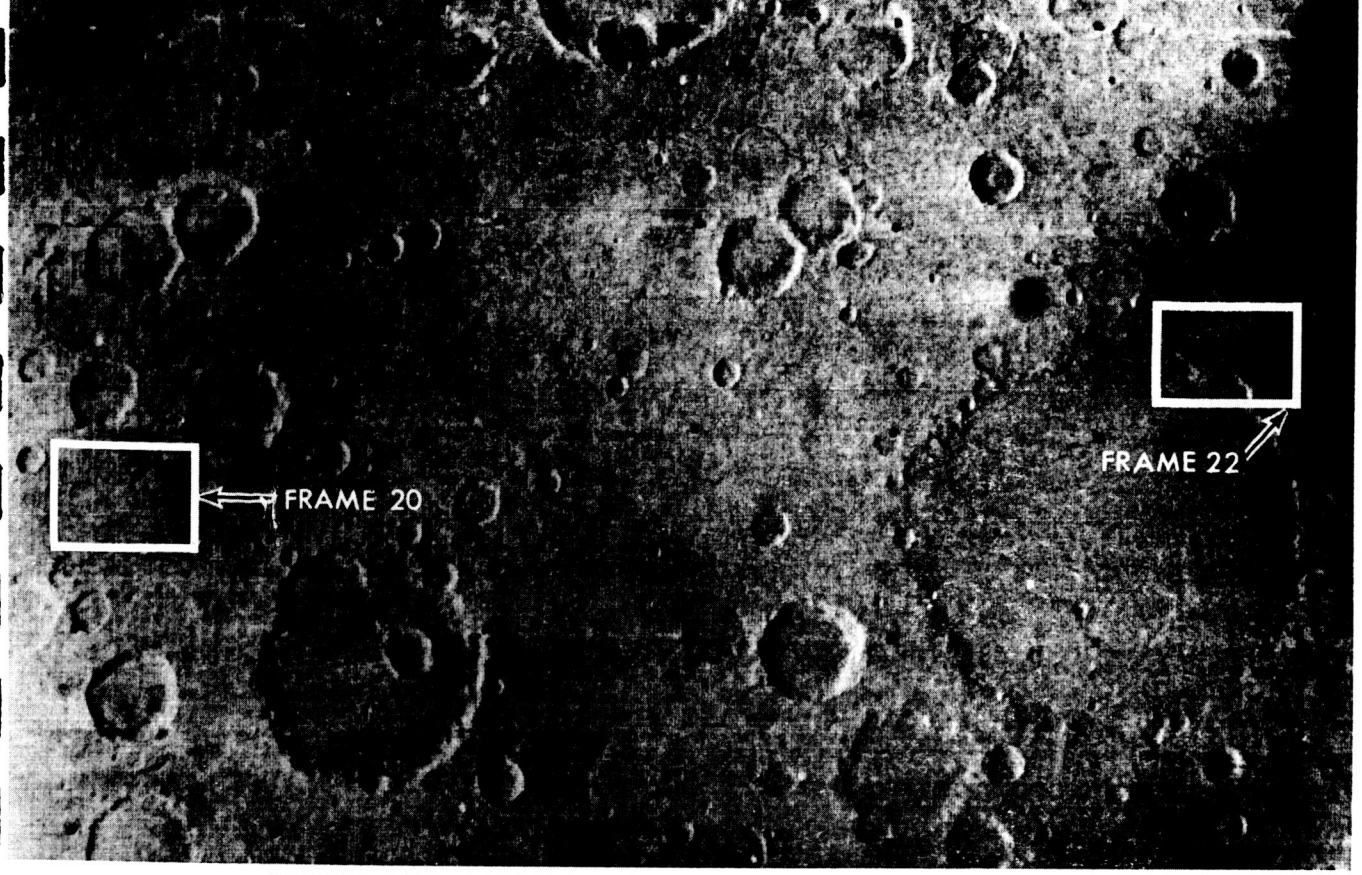

	Near-encounter frame number	Filter	Distance to martian surface (km)	Mars coordinates (*3*)	North-south by east-west dimensions (km)	Viewing angle from vertical	Solar zenith angle (deg)
Fig. 7	19	Green	3613	17°S, 3.2°E	717 × 994	24.4°	58.6°
Fig. 8	20	Minus blue	3544	16.6°S, 9.0°E	73 × 88.5	20.4°	64.3°
Fig. 9	21	Red	3499	16.2°S, 15.1°E	697 × 899	16.4°	70.4°
Fig. 10	22	Minus blue	3497	15.3°S, 20.6°E	72 × 84	15.0°	75.8°

ridges faintly seen extending northward through both Figs. 8 and 9.

Differences between lunar and martian terrains lie in the seemingly more subdued relief of many martian craters, their flatter floors, fewer central peaks, more subdued debris blankets, absence of obvious secondary craters and rays, and possibly greater abundance of "ghost" craters. A striking double concentric "ghost," similar to prominent double concentric craters seen on the back side of the Moon is faintly visible in the western part of Fig. 8. A more facile isostatic adjustment of the martian crust could also be a contributing factor.

No sinuous rilles have yet been identified on the Mariner 6 photos. Furthermore, no distinctive Earth-like phenomena such as mountain ranges, tectonic basins, streamcut topographs, dune fields, playa flats, or other arid-region features have been recognized. On the other hand, a remarkable variety of albedo markings are apparent in the encounter photographs at high solar angle. Such albedo markings, however, are particularly susceptible to spurious effects in the present preliminary form, and their analysis must await reconstruction of the digital and analog data.

ROBERT B. LEIGHTON
NORMAN H. HOROWITZ
BRUCE C. MURRAY, ROBERT P. SHARP
California Institute of Technology, Pasadena 91103

ALAN G. HERRIMAN
ANDREW T. YOUNG
Jet Propulsion Laboratory, Pasadena California 91103

BRADFORD A. SMITH
New Mexico State University, Las Cruces 88001

MERTON E. DAVIES
RAND Corporation, Santa Monica, California 90406

CONWAY B. LEOVY
University of Washington, Seattle 98055

References and Notes

1. R. B. Leighton, B. C. Murray, R. P. Sharp, J. D. Allen, R. K. Sloan, *Science* **149**, 627 (1965).
2. A. T. Young, *Bull. Amer. Astron. Soc.* **1**, 218 (1969).
3. Longitude measured eastward on Mars from the standard ephemeris zero meridian. Ephemeris longitude is measured westward from this meridian.
4. We acknowledge the support and encouragement of the National Aeronautics and Space Administration. We also thank the Mariner Mars '69 project manager, H. M. Schurmeier, and his staff at the Jet Propulsion Laboratory, California Institute of Technology, without whose skill, expert knowledge, and devoted labor Mariner 6 could not have succeeded.

Reprinted from
22 August 1969, Volume 165, pp. 787-795

SCIENCE

Mariner 7 Television Pictures: First Report

Robert B. Leighton, Norman H. Horowitz, Bruce C. Murray, Robert P. Sharp, Alan G. Herriman, Andrew T. Young, Bradford A. Smith, Merton E. Davies and Conway B. Leovy

Fig. 1. Approximate locations of Mariner 7 near-encounter pictures. Heavy lines delineate the wide-angle frames. Small rectangles mark the narrow-angle frames.

Mariner 7 Television Pictures: First Report

Initial results of the television experiment carried by Mariner 6 were recently reported (*1*). This is a similar report of the television experiment aboard Mariner 7. These reports are presented primarily to communicate significant results to the scientific community as rapidly as possible. A more comprehensive, but still preliminary, review of the results of both experiments, and of their implications concerning the atmosphere and surface of Mars, is in preparation for submission to this journal.

The Mariner 7 television camera and data systems are essentially the same as those of Mariner 6. The relevant instrumental characteristics, and the rather complex nature of the returned signal information, have been described (*1*). Both Mariner 7 cameras operated normally. Compared with Mariner 6, the electrical noise (pickup by the camera system aboard the spacecraft) proved to be less, and the sensitivity of the high-resolution (narrow-angle) camera proved to be somewhat higher, as immediately apparent in the far-encounter mode of Mariner 7.

The mission profile of Mariner 7 permitted acquisition of 93 far-encounter pictures and 33 near-encounter pictures. In all, 126 pictures were acquired by Mariner 7, compared with 74 for Mariner 6.

The near-encounter picture fields superimposed on a "map" of Mars are shown in Fig. 1. They show that the instrument platform was slued after picture 9 onto a track leading across the south polar cap and slued again after picture 20 in order to provide a second limb-crossing for the ultraviolet spectrometer slit and so as to cross the classical dark area Hellespontus and the classical bright desert Hellas. During the initial traversal of the bright limb, the limb appeared in the field of the narrow-angle camera. Overlapping wide-angle coverage with the track of Mariner 6 was obtained in the vicinity of Meridiani Sinus.

Principal results of initial study of Mariner 7 pictures, in addition to confirming the first reported results of Mariner 6, are (i) additional physiographic interpretations of classically observed features are made; (ii) the surface of the south polar cap is generally visible and many large topographic forms are entirely coated with "snow"; (iii) the edge of the cap is apparently defined by local topographic configurations, but "snow"-free areas are apparent within the polar regions; and (iv) the Hellas region appears devoid of craters, thus implying the operation of more effective, more recent, and more geographically confined surface processes than heretofore evidenced.

The far-encounter sequence of Mariner 7 shows mottling within the maria, an effect noted in ground-based telescopic observations. It is here found that the mottled appearance is, in fact, caused by large numbers of craters with diameters of up to several hundred kilometers, most of which appear to have dark floors with lighter rims. Several examples can be seen in Figs. 2 and 3. The borders of the maria are sharply defined in some locations and diffuse in others. In one localized region, on the north edge of Sabaeus Sinus (left side of Fig. 3), the transition between mare and desert takes place within a few tens of kilometers. The borders of the maria occasionally show long, dark, fingerlike projections intruding into the bright areas. Several examples can be seen in both figures. Although this configuration suggests an association with craters or parts of craters, conclusive identification is not possible at this stage of picture processing.

Far-encounter photographs have been examined for evidence of martian canals, defined here as those dark, diffuse, more or less linear features, generally of low contrast, which have been recorded by visual observers and telescopic photographs. Although the Mariner pictures are still in a relatively rough form, several previously identified canals appear as well-defined features. Examples include Agathodaemon, the dark linear feature halfway between the center and the evening (right) limb of Fig. 4 and Cerberus, the large dark feature above and to the right of center in Fig. 2. Other canals appear to be resolved into a sequence of dark patches of varying size and contrast. In some cases the individual dark areas seem unrelated, suggesting that many canals involve the chance alignment of randomly distributed dark patches. Variegated shading has been noted in some of the well-defined canals, but the true physical nature of these features is still unknown.

Figure 5 shows two successive far-encounter frames arranged for stereoscopic viewing. Nix Olympica and the curious bright streaks mentioned in the Mariner 6 report (see *1*) are clearly seen.

The boundary of the south polar cap was seen at longitude 335°E, latitude 61°S, at a solar elevation of 33° (Fig. 6). The area is heavily cratered, and the cap edge is strongly influenced by local topographic features. Even so, the transition between bare ground and complete coverage by "snow" is remarkably sharp: the entire transition spans only about 2° of latitude. This suggests that the slopes at and even below the scale resolved by the wide-angle camera are of this same order and are thus similar to those seen at lower latitudes. This comparison, when evaluated more quantitatively, will be important in singling out mechanisms of surface modification most active on Mars. No indication of a dark "polar collar" is found.

Several wide- and narrow-angle views of the cap itself were obtained (Figs. 7 to 10). Since these show craters entirely covered by "snow," the cap material generally must be thick enough not to evaporate away during the day on sunward-facing slopes. At the same time, dark areas well within the cap (particularly on crater floors) suggest a deposit thin enough to be removed by surface winds or other meteorological factors in some places.

(Continued on page 10)

← Fig. 2

Fig. 3

Figs. 2 to 5. The phase angles are 25°. The approximate subspacecraft latitudes are −4°.

	Far-encounter frame number	Distance to martian surface (km)	Time of picture G.M.T. 8/4/69 (hr : min)	Central meridian east longitude (*2*) (deg)	Typical features
Fig. 4	72	492,000	09:41	256.2	Solis Lacus, Tharsis
Fig. 5 (left)	74	452,100	11:15	233.3	Tharsis, Mare Sirenum
Fig. 5 (right)	75	432,600	12:01	222.0	Tharsis, Mare Sirenum
Fig. 2	81	292,000	17:31	142.2	Cerberus, Elysium, Mare Cimmerium
Fig. 3	92	131,500	23:48	50.9	Syrtis Major, Deltaton Sinus

Fig. 4

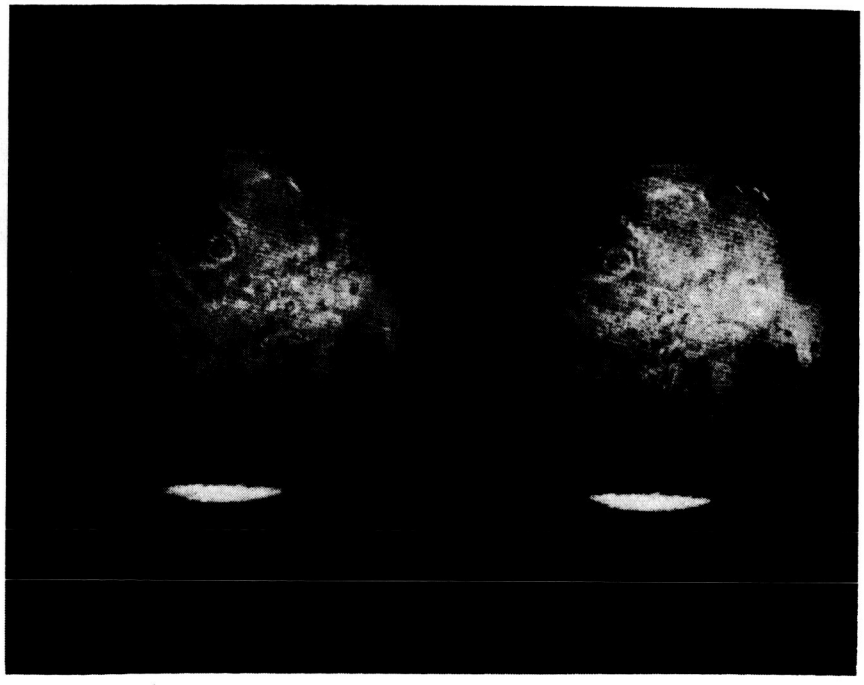

Fig. 5

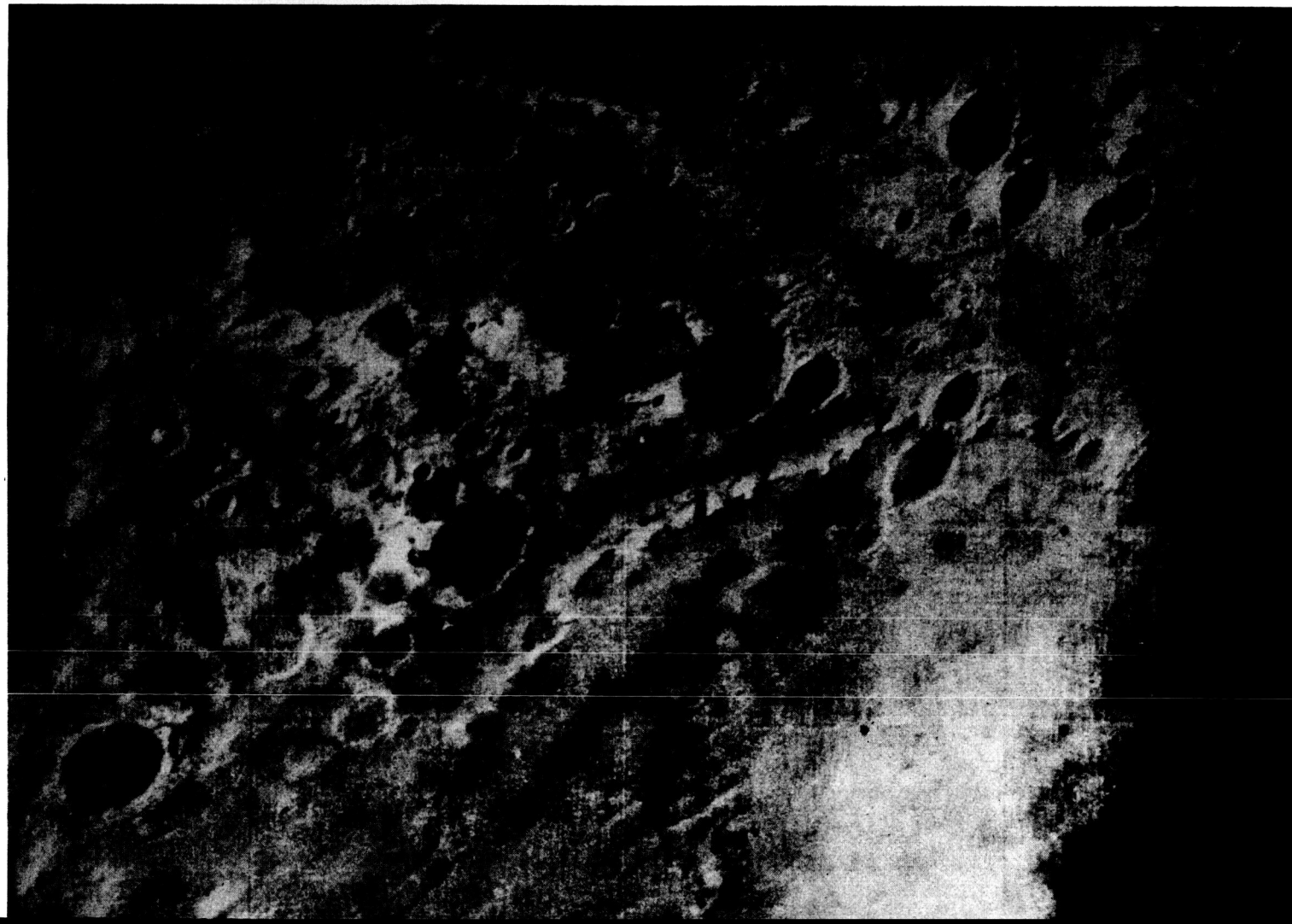

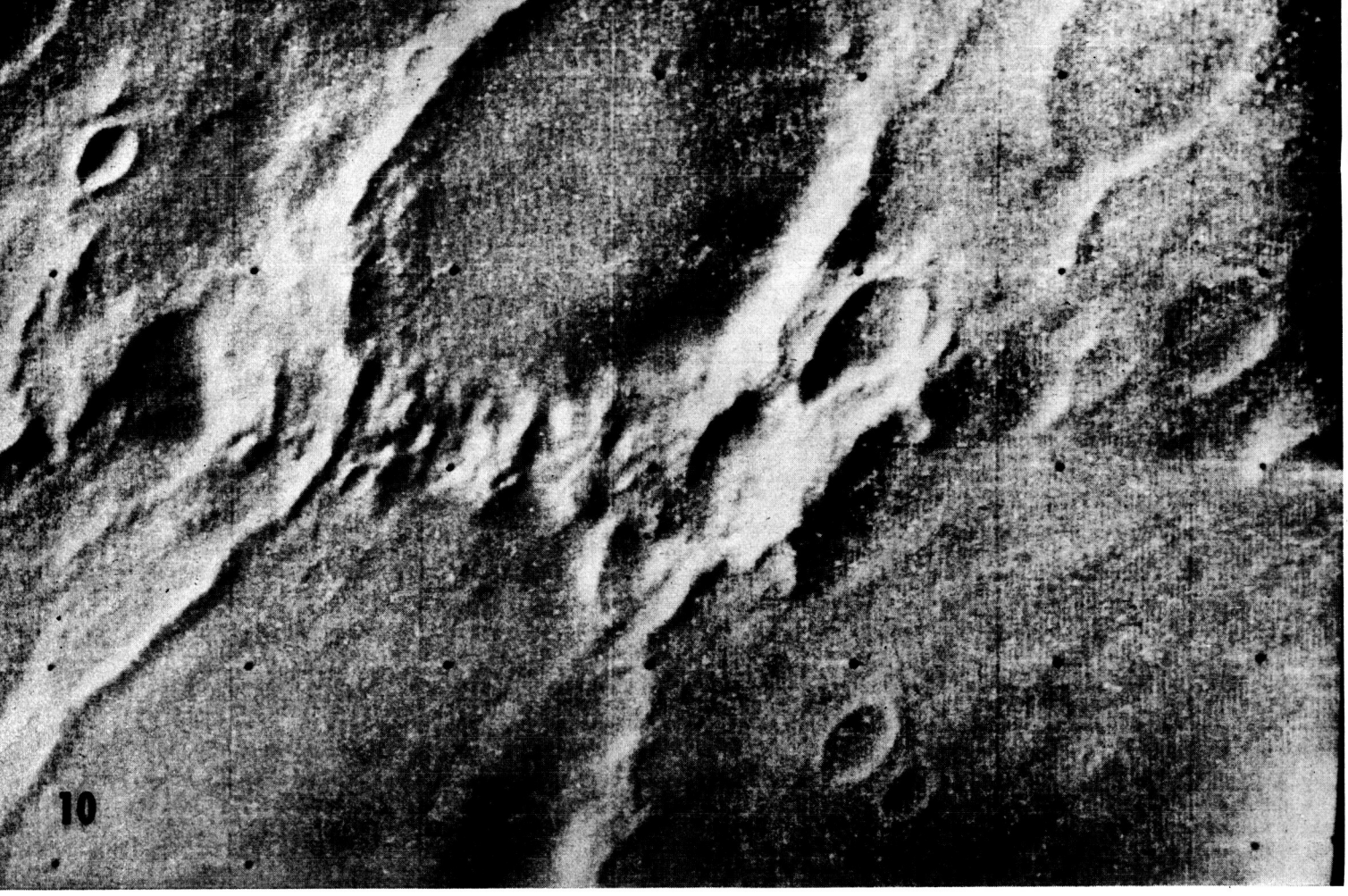

10

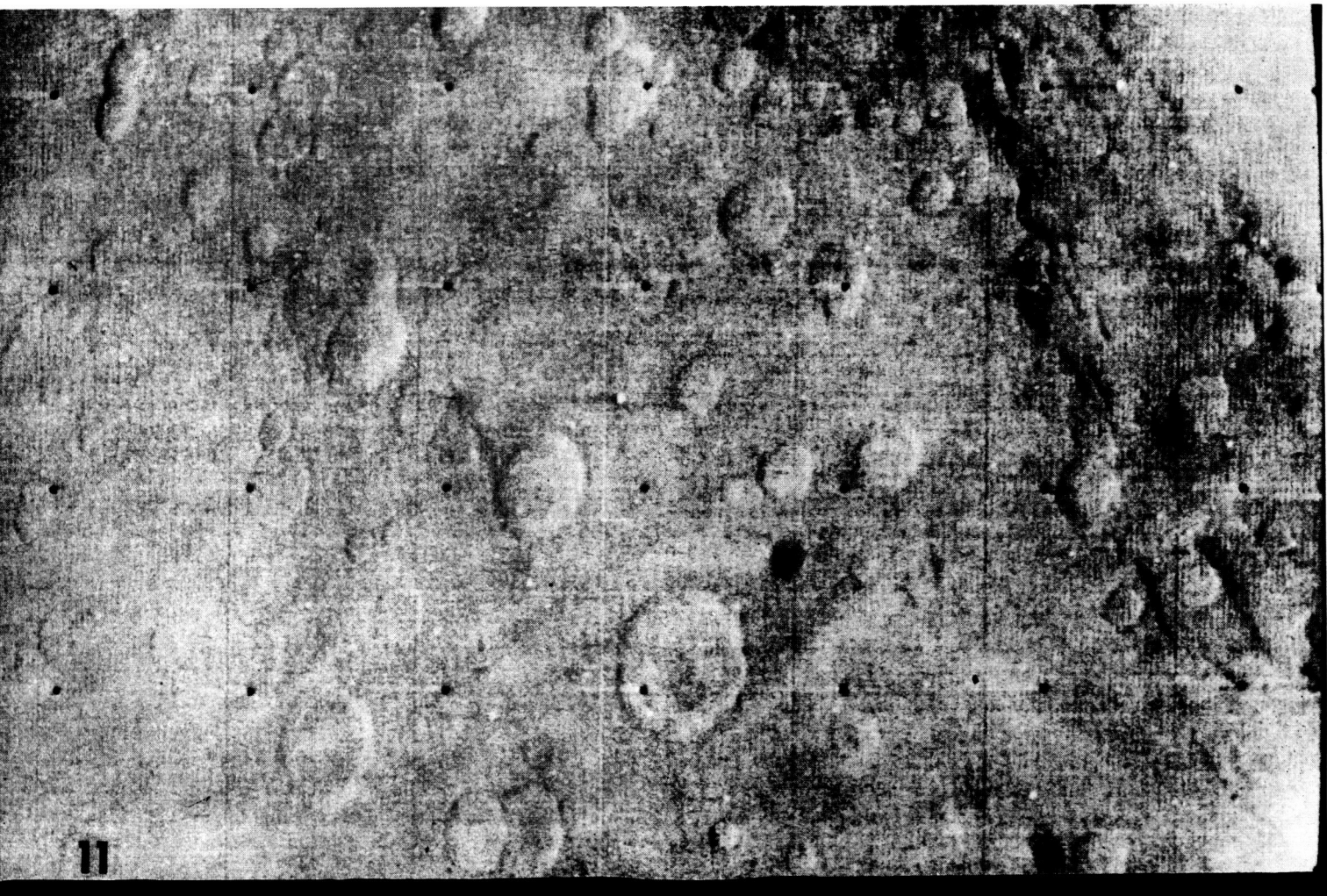

11


12

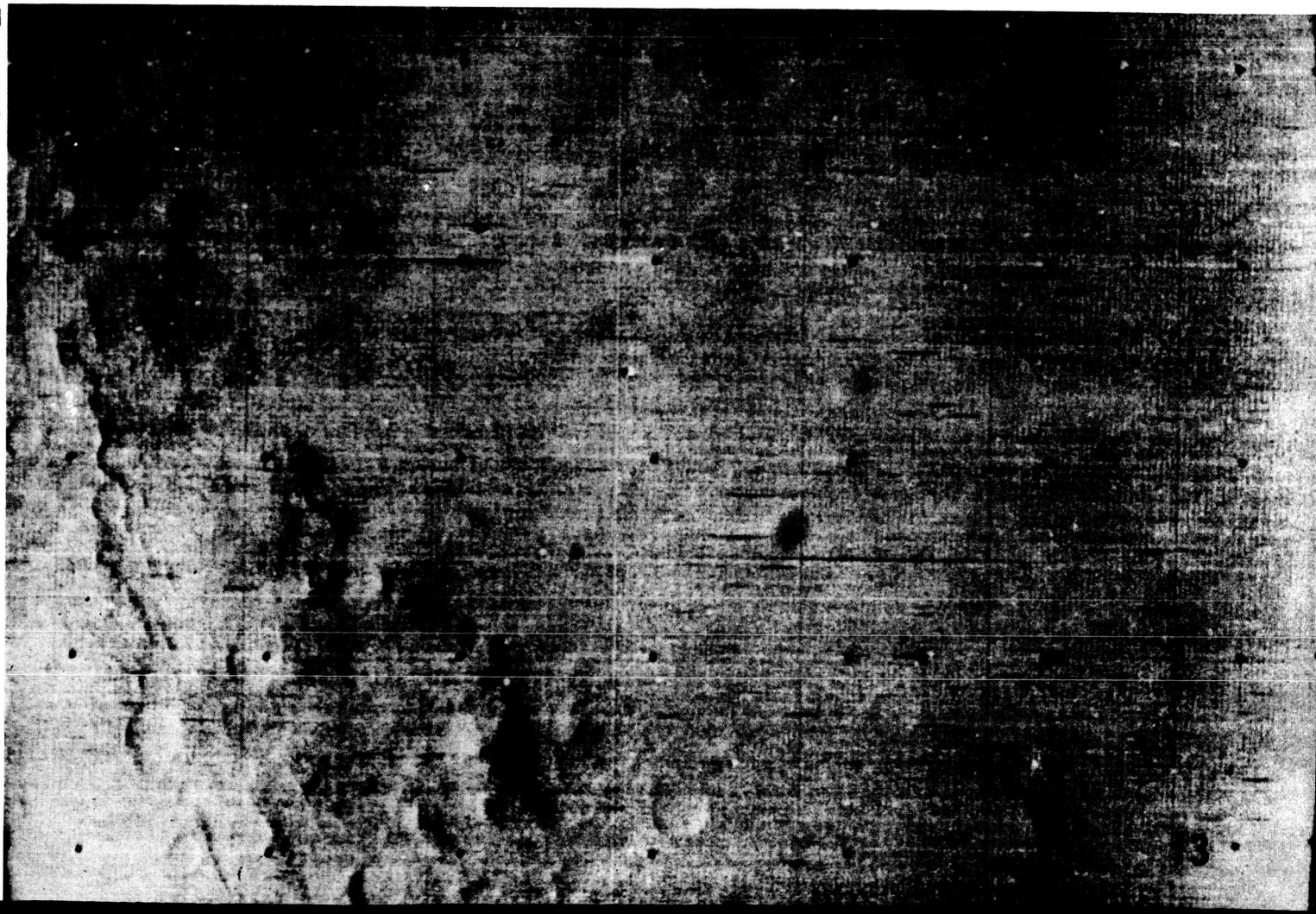
13

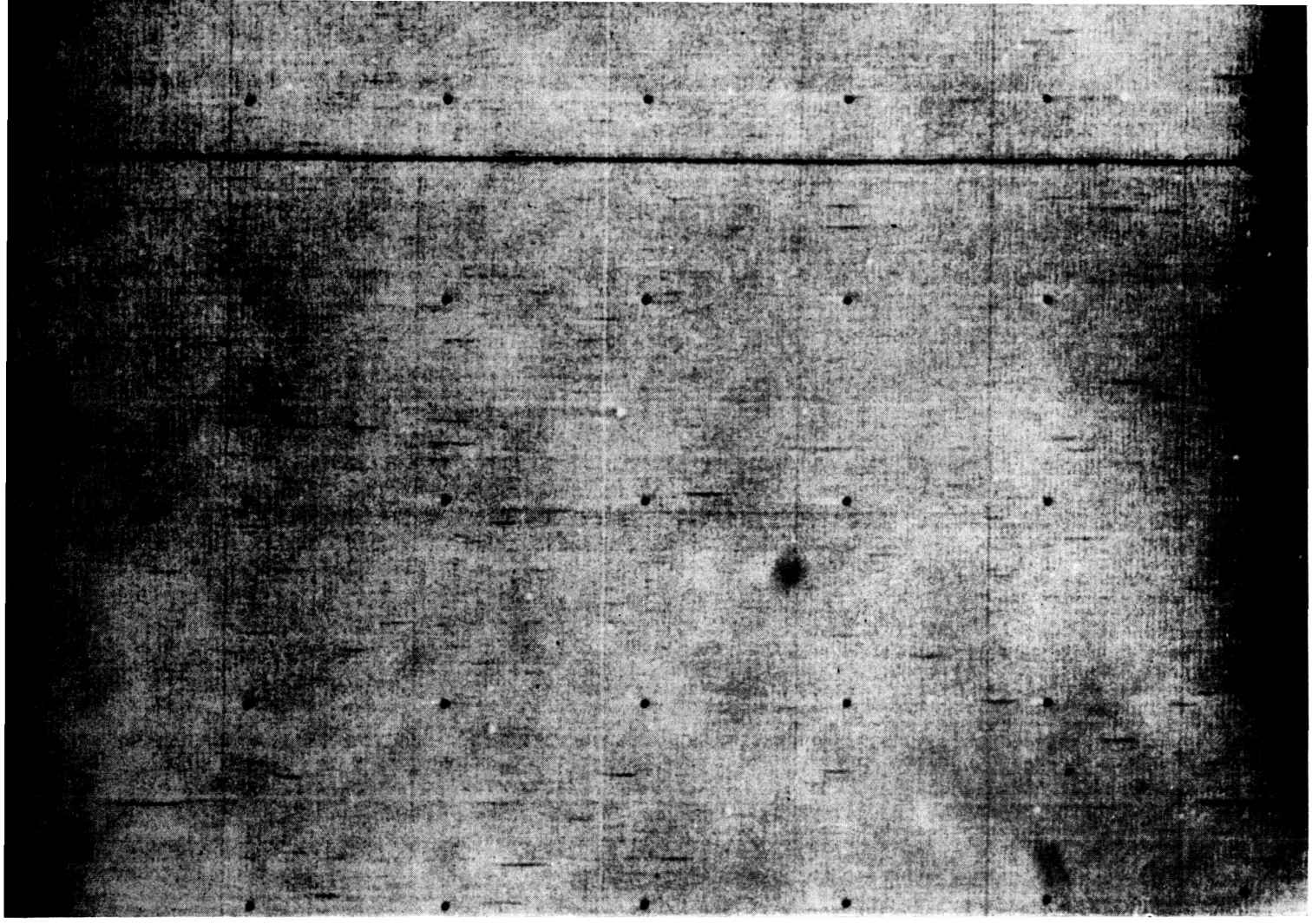

Figs. 6 to 14. Figures 6, 7, 9, 11, and 13 (frames 13, 17, 19, 25, and 27 of the Mariner 7 near-encounter series) are wide-angle photos, often with overlap, and a resolution of about 3 km. Figures 8, 10, 12, and 14 (frames 18, 20, 26, and 28) cover small areas within the wide-angle photos with a resolution of about 300 m. Figures 6 to 10 are within the south polar cap. Figures 11 to 14 are within the areas Hellespontus and Hellas in the eastern part of the Mariner 7 near-encounter path, approaching the evening terminator. North is approximately toward the top. The south pole of Mars appears in Fig. 7 near the lower edge and about one-third of the picture width from the right edge.

	Near-encounter frame No.	Filter	Distance to martian surface (km)	Mars coordinates (deg)	Approximate north-south by east-west dimensions (km)	Viewing angle from vertical (deg)	Solar zenith angle (deg)
Fig. 6	13	Green	5909	65 S 341 E	1500 × 1700	44	57
Fig. 7	17	Blue	5210	77 S 25 E	1400 × 1600	46	69
Fig. 8	18	Minus blue	5092	78 S 46 E	130 × 145	47	73
Fig. 9	19	Green	5040	79 S 71 E	1350 × 1850	51	78
Fig. 10	20	Minus blue	4998	76 S 94 E	130 × 170	54	82
Fig. 11	25	Blue	3913	43 S 36 E	770 × 1220	33	48
Fig. 12	26	Minus blue	3755	45 S 44 E	75 × 100	27	54
Fig. 13	27	Green	3636	46 S 52 E	720 × 990	23	60
Fig. 14	29	Red	3619	40 S 69 E	780 × 940	27	62

(Continued from page 788)

Several areas of relatively thin "snow" cover within the cap are indicated by lower surface brightness or by the configuration of their boundaries, or both (Figs. 7 and 9). Often these are of irregular outline and differ from craters and other topographic features seen outside the polar cap in the picture series of either spacecraft. If the boundaries of these areas are produced by variations of "snow" depth, local depths of many meters may be indicated. No effects clearly identifiable with haze or clouds were seen over the polar cap, although several features suggestive of low clouds are present (Figs. 8 and 9). Definitive analysis requires merging of the digital and analog video data.

The sequence of frames shown in

Figs. 11 to 14 illustrates a striking change in surface morphology eastward from the elongate dark area, Hellespontus, into the large circular bright area, Hellas. In Figs. 11 and 12, Hellespontus and the intervening scarped and ridged transition zone to Hellas display abundant craters of good size, but in Figs. 12 and 14 the floor of Hellas is seen to be virtually devoid of discernible craters, except within a narrow marginal zone where they are faintly visible. Small craters disappear even earlier, being unrecognizable in the transition zone and on the near edge of Hellespontus, even in high resolution photos (Fig. 13).

Various considerations suggest that this disappearance of craters is not the result of an atmospheric haze or fog hanging over the Hellas area, but rather the product of some difference in processes acting, or materials present (or both), which results in abnormally rapid obscuration of craters on the floor of Hellas. The transition area between Hellespontus and Hellas with its short en echelon scarps and ridges constitutes the most distinct structural border yet seen between a light and dark area on Mars.

ROBERT B. LEIGHTON
NORMAN H. HOROWITZ
BRUCE C. MURRAY
ROBERT P. SHARP
California Institute of Technology, Pasadena 91109

ALAN G. HERRIMAN
ANDREW T. YOUNG
Jet Propulsion Laboratory, Pasadena 91103

BRADFORD A. SMITH
New Mexico State University, Las Cruces 88001

MERTON E. DAVIES
RAND Corporation, Santa Monica, California 90406

CONWAY B. LEOVY
University of Washington, Seattle 98055

References and Notes

1. R. B. Leighton, N. H. Horowitz, B. C. Murray, R. P. Sharp, A. R. Herriman, A. T. Young, B. A. Smith, M. E. Davies, C. B. Leovy, *Science* **165**, 684 (1969).
2. Longitude measured eastward on Mars from the standard ephemeris zero meridian. Ephemeris longitude is measured westward from this meridian.
3. We acknowledge the support and encouragement of the National Aeronautics and Space Administration. We also thank the Mariner Mars '69 project manager, H. M. Schurmeier, and his staff at the Jet Propulsion Laboratory, California Institute of Technology, without whose skill, expert knowledge, and devoted labor Mariner 7 could not have succeeded.

Reprinted from
3 October 1969, volume 166, pages 49–67

SCIENCE

Mariner 6 and 7 Television Pictures: Preliminary Analysis

R. B. Leighton, N. H. Horowitz, B. C. Murray
R. P. Sharp, A. H. Herriman, A. T. Young
B. A. Smith, M. E. Davies, C. B. Leovy

Mariner 6 and 7 Television Pictures: Preliminary Analysis

R. B. Leighton, N. H. Horowitz, B. C. Murray, R. P. Sharp, A. H. Herriman, A. T. Young, B. A. Smith, M. E. Davies, C. B. Leovy

Before the space era, Mars was thought to be like the earth; after Mariner 4, Mars seemed to be like the moon; Mariners 6 and 7 have shown Mars to have its own distinctive features, unknown elsewhere within the solar system.

The successful flyby of Mariner 4 past Mars in July 1965 opened a new era in the close-range study of planetary surfaces with imaging techniques. In spite of the limited return of data, Mariner 4 established the basic workability of one such technique, which involved use of a vidicon image tube, on-board digitization of the video signal, storage of the data on magnetic tape, transmission to the earth at reduced bit rate by way of a directional antenna, and reconstruction into a picture under computer control. Even though the Mariner 4 pictures covered only about 1 percent of Mars's area, they contributed significantly to our knowledge of that planet's surface and history (*1, 2, 19, 21*).

The objectives of the Mariner 6 and 7 television experiment were to apply the successful techniques of Mariner 4 to further explore the surface and atmosphere of Mars, both at long range and at close range, in order to determine the basic character of features familiar from ground-based telescopic studies; to discover possible further clues as to the internal state and past history of the planet; and to provide information germane to the search for extraterrestrial life.

The Mariner 6 and 7 spacecraft successfully flew past Mars on 31 July and 5 August 1969, respectively; first results of the television experiment, based upon qualitative study of the uncalibrated pictures, have been reported (*3, 4*). The purpose of this article is to draw together the preliminary television results from the two spacecraft; to present tentative data concerning crater size distributions, wall slopes, and geographic distribution; to discuss evidences of haze or clouds; to describe new, distinctive types of topography seen in the pictures; and to discuss the implications of the results with respect to the present state, past history, and possible biological status of Mars.

The data presented here and in the two earlier reports were obtained from inspection and measurement of a partial sample of pictures in various stages of processing. As such, the results must be regarded as tentative, subject to considerable expansion and possible modification as more complete sets, and better-quality versions, of the pictures become available over a period of several months. They are offered at this time because of their unique nature, their wide interest, and their obvious relevance to the forthcoming Mariner 1971 (orbiter) and Viking 1973 (lander) missions.

Drs. Leighton, Horowitz, Murray, and Sharp are affiliated with the California Institute of Technology, Pasadena; Mr. Herriman and Dr. Young, with the Jet Propulsion Laboratory, Pasadena; Mr. Smith, with New Mexico State University, Las Cruces; Dr. Davies, with the RAND Corporation, Santa Monica, California; and Dr. Leovy, with the University of Washington, Seattle.

Television System Design

The experience and results of Mariner 4 strongly influenced the basic design of the Mariner 6 and 7 television experiment. The earlier pictures showed Mars to be heavily cratered, but to have subdued surface relief and low photographic contrast, and possibly to have a hazy atmosphere. It was also found that a vidicon-type camera tube has a most important property: the "target noise," analogous to photographic grain, is less than that of a photographic emulsion by perhaps a factor of 10 (*2*) and is the same from picture to picture. Thus the 64-level (6-bit) encoding scheme of Mariner 4 was able to cope with the extremely low contrast conditions because intensity calibration and contrast enhancement by computer techniques could be effectively applied to the data to produce pictures of useful quality.

Early design studies for Mariner 6 and 7 centered around 256-level (8-bit) encoding—at least a tenfold increase in data return over that from Mariner 4; overlapping two-color coverage along the picture track (similar to that of Mariner 4); use of two cameras of different focal lengths to provide higher-resolution views of areas nested within overlapping, wider-angle frames; and use of the camera of longer focal length to obtain a few full-disk photographs showing all sides of Mars as the spacecraft approached the planet. A third filter color, "blue," was added to the "red" and "green" of Mariner 4 for the purpose of studying atmospheric effects.

Limitations of volume, money, and schedule prevented use of a suitable digital recorder system with the necessary data storage capacity, but, through a hybrid system which uses both digital and analog tape recorders, it ap-

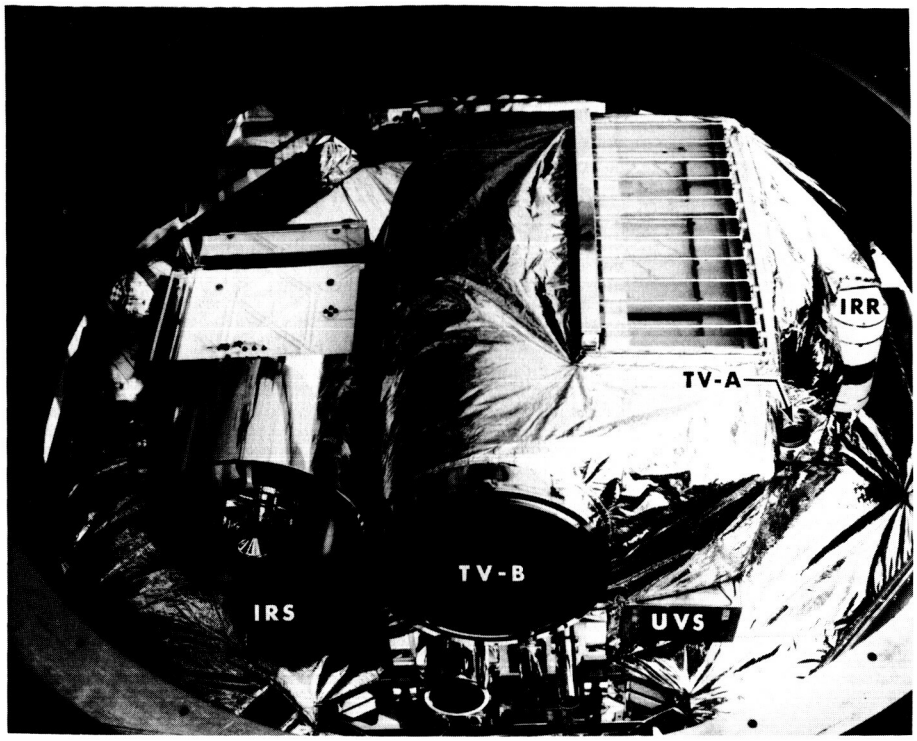

Fig. 1. Mariner 6 instruments and scan platform, mounted on the spacecraft. The five principal instruments are an infrared spectrometer (IRS), television camera B (TV-B), an ultraviolet spectrometer (UVS), television camera A (TV-A), and an infrared radiometer (IRR).

peared possible to achieve sufficient data storage capacity, albeit at the expense of complexity.

In its final form, the television experiment employed a two-camera system in which the picture formats and electronic circuits of the cameras were identical (for economy and for efficient use of the tape recorders); a digital tape recorder to store the six lowest-order bits of an 8-bit encoded word for every seventh picture element ("pixel") along each TV picture line (referred to as 1/7 digital data; see *5*); and a second, similar tape recorder to store analog data for all pixels (*6*).

In order to reduce the "noise" introduced by analog recording, the average signal level was held nearly constant and the modulation index was increased by automatic gain control (AGC) and a cube-law "contrast enhancement" circuit. This signal processing increased the data return by a factor of about 5; it also made necessary an elaborate program of computer restoration of the pictorial data after receipt on the earth.

Some technical data relating to the

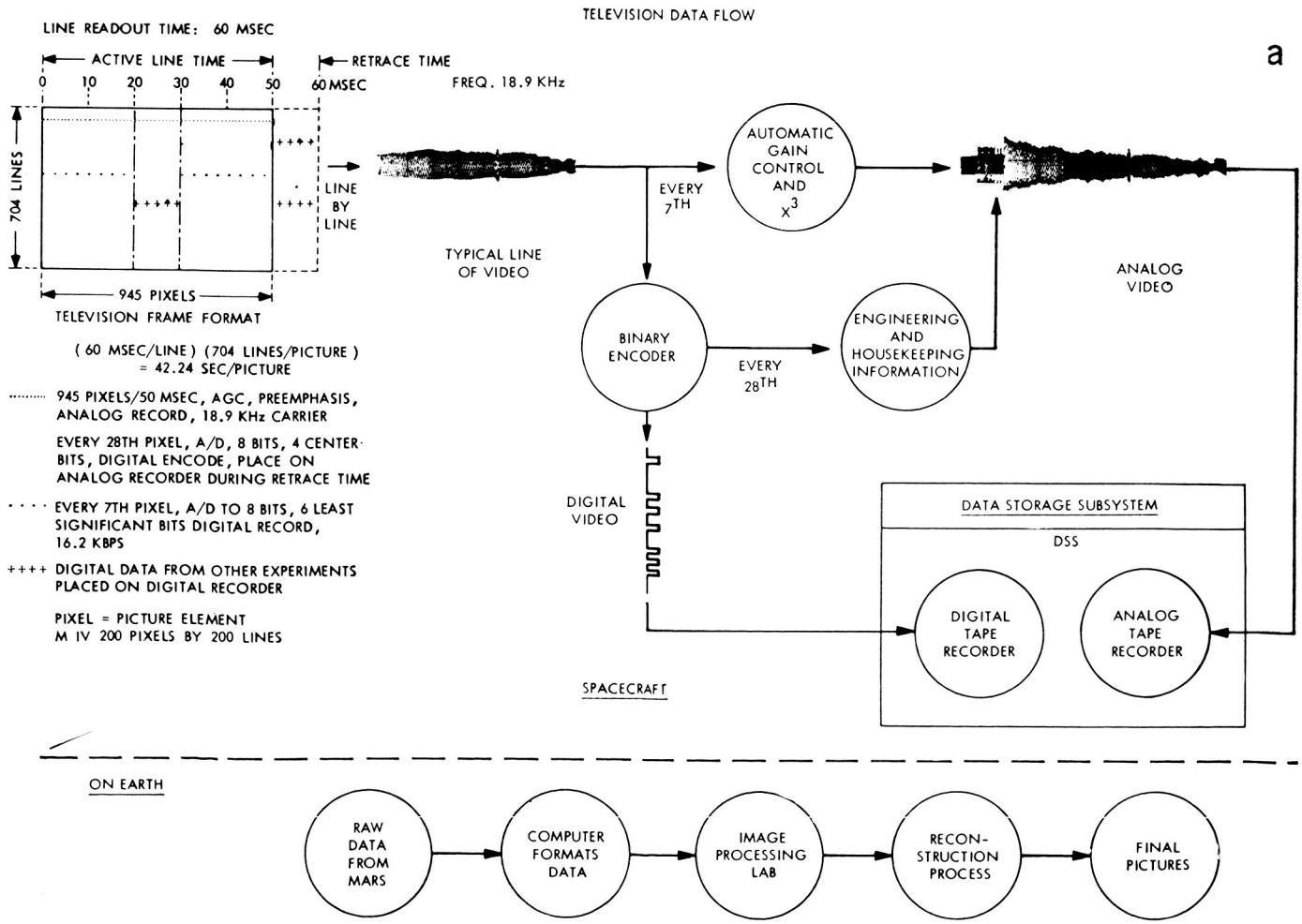

Fig. 2. (a) Schematic diagram illustrating video signal processing. (b) Spectral sensitivity curves of Mariner 6 and 7 cameras, with and without filters.

camera system are given in Leighton *et al.* (*3*), and more complete data will be given elsewhere (*6*). Briefly, one camera, called camera A, has a field of view 11° × 14° and a rotary shutter which carries four colored filters in the sequence red, green, blue, green, and so on. Alternating exposures with camera A is camera B, which has a focal length 10 times as great and a field of view 1°.1 × 1.°4. Camera B carries only a minus-blue haze filter.

Certain further aspects of the camera-operation and on-board signal processing are shown in Figs. 1 and 2. Figure 1 shows the cameras mounted on the spacecraft. Figure 2a shows the effect of automatic gain control on the analog signal, an effect similar to that of a high-pass filter in that it diminishes the amplitude of long-spatial-wavelength (low-frequency) signals. The response time of the AGC, about 6 milliseconds, corresponds to about one-tenth of a picture line, and its characteristic effects are apparent in all near-encounter pictures, especially those of high contrast: the polar cap boundary, the planet limb, and the terminator.

To illustrate the nature of the picture restoration process, we list some of the steps in the computer reduction: Restore the two highest-order bits to the digital data (*7*); remove effects of AGC and "cuber" in the analog data; combine digital and analog data; measure and remove electronic "pickup" noise (*7*); measure pixel locations of reseau marks on flight pictures and calibration pictures (*8*); bring pictorial calibration and flight data, by interpolation, into agreement with the known reseau pattern; measure and correct for optical distortions; measure and remove effects of residual image from calibration and flight data; evaluate the sensitometric response of each pixel from calibration data and deduce the true photometric exposure for each flight pixel (*9*); correct for the effects of shutter-speed variations and light leakage (camera B); and evaluate and correct for the modulation-transfer function of the camera system. Some of these steps have been applied to a few of the flight pictures on an experimental, ad hoc basis, pending receipt of complete, corrected telemetry data from the six playbacks of the recorded close-up pictures.

Mission Design and Television Data Return

As was described in Leighton *et al.* (*3*), the planetary encounter period for each spacecraft was divided into two parts: a far-encounter (FE) period beginning 2 or 3 days prior to, and extending to within a few hours of, closest approach, and a near-encounter (NE) period bracketing the time of closest approach.

As the Mariner 6 and 7 mission was originally conceived, the analog data for eight FE B-camera pictures and 25 NE pictures, and the 1/7 digital NE picture data (and other NE science data) were to be recorded and later transmitted to the earth at 270 bits per second over a 5-day period for each spacecraft. However, a 60-fold increase in transmission rate was realized during the development of the spacecraft, so that *real-time* transmission of the 1/7 digital data stream, or of the digitized analog data during picture playback, became possible. This capability thus led to the extended FE picture sequences actually used, in which the analog tape recorder was filled and played back several times. In addition, several hundred 1/7 digital pictures were transmitted directly to the earth in real time. Some of these digital pictures, taken during the very late FE period of Mariner 7, contain valuable three-color camera-A photometric data for large areas of Mars at a resolution greatly superior to that attainable from the earth. In all, 50 FE pictures, 26 NE pictures, and 428 useful (*10*) real-time 1/7 digital pictures were returned from Mariner 6, and 93 FE pictures, 33 NE pictures, and 749 useful real-time digital pictures were returned from Mariner 7. This further ninefold increase in the number of FE pictures and 18 percent increase in the number of NE pictures over the original plan represents a total data return 200 times that of Mariner 4, not counting the real-time digital frames.

The pictures are designated by spacecraft, camera mode, and frame number. Thus "6N17" means Mariner 6 NE frame 17; "7F77" means Mariner 7 FE frame 77; and so on. The first NE picture from each spacecraft was a camera-A, blue-filter picture. Thus, in near-encounter, all odd-numbered frames are camera-A (wide-angle, low-resolution) frames.

During each day of the FE period, camera B was used to record a series of up to 33 full-disk analog pictures of Mars with the AGC clamped. These pictures were transmitted to the earth during each daily period when the 16.2-kilobits-per-second signal could be received by the 210-foot antenna of the Goldstone, California, station of the NASA deep-space net. These pictures showed all sides of the planet as it rotated each day, and, within the total 5-day series, each face of Mars was recorded at a number of different scales and under many different viewing conditions. The phase angle was nearly constant throughout the far-encounter for both spacecraft (25°, morning terminator visible).

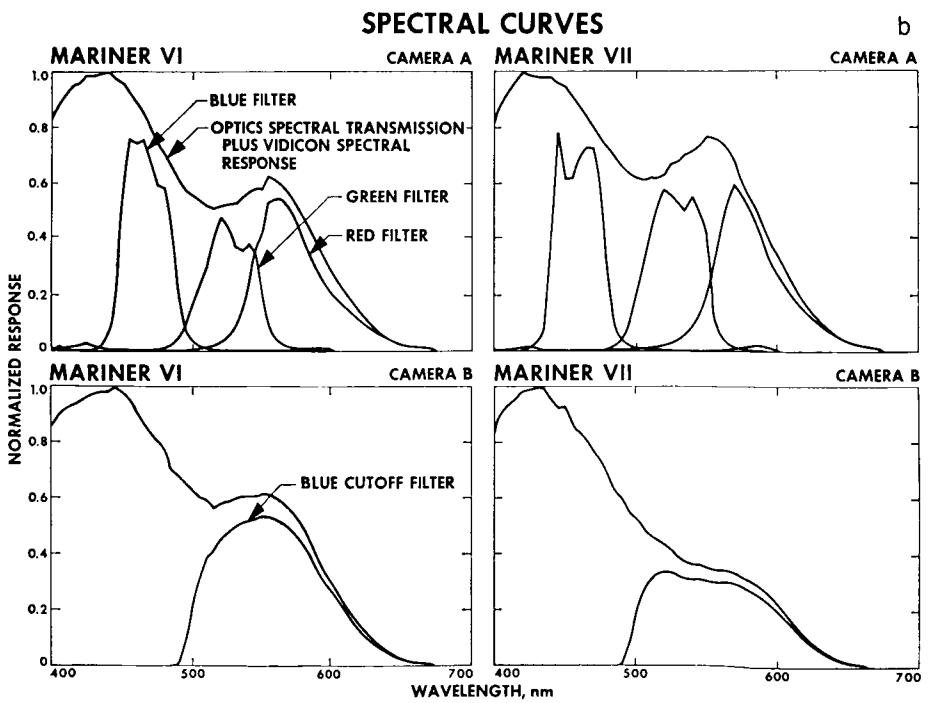

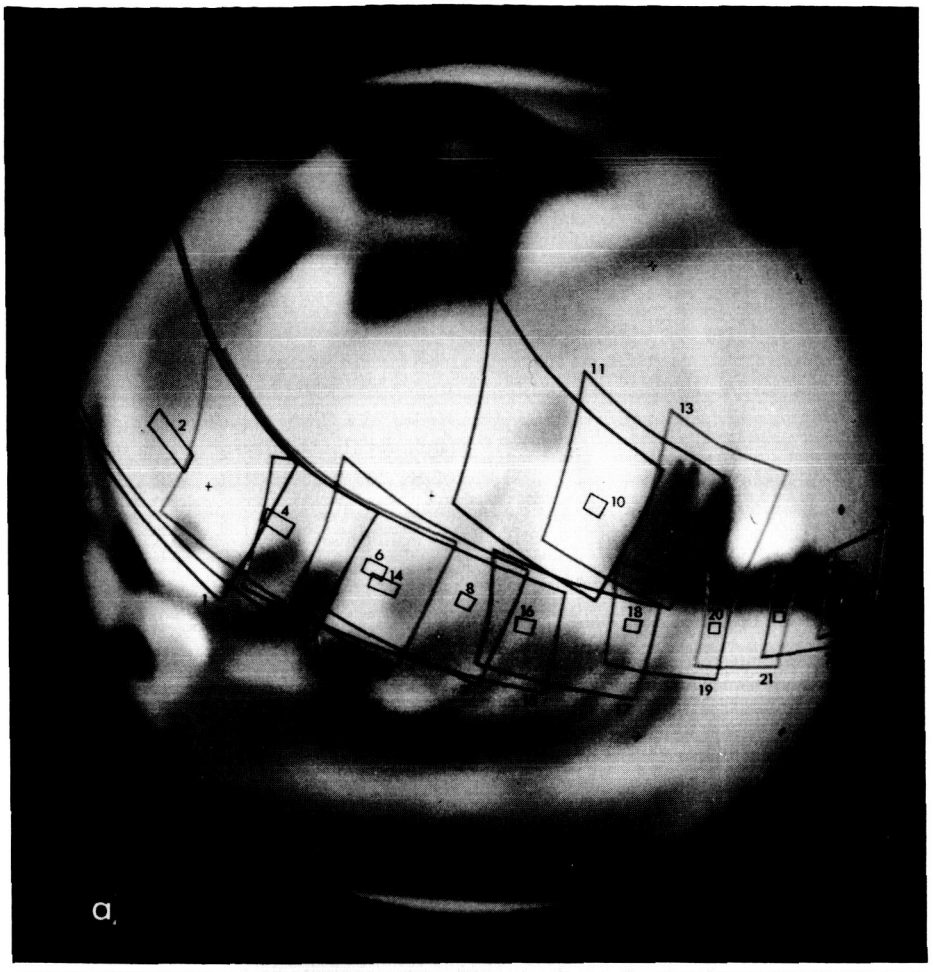

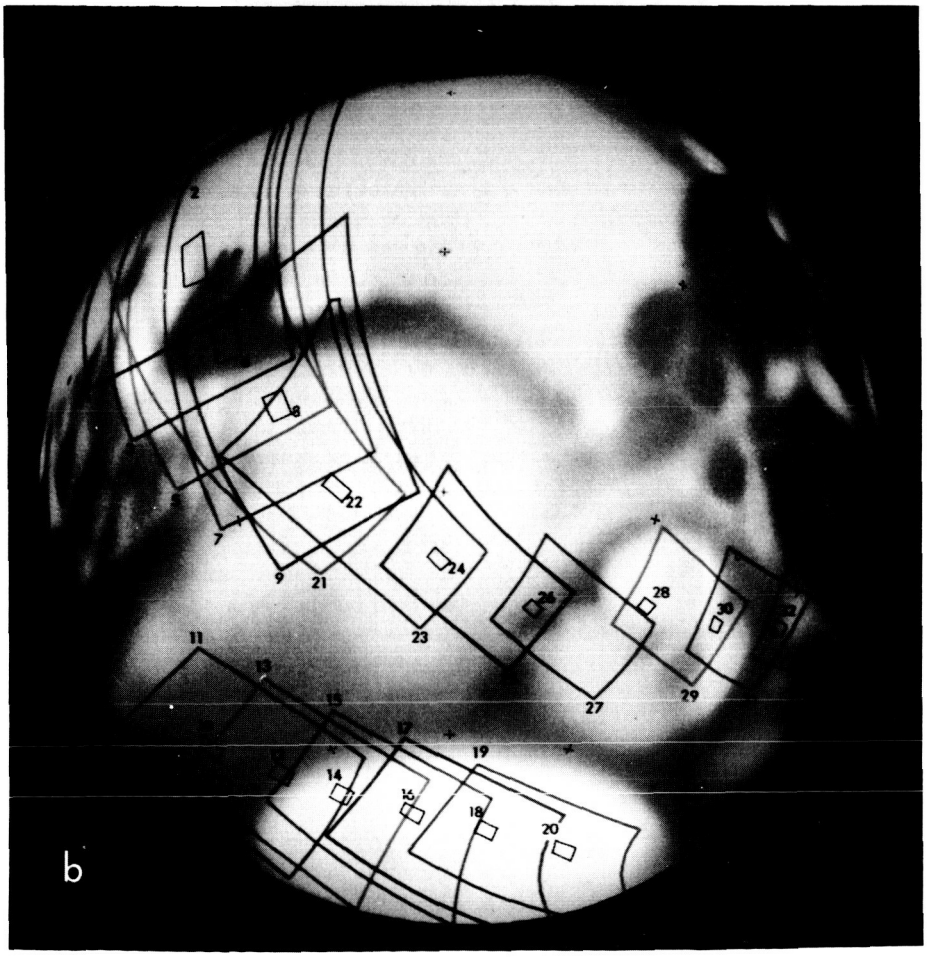

Fig. 3. (a) Mariner 6 NE picture locations, plotted on a painted globe of Mars. The first picture is taken with a blue filter. The camera-A filter sequence is blue, green, red, green, and so on. Wide-angle (camera A) frames and narrow-angle (camera B) frames alternate. (b) Mariner 7 NE picture locations. The filter sequence is the same as for Mariner 6.

The approximate near-encounter picture locations for the two spacecraft are shown in Fig. 3, and the relevant data are given in Tables 1 and 2. The picture tracks were chosen, in concert with investigators for other on-board experiments, on the basis of several considerations and constraints. First, the choice of possible arrival dates was limited by engineering considerations to the interval 31 July to 15 August 1969. Second, on any given arrival date, the time of closest approach was limited to an interval of about 1 hour by the requirement that the spacecraft be in radio view of Goldstone tracking station during a period of several hours which bracketed the time of closest approach. These two constraints and the approximate 24-hour rotation period of Mars considerably limited the possible longitudes of Mars that could effectively be viewed; in particular, the most prominent dark area, Syrtis Major, could not be seen under optimum conditions. Fortunately, Meridiani Sinus, a prominent dark area almost as strong and permanent as Syrtis Major, and various other important features well known from Earth observation, were easily accessible.

The cameras and other instruments were mounted on a two-axis "scan platform" which could be programmed to point the instruments in as many as five successive directions during the near-encounter. The particular orbit and platform-pointing strategy adopted for each spacecraft was designed to achieve the best possible return of scientific data within a context of substantial commonality but with some divergence of needs of the various experiments. The television experimenters placed great weight upon viewing a wide variety of classical features, including the polar cap; continuity of picture coverage; substantial two-color overlap and some three-color overlap if possible; stereoscopic overlap; viewing the planet limb in blue light; viewing the same area at two different phase angles; and seeing the same area under different viewing conditions at nearly the same phase angle.

Table 1. Mariner 6 near-encounter picture data at center of frame.

Picture No.	Slant range (km)	View angle from vertical (deg)	Solar zenith angle (deg)	Latitude (deg)	East longitude (deg)	Area ("height × width") (km)
1	Center of picture does not intercept planet					Limb
2	7401	70.2	18.8	4.3	292.3	157.2 × 556.4
3	6614	57.3	6.8	− 2.0	303.2	Limb
4	6130	49.8	4.9	− 5.2	310.3	125.6 × 229.1
5	5682	41.8	11.1	− 8.6	317.3	Limb
6	5348	36.2	17.1	− 10.6	323.0	109.1 × 158.7
7	5028	29.7	23.5	− 12.9	329.1	1112 × 1597
8	4777	25.2	28.9	− 14.1	334.4	97.4 × 125.7
9	4920	40.5	41.3	− 0.1	346.0	1679 × 1861
10	4737	39.4	45.8	− 1.2	350.7	119.1 × 122.1
11	4558	38.1	50.8	− 2.7	355.8	1309 × 1378
12	4439	38.8	55.6	− 3.0	0.6	113.9 × 108.4
13	4333	39.6	60.9	− 3.7	5.8	1191 × 1243
14	4832	59.5	20.5	− 13.0	324.8	99.8 × 231.4
15	4382	49.3	30.6	− 15.9	334.7	Limb
16	4103	42.1	38.2	− 17.3	342.3	83.7 × 132.8
17	3868	34.6	45.7	− 18.5	349.9	858 × 1289
18	3738	30.3	52.1	− 16.6	356.6	77.1 × 102.5
19	3613	24.4	58.5	− 16.9	3.1	773 × 1036
20	3543	20.4	64.2	− 16.6	8.9	73.1 × 88.8
21	3498	16.3	70.3	− 16.2	15.1	723 × 929
22	3497	14.9	75.8	− 15.2	20.5	72.3 × 84.4
23	3522	15.0	81.7	− 14.2	26.4	718 × 921
24	3584	17.6	87.2	− 12.7	31.7	74.8 × 87.0
25	3622	19.1	90.0	− 12.1	34.4	765 × 973
26	3680	21.3	93.0	− 11.0	37.3	77.4 × 91.1

Table 2. Mariner 7 near-encounter picture data at center of frame.

Picture No.	Slant range (km)	View angle from vertical (deg)	Solar zenith angle (deg)	Latitude (deg)	East longitude (deg)	Area ("height × width") (km)
1	Center of picture does not intercept planet					Limb
2	Center of picture does not intercept planet					Limb
3	9243	69.6	25.8	14.4	350.3	Limb
4	8533	59.7	15.6	5.3	354.9	175.3 × 412.5
5	7993	52.3	8.2	− 1.4	357.7	Limb
6	7533	46.1	2.5	− 7.0	1.3	152.9 × 262.0
7	7129	40.6	4.7	− 12.0	3.8	Limb
8	6771	35.8	10.2	− 16.4	7.3	137.7 × 200.4
9	6443	31.4	15.1	− 20.5	10.0	1503 × 2233
10	6654	47.5	50.5	− 53.1	328.3	197.0 × 165.7
11	6377	45.6	52.1	− 57.1	332.4	2282 × 1672
12	6084	42.9	53.4	− 60.6	338.9	166.6 × 147.5
13	5864	42.4	55.9	− 64.2	344.1	2049 × 1912
14	5631	41.1	58.2	− 67.4	352.3	148.8 × 139.4
15	5462	41.9	61.4	− 70.7	0.1	2098 × 2058
16	5285	42.1	64.5	− 73.2	12.5	137.4 × 138.9
17	5167	44.2	68.3	− 75.9	26.6	1368 × 1561
18	5049	45.8	72.1	− 76.8	46.3	131.69 × 147.2
19	4994	49.2	76.7	− 77.3	68.6	1343 × 1862
20	4949	52.4	81.4	− 75.4	89.4	133.5 × 171.7
21	5314	65.7	14.0	− 20.6	6.1	Limb
22	4776	55.0	24.9	− 28.5	14.2	97.9 × 201.3
23	4405	46.8	33.3	− 34.3	21.2	1383 × 2488
24	4130	39.9	40.7	− 38.3	28.8	84.5 × 128.9
25	3917	33.7	47.3	− 41.7	36.2	874 × 1291
26	3759	28.4	53.6	− 43.7	44.2	77.2 × 101.4
27	3638	23.6	59.5	− 45.3	52.0	775 × 1035
28	3664	28.1	65.6	− 40.4	62.1	80.7 × 92.2
29	3619	26.6	71.1	− 40.4	69.3	823 × 995
30	3621	27.3	76.7	− 39.1	76.3	81.5 × 87.7
31	3646	28.4	82.1	− 37.7	83.1	831 × 987
32	3722	31.6	87.7	− 35.0	89.5	87.1 × 90.8
33	3822	34.9	93.4	− 32.2	95.5	996 × 1116

The Mariner 6 picture track was chosen to cover a broad longitude range at low latitudes in order to bring into view a number of well-studied transitional zones between light and dark areas, two "oases" (Juventae Fons and Oxia Palus), and a variable light region (Deucalionis Regio). The picture track of Mariner 7 was selected so that it would cross that of Mariner 6 on the dark area Meridiani Sinus, thereby providing views of that important region under different lighting conditions. The track was also specifically arranged to include the south polar cap and cap edge, to intersect the "wave-of-darkening" feature Hellespontus, and to cross the classical bright circular desert Hellas.

Camera Operation and Picture Appearance

With minor exceptions, both camera systems operated normally, well within expected ranges of the various ambient parameters. The principal exceptions were the following: the contrast of the FE pictures of Mariner 6 was lower than expected, because of an unaccountably low signal level; the electronic "pickup" noise from the square-wave power system was somewhat greater than anticipated for both spacecraft; the first track of the Mariner 6 analog tape recorder showed a 50 percent drop in amplifier gain between FE and NE playback; and the fourth track of the analog tape recorder of Mariner 7 showed greater than normal "dropout" noise. These deficiencies not only affected the subjective appearance of the pictures but also necessitate more elaborate processing of the data before accurate, high-resolution photometric measurements can be made.

The first impression of Mars conveyed by the pictures is that the surface is generally visible and is not obscured by clouds or haze except perhaps in the polar regions and in a few areas marked by the appearance of afternoon "clouds." The classical martian features stand out clearly in the far-encounter pictures, and, as the image grows, these features transform into areas having recognizable relationships to the numerous craters which mark the surface. The near-encounter pictures seem to show a Moon-like terrain. However, one must bear in mind the fact that the camera system was designed to enhance the contrast of local brightness

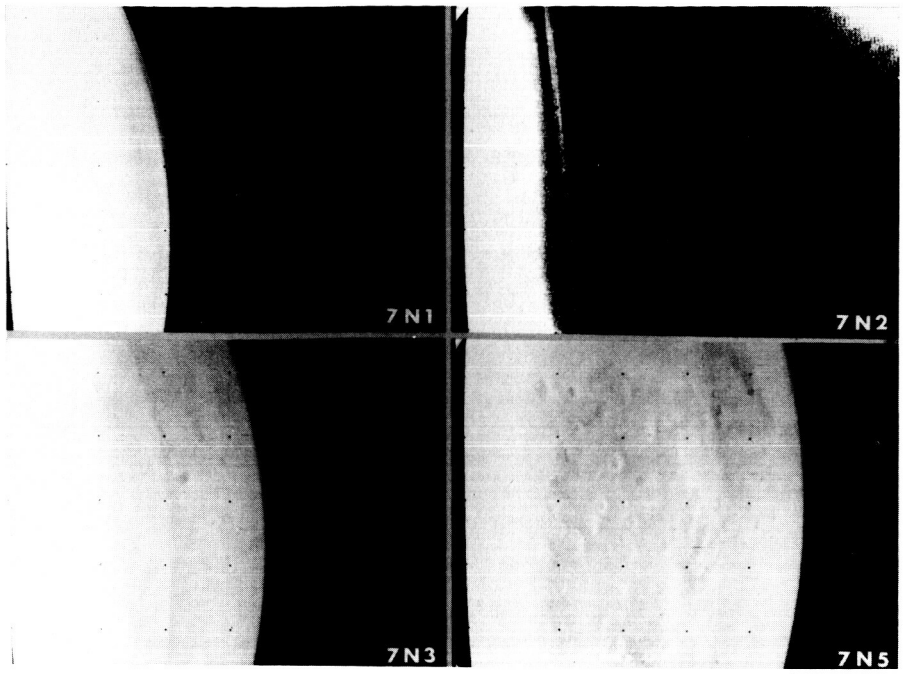

Fig. 4. Mariner 7 limb frames 7N1, 2, 3, and 5. Note the sharp haze layer adjacent to the limb in frames 7N1, 3, and 5, and the magnified view (tenfold magnification) in 7N2. The prominent, cratered dark feature in frame 7N5 is Meridiani Sinus. North is approximately toward the right.

fluctuations by a factor of 3, and that the contrast of the pictures is often further enhanced in printing. Actually, although the surface is generally visible, its contrast is much less than that of the moon under similar lighting conditions. Fewer shadows are seen near the terminator.

The determination of true surface contrast depends critically upon the amount of haze or veiling glare in the picture field. Although the pictures appear to be free of such effects, more refined photometric measurements may well reveal the presence of veiling glare or a general atmospheric haze. Definite conclusions must await completion of the photometric reduction of the pictures, including corrections for vidicon dark current, residual images, shutter light leaks, and possible instrumental scattering.

Observed Atmospheric Features

Aerosol scattering. Clear-cut evidence for scattering layers in the atmosphere is provided by the pictures of the northeastern limb of Mariner 7. The limb appears in frames 7N1, 2, 3, 5, and 7, and in a few real-time digital A-camera frames received immediately prior to frame 7N1. The limb appears again in frame 7N21 after the platform slew which began the track across Hellas. Thus the limb coverage includes each of the filters of the A camera and one B-camera frame.

Several characteristics of the scattering layer shown in Fig. 4 are evident even at this early stage. (i) The scattering is distinctly stratified in horizontal layers, just as scattering from aerosol layers in the earth's atmosphere is. (ii) The intensity of the scattering varies substantially over distances of a few hundred kilometers and is more intense toward the west or toward earlier local times of day. (iii) The thickness of the scattering layer is about 10 kilometers. (iv) The height of the layer is difficult to determine because of the difficulty of locating the true planetary limb, but it is estimated to be between 15 and 25 kilometers in the region covered by frames 7N1 to 7N7 and up to 40 kilometers in frame 7N21. (v) The layer is about 50 percent brighter in the blue-filter pictures than in the red or green. This is less difference in intensity than would be expected for Rayleigh scattering, but corresponds more closely to λ^{-2} wavelength dependence.

The relationship between this scattering layer and the martian tropopause is obviously of great interest and will be studied carefully as more refined data become available.

The normal-incidence optical depth, isotropic scattering being assumed, is estimated as 0.01 in the red and about 0.03 in the blue. A λ^{-2} dependence suggests that scattering should be predominantly forward, so these very small values should be underestimates.

The real-time digital data reveal an apparent limb haze near the south polar cap, and over the regions of Mare Hadriaticum and Ausonia just east of Hellas. The haze over these regions is not as bright as the haze discussed above, so it is unlikely that it is sufficiently dense to obscure surface features seen at NE viewing angles. A faint limb haze may also be present in the Mariner 6 limb frames.

The "blue haze." Despite these evidences of very thin aerosol hazes, visible tangentially on the limb, there is no obscuring "blue haze" sufficient to account for the normally poor visibility of dark surface features seen or photographed in blue light and for their occasional better visibility—the so-called "blue-clearing" phenomenon (*11, 12*).

The suitability of the Mariner blue pictures for "blue haze" observations was tested by photographing Mars through one of the Mariner blue filters on Eastman III-G plates, whose response in this spectral region is similar to that of the vidicons used in the Mariner camera. Conventional blue photographs on unsensitized emulsions and green photographs were taken for comparison. A typical result is shown in Fig. 5; the simulated TV blue picture is very similar to the conventional blue photographs. The effective wavelength of the actual blue TV pictures should be even shorter, owing to a lower ambient temperature and to the absence of reddening due to the earth's atmosphere.

The blue pictures taken by Mariners 6 and 7 clearly show craters and other surface features, even near the limb and terminator, where atmospheric effects are strong. Polar cap frame 7N17 shows sharp surface detail very near the terminator. The blue limb frame 6N1 shows surface detail corresponding to that seen in the subsequent overlapping green frame 6N3. Figure 6 includes blue, green, and red pictures in the region of Sinus Meridiani. Although craters show clearly in all three colors, albedo variations, associated both with craters and with larger-scale features, are much more pronounced in green and red than in blue. Blue photographs obtained from the earth

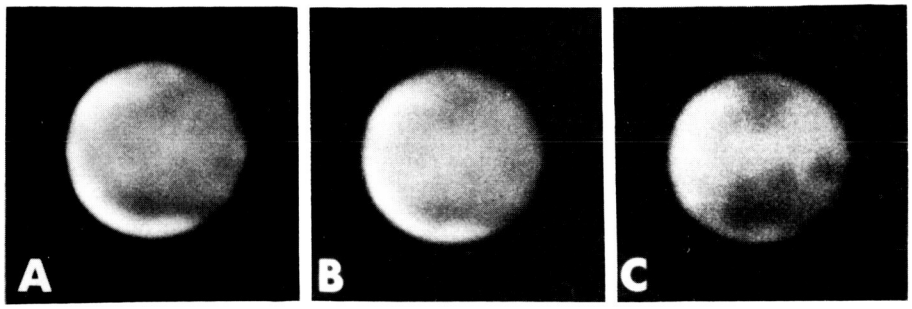

Fig. 5. Photographs of Mars from the earth, taken to compare Mariner-type blue-filter pictures with "standard" green and blue pictures of Mars. The pictures were taken 24 May 1969 at New Mexico State University Observatory. (A) "Standard" blue (0915 U.T.); (B) Mariner blue (0905 U.T.); (C) standard green (0844 U.T.). North is at the top.

during the Mariner encounters show the normal "obscured" appearance of Mars.

South polar cap shading. Another possible indication of atmospheric haze is the remarkable darkening of the south polar cap near both limb and terminator in the FE pictures (Fig. 7). This darkening is plainly *not* due to cloud or thick haze since, during near-encounter, surface features are clearly visible everywhere over the polar cap. It may be related to darkening seen in NE Mariner 7 frames near the polar cap terminator, and to the decrease in contrast with increasing viewing angle between the cap and the adjacent mare seen in frame 7N11 (Fig. 8b). The darkening may be due to optically thin aerosol scattering over the polar cap, or possibly to unusual photometric behavior of the cap itself. In either case, it may be complicated by systematic diurnal or latitudinal effects.

North polar phenomena. Marked changes seem to have occurred, between the flybys of Mariners 6 and 7, in the appearance of high northern latitudes. Some of these changes are revealed by a comparison of frames 6F34 and 7F73, which correspond to approximately the same central meridian and distance from Mars (Fig. 7). A large bright tongue (point 1 in frame 73) and a larger bright region near the limb (point 2) appear smaller and fainter in the Mariner 7 picture, despite the generally higher contrast of Mariner 7 FE frames. Much of the brightening near point 2 has disappeared entirely between the two flybys; in fact, it was not visible at all on pictures taken by Mariner 7 during the previous Mars rotation, although it was clearly visible in several Mariner 6 frames taken over the same range of distances. The bright tongue (point 1) increases in size and brightness during the martian day, as may be clearly seen from a comparison of frames 7F73 and 7F76 (Fig. 7).

The widespread, diffuse brightening covering much of the north polar cap region (point 3) apparently corre-

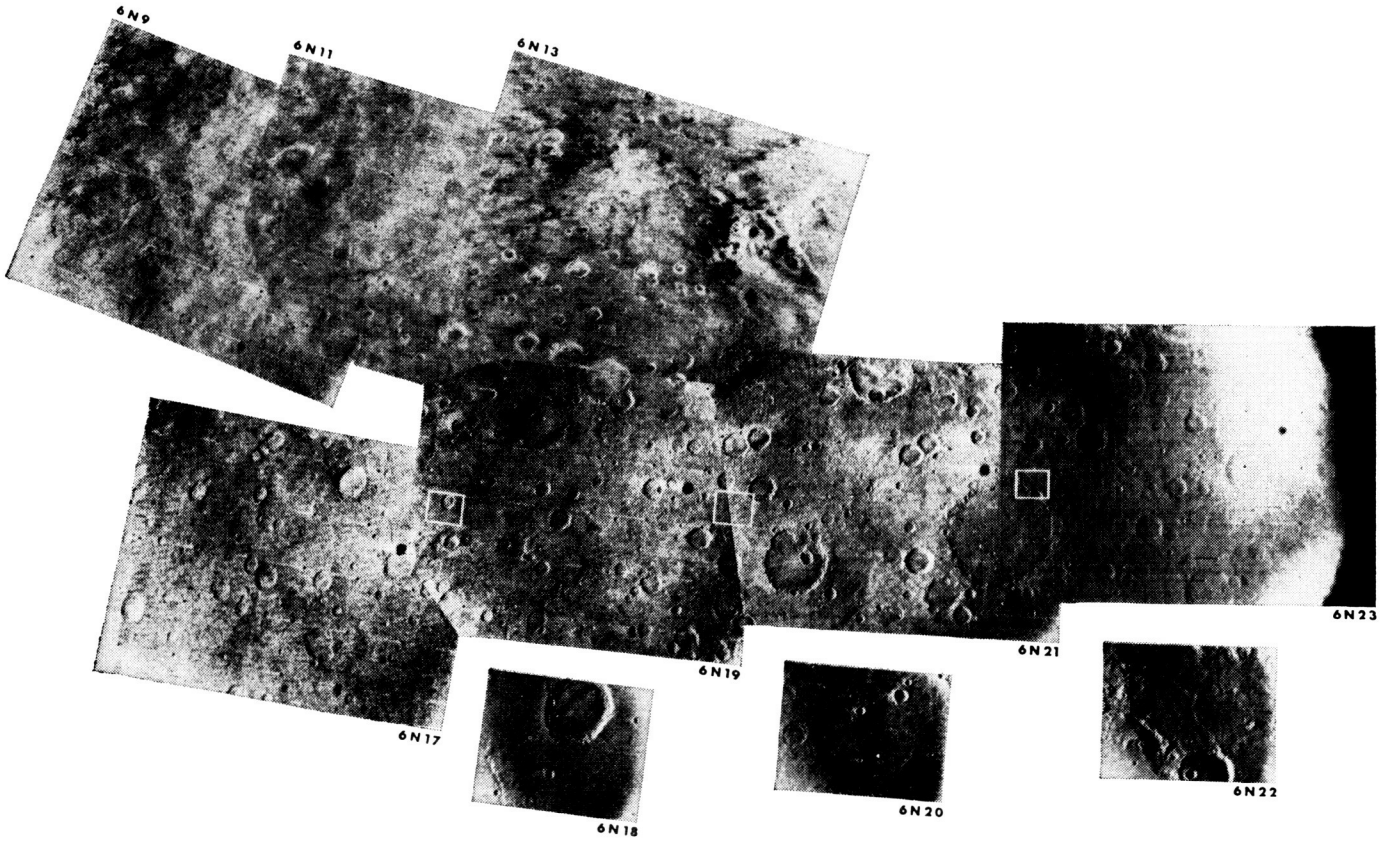

Fig. 6. Composite of ten Mariner 6 pictures showing cratered terrain in the areas of Margaritifer Sinus (top left), Meridiani Sinus (top center), and Deucalionis Regio (lower strip). Large-scale contrasts are suppressed by AGC and small-scale contrast is enhanced (see text). Craters are clearly visible in blue frames 6N9 and 6N17, but albedo variations are subdued. Locations of three camera-B frames are marked by rectangles. North is approximately toward the top, and the sunset terminator lies near the right edge of 6N23.

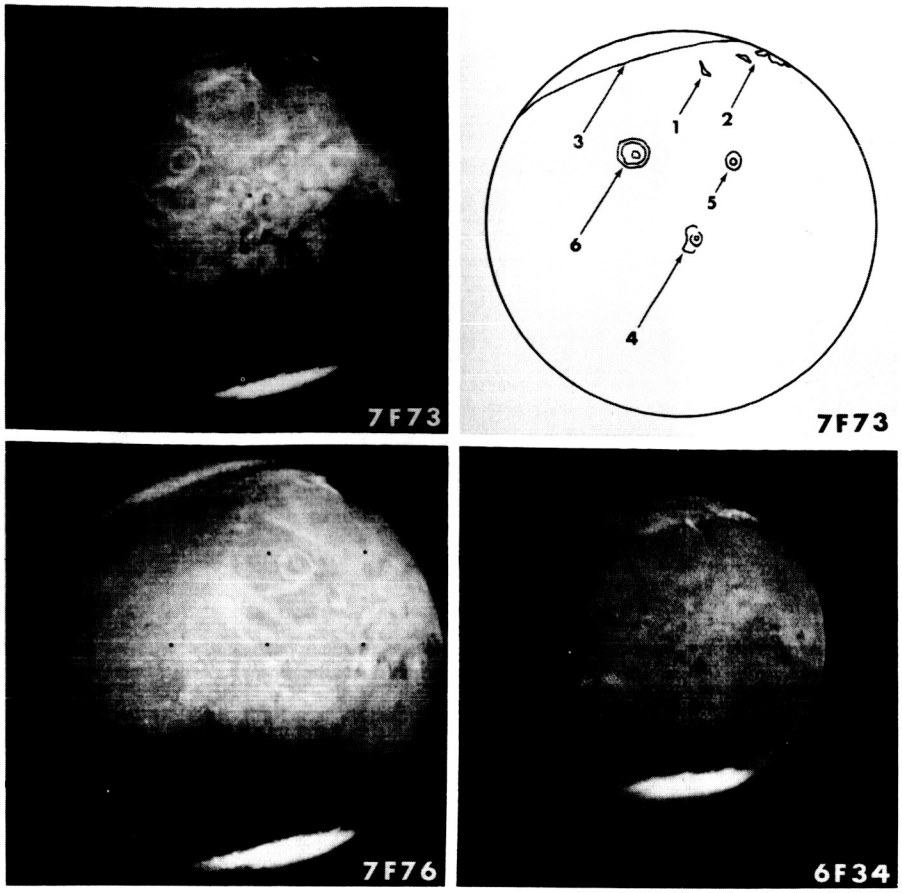

Fig. 7. Far-encounter pictures showing atmospheric and atmosphere-surface effects. Picture shutter times were as follows: 6F34, 30 July 0732 U.T.; 7F73, 4 August 1115 U.T.; 7F76, 4 August 1336 U.T.

sponds to the "polar hood" which has been observed from the earth at this martian season (northern early autumn). The extent of this hood is smaller in Mariner 7 than in Mariner 6 pictures; the region between, and just north of, points 1 and 2 appears to be covered by the hood in the Mariner 6 frames, but shows no brightening in the Mariner 7 frames.

The different behaviors of the discrete bright regions and the hood suggest different origins for these features, although both apparently are either atmospheric phenomena or else result from the interaction of the atmosphere and the surface. The discrete bright regions have fixed locations suggesting either surface frost or orographically fixed clouds. The fluctuation in the areal extent of the diffuse hood suggests cloud or haze. An extensive cloud or haze composed of either CO_2 or CO_2 and H_2O ice would be consistent with the atmospheric temperature structure revealed by the Mariner 6 occultation experiment (*13*).

Diurnal brightening. Other variable bright features which may be indicative of atmospheric processes appear throughout the Tharsis, Candor, Tractus Albus, and Nix Olympica regions (Fig. 7, frame 7F73; see also *3*). The brightness of these areas is observed to develop during the forenoon and increase during the martian afternoon, both in the Mariner pictures and in photographs taken from the earth. The structure and locations in the FE pictures do not change over the 6-day time span during which the region was observed. Particularly striking are several long light streaks near Nix Olympica (point 6 in frame 7F73) and numerous circular features resembling craters, which have bright centers and dark edges. Several of the circular features exhibit one or more concentric circles similar to, but less striking than, those near Nix Olympica. Two features of this type form two of the westernmost points of the classical "W-cloud" (points 4 and 5). No morphology associated with clouds—such as waves, billows, or cirriform streaks—appear in this region, although at the 30-kilometer resolution of these pictures such features would be visible in terrestrial clouds.

Search for local clouds and fog. All NE frames from both spacecraft were carefully examined for evidences of clouds or fog. Away from the south polar cap there are no evidences of such atmospheric phenomena. Over the polar cap and near its edge a number of bright features which may be atmospheric can be seen, although no detectable shadows are present and no local differences in height can be detected by stereoscopic viewing of overlapping regions whose stereo angles lie between 5° and 12°. Little or no illumination is evident near and beyond the polar cap terminator. On the other hand, frames 7N11, 12, and 13 (Fig. 8) show several diffuse bright patches suggestive of clouds near the polar cap edge. Also, on the cap itself a few local diffuse bright patches are present in frames 7N15 (green) and 7N17 (blue). Unlike most polar cap craters, which appear sharp and clear, a few crater rims and other topographic forms appear diffuse (frames 7N17, 18, and 19). In frames 7N17 (blue) and 7N19 (green), remarkable curved, quasi-parallel bright streaks are visible near the south pole itself. While these show indications of topographic form or control, including some crater-like shapes, their possible cloud-like nature is suggested by lack of shading. Also frames 7N17 and 7N19 show faint but definite streaks and mottles very near the terminator, superimposed on a sparsely cratered surface.

Observed Surface Features

A primary objective of the Mariner 6 and 7 television experiment was to examine, at close range, the principal types of martian surface features seen from the earth.

Mariners 6 and 7, while confirming the earlier evidence of a Moon-like cratered appearance for much of the martian surface, have also revealed significantly different terrains suggestive of more active, and more recent, surface processes than were previously evident. Preliminary analyses indicate that at least three distinctive terrains are represented in the pictures, as well as a mixture of permanent and transitory surface features displayed at the edge of, and within, the south polar cap; these terrains do not exhibit any simple correlation with the light and dark markings observed from the earth.

Cratered terrains. Cratered terrains

are those parts of the martian surface upon which craters are the dominant topographic form (Fig. 6). Pictures from Mariners 4, 6, and 7 all suggest that cratered terrains are widespread in the southern hemisphere.

Knowledge of cratered terrains in the northern hemisphere is less complete. Cratered areas appear in some Mariner frames as far north as latitude 20°. Nix Olympica, which in far-encounter photographs appears to be an unusually large crater, lies at 18°N. Numerous craters are visible in the closer-range FE frames. These are almost exclusively seen in the dark areas lying in the southern hemisphere, few being visible in the northern hemisphere. This difference may result from an enhancement of crater visibility by reflectivity variations in dark areas. However, poor photographic coverage, highly oblique views, and unfavorable sun angles combine to limit our knowledge of the northern portion of the planet.

Preliminary measurements of the diameter-frequency distribution of martian craters in the region Deucalionis Regio were made on frames 6N19 to 6N22 and are shown in Fig. 9a. The curves are based upon 104 craters more than 0.7 kilometer in diameter seen on frames 6N20 and 22, and upon 256 craters more than 7 kilometers in diameter seen on frames 6N19 and 21. The most significant result is the existence of two different crater distributions, a dichotomy also apparent in morphology. The two morphological crater types are (i) large and flat-bottomed and (ii) small and bowl-shaped. Flat-bottomed craters are most evident on frames 6N19 and 6N21. The diameters range from a few kilometers to a few hundred kilometers, with estimated diameter-to-

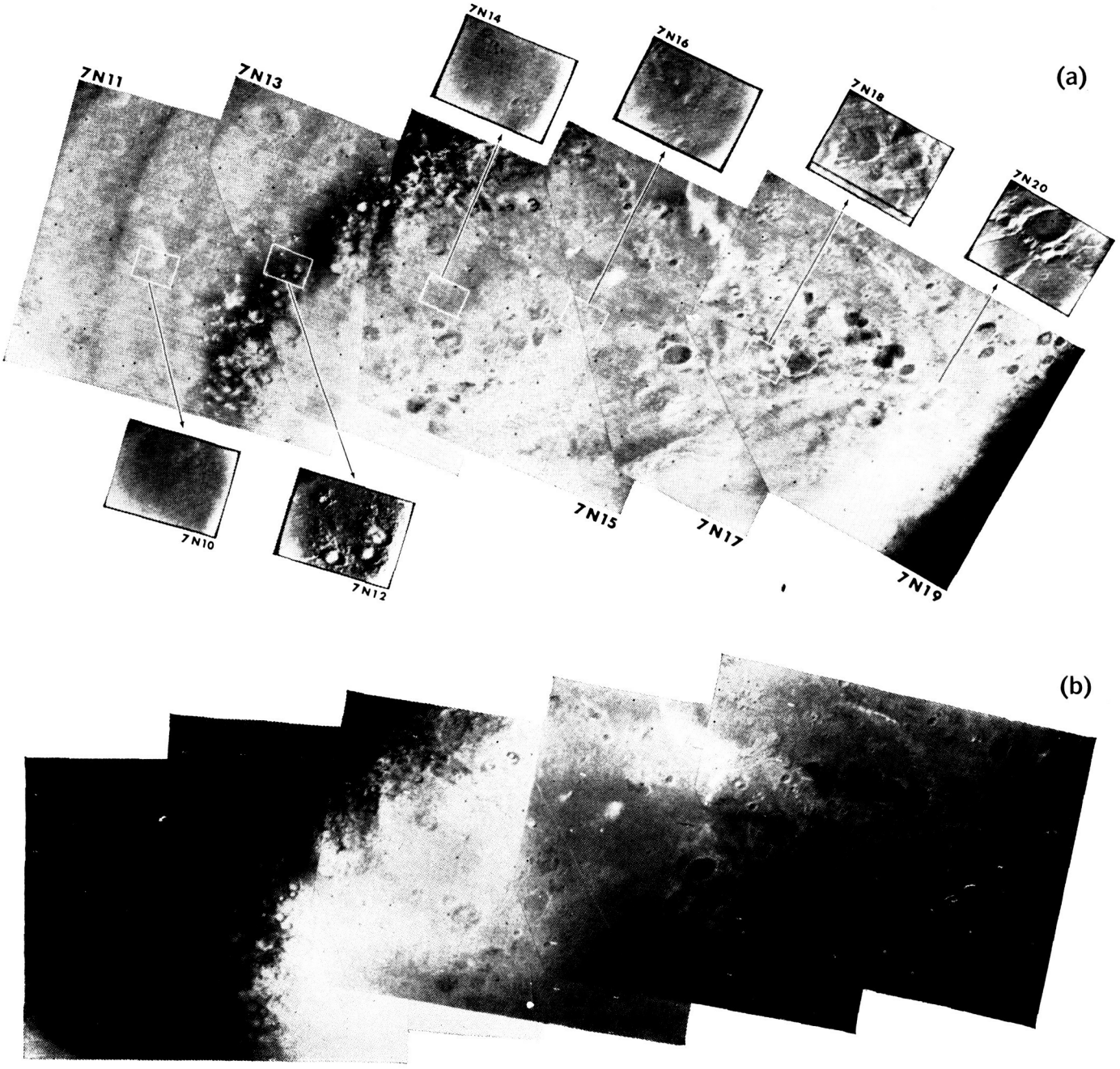

Fig. 8. (a) Composite of polar cap frames 7N10 to 7N20. Effects of AGC are clearly evident near the terminator (right) and at cap edge. (b) Composite of poplar cap camera-A frames 7N11 to 7N19. The effects of AGC have been partially corrected, but contrast is enhanced. The south pole lies near the parallel streaks in the lower right corner of frame 7N17.

depth ratios on the order of 100 to 1. The smaller, bowl-shaped craters are best observed in frames 6N20 and 6N22 and resemble lunar primary-impact craters. Some of them appear to have interior slopes steeper than 20 degrees.

The diameter-frequency distribution of large flat-bottomed craters is compared in Fig. 9b with the distribution of craters in the uplands on the far side of the moon near Tsiolkovsky. This particular lunar region was chosen for comparison because it is evidently a primordial surface, devoid of large post-upland features which might have modified the original crater distribution. The distribution of the small bowl-shaped craters is compared in Fig. 9c with the distribution of craters on the lunar maria (*14*). The distribution curve for small martian craters larger than about 1 kilometer in diameter has a slope of about -2, which is similar to the curve for primary craters larger than 3 kilometers in diameter on the lunar maria.

There are large variations in crater morphology among different cratered terrains. The craters of the dark area Meridiani Sinus (Fig. 6) have more marked polygonal outlines and more central peaks than craters in some other martian areas; the especially distinctive lighter marking in the northwest portions of the crater floors is also, but less clearly, seen in some FE frames. Many of the primary and secondary features associated with large lunar impact craters can be found on the martian terrain (see, for example, frame 6N18); however, certain others, such as rays and secondary crater swarms, appear to be absent. Also, ejecta blankets appear to be much less well developed. The missing features are generally those most easily removed or hidden by erosion or blanketing—a pattern consistent with the observation that the martian craters are generally shallower and more smooth than lunar ones.

On frame 6N20 there are low irregular ridges similar to those seen on the lunar maria. However, no straight or sinuous rills have been identified with confidence. Similarly, no Earth-like tectonic forms possibly associated with mountain building, island-arc formation, or compressional deformation have been recognized.

Chaotic terrains. Mariner frames 6N6, 14, and 8 (Fig. 10a) show two types of terrain—a relatively smooth cratered surface that gives way abruptly to irregularly shaped, apparently lower areas of chaotically jumbled ridges. This chaotic terrain seems characteristically to display higher albedo than its surroundings. On that basis, we infer that significant parts of the overlapping frames 6N5, 7, and 15 may contain similar terrain, although their resolution is not great enough to reveal the general morphological characteristics. As shown in Fig. 10a, frames 6N6, 14, and 8 all lie within frame 6N7, for which an interpretive map of possible chaotic terrain extent has been prepared (Fig. 11).

About 10^6 square kilometers of chaotic terrain may lie within the strip, 1000 kilometers wide and 2000 kilometers long, covered by these Mariner 6 wide-angle frames. Frames 6N9 and 10 contain faint suggestions of similar features. This belt lies at about 20°S, principally within the poorly defined, mixed light-and-dark area between the dark areas Aurorae Sinus and Margaritifer Sinus.

Chaotic terrain consists of a highly irregular plexus of short ridges and depressions, 1 to 3 kilometers wide and 2 to 10 kilometers long, best seen in frame 6N6 (Fig. 10a). Although irregularly jumbled, this terrain is different in setting and pattern from crater ejecta sheets. Chaotic terrain is practically uncratered; only three faint possible craters are recognized in the 10^6-square-kilometer area. The patches of chaotic terrain are not all integrated, but they constitute an irregular pattern with an apparent N to N 30°E grain.

Featureless terrains. The floor of the bright circular "desert," Hellas, centered at about 40°S, is the largest area of featureless terrain so far identified. Even under very low solar illumination the area appears devoid of craters down to the resolution limit of about 300 meters. No area of comparable size and smoothness is known on the moon. It may be that all bright circular "deserts" of Mars have smooth featureless floors; however, in the present state of our knowledge it is not possible to define any significant geographic relationship for featureless terrains.

The Mariner 7 traverse shows that the dark area Hellespontus, lying west of Hellas, is heavily cratered. The 130- to 350-kilometer-wide transitional zone is also well cratered and appears to slope gently downward to Hellas, interrupted by short, en echelon scarps and ridges (Fig. 12). It gives way abruptly along an irregular foot to the flat floor of Hellas. Craters are observed within the transitional zone but abruptly become obscured within the first 200 kilometers toward the center of Hellas.

The possibility that a low haze or fog may be obscuring the surface of Hellas, and that the featureless images are therefore not relevant to the true surface, has been considered. However, in frame 7N26 the ridges of the Hellas-Hellespontus boundary are clearly visible, proving that the surface is seen; yet there are virtually no craters within that frame. Thus the absence of well-defined craters appears to be a real effect.

South polar cap features. The edge of the martian south polar cap was visible at close range over a 90° span of longitude, from 290°E to 20°E, and the cap itself was seen over a latitude range from its edge, at $-60°$, southward to, and perhaps beyond, the pole itself. Solar zenith angles ranged from 51° to 90° and more; the terminator is clearly visible in one picture. The phase angle for the picture centers was 35°. The superficial appearance is that of a clearly visible, moderately cratered surface covered with a varying thickness of "snow." The viewing angle and the unfamiliar surface conditions make quantitative comparison with other areas of Mars difficult with respect to the number and size distributions of craters. Discussion here is therefore confined to those qualitative aspects of the polar cap which seem distinctive to that region.

The edge of the cap was observed in the FE pictures to be very nearly at 60°S, as predicted from Lowell Observatory measurements (*15*); this lends confidence to Earth-based observations concerning the past behavior of the polar caps.

The principal effect seen at the cap edge is a spectacular enhancement of crater visibility and the subtle appearance of other topographic forms. In frames 7N11 to 7N13, where the local solar zenith angle was about 53°, craters are visible both on and off the cap. However, in the transition zone, about 2 degrees of latitude in width, the population density of visible craters is several times greater, and may equal any so far seen on Mars. This enhancement of crater visibility results mostly from the tendency, noted in Mariner 4 pictures 14 and 15, for snow to lie preferentially on poleward-facing slopes.

In frame 7N12 the cap edge is seen in finer detail. The tendency mentioned above is here so marked as to cause confusion concerning the direction of the

illumination. There are several tiny craters as small as 0.7 kilometer in diameter, and areas of fine mottling and sinuous lineations are seen near the larger craters. The largest crater shows interesting grooved structure, near its center and on its west inner wall, which appears similar to that in frame 6N18.

On the cap itself, the wide-angle views show many distinct reflectivity variations, mostly related to moderately large craters but not necessarily resulting from slope-illumination effects. Often a crater appears to have a darkened floor and a bright rim, and in some craters having central peaks the peaks seem unusually prominent. In frames 7N17 and 7N19 several large craters seem to have quite dark floors.

In contrast, the high-resolution polar cap frames 7N14 to 7N20 suggest a more uniformly coated surface whose brightness variations are mostly due to the effects of illumination upon local relief. Several craters are visible in each frame, some quite small; but, unlike most other areas of Mars, regions of positive relief are also visible, notably in frames 7N14 and 7N16. Also distinctive in these frames are areas of fine, irregular, quasi-parallel bright boundaries and irregular, shallow depressed regions. In frame 7N14, three such regions lie on the floor of a crater. Other irregular, shallow depressions apparently unrelated to craters appear in frames 7N15 and 7N17. Some of these are tens of kilometers in diameter and have no known counterparts elsewhere in the picture series of either spacecraft.

Finally, in frame 7N19 a curved, scalloped escarpment is seen, forming a boundary between a well-cratered area on its convex side and a relatively crater-free area on its concave side; this feature suggests the large circular structures associated with the mare basins on the moon.

Relationship of terrain to light and dark markings. The contrast of light and dark markings on Mars varies with wavelength, a fact long known from telescopic photography. In violet light, "bright" and "dark" areas are essentially indistinguishable, as they have approximately the same reflectivity. With increasing wavelength, contrast is enhanced as redder areas become relatively brighter. Frame 6N13 (Fig. 6) shows craters in a dark area that have partially bright rims and floors, while craters in bright areas have rim and floor reflectivities similar to the reflectivity of the surroundings. These differences tend to increase the visibility of craters in dark areas, but only in photographs taken in red or green light. West of Meridiani Sinus (frames 6N9 and 6N11), and in some other parts of the planet, there are a number of dark-floored craters within bright areas, which, although otherwise relatively conspicuous, are difficult to see in blue light. The floors of these craters thus exhibit the same general dependence of reflectivity on wavelength that the larger dark areas do.

The distinction between bright and dark areas on the martian surface is generally more obvious in FE than in NE views. At higher resolution, the boundaries tend to become dispersed and indistinct. Exceptions are the sharp northeast and southern boundaries of Meridiani Sinus (frame 6N13) and the east edge of Hellespontus. The clearest structural relationship seen between a dark and a bright area is that of Hellespontus and Hellas (Fig. 12).

Chaotic terrain appears to be lower and to have a somewhat higher reflectivity than adjacent cratered areas. Whether chaotic terrain is extensive enough to comprise any previously identified bright areas remains to be determined.

Some of the classical "oases" observed from the earth have now been identified with single, large, dark-floored craters (such as Juventae Fons, see *4* and Fig. 4) or groups of such craters (such as Oxia Palus, frame 7N5). At least two classical "canals" (Cantabras and Gehon) have been found to coincide with quasi-linear alignment of several dark-floored craters, shown also in frame 7N5 (Fig. 13). As reported elsewhere (*4*), other canals are composed of irregular dark patches. It is probable

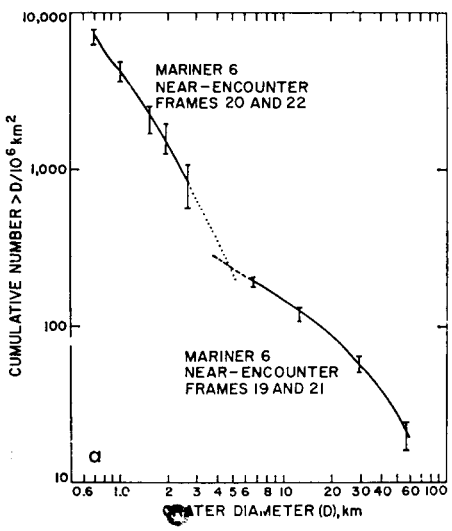

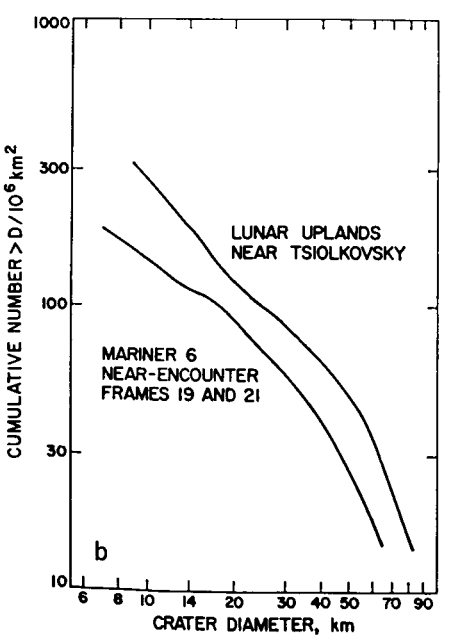

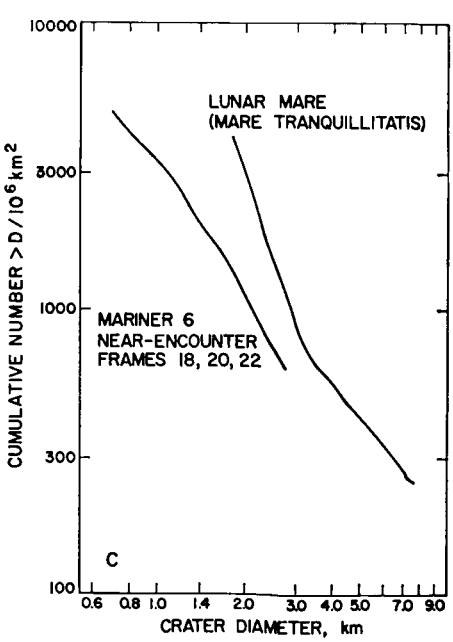

Fig. 9. (a) Preliminary cumulative distribution of crater diameters. Solid curve at right is based upon 256 counted craters in frames 6N19 and 6N21 having diameters $\geqslant$ 7 kilometers. The solid curve at left is based upon 104 counted craters in frames 6N20 and 6N22. The error bars are from counting statistics only ($N^{1/2}$). (b) Comparison of size distribution of large craters on Mars and on the lunar uplands. (c) Comparison of size distribution of small craters on Mars and on a lunar mare.

that most canals will, upon closer inspection, prove to be associated with a variety of physiographic features, and that eventually they will be considered less distinctive as a class.

Some early drawings and "maps" of Mars show a circular bright area within the dark area south of Syrtis Major and east of Sabaeus Sinus, very nearly in the place occupied by a large crater (*4*, fig. 3; *16*). Further comparison of the Mariner pictures with early maps and photographs may prove fruitful in revealing long-term aspects of topographic associations of dark-area boundaries.

It is possible to make a few rough comparisons between the Mariner 6 and 7 pictures and estimates of Mars topographic elevations based on Mariner occultations (*13*), Earth-based radar measurements (*17*), or CO_2 equivalent-width spectral measurements (*18*).

The long stretch of cratered terrain in Deucalionis Regio (Fig. 6) is located on what Earth-based radar and CO_2 measurements both suggest to be a very gradual slope rising westward. Here, at least, cratered terrain is not restricted to regionally high or to regionally low areas; like dark and light areas, it may not exhibit any particular correlation with planetary-scale relief.

The chaotic terrain viewed in Mariner 6 NE frames occurs in what appears to be the topographically lowest area surveyed by the spacecraft, if Earth-based CO_2 measurements are correct. Thus, it is at least possible that chaotic terrain is related in some consistent way to planetary-scale relief.

Mariner 7's occultation point occurred near Hellespontica Depressio, near latitude 55°S, longitude 20°E. A very low surface pressure was measured there, suggesting highly elevated terrain. If Hellespontica Depressio is elevated, Hellespontus may be also. This relationship would be consistent with the impression gained from the Mariner pictures that the floor of Hellas, with its featureless terrain, is a local basin rimmed by higher areas.

Inferences concerning Processes and Surface History

The features observed in the Mariner 6 and 7 pictures are the result of both present and past processes; therefore, they provide the basis of at least limited conjecture about those processes and their variations through time. In this section we consider the implications of (i) the absence of Earth-like tectonic features; (ii) the erosion, blanketing, and secondary modification evidenced in the three principal terrains; and (iii) the probable role of equilibrium between CO_2 solid and vapor in the formation of features of the south polar cap. We also consider the possible role of equilibrium between H_2O solid and vapor as an explanation of the diurnal brightenings observed in the FE photographs and biological implications.

Significance of the absence of Earth-like forms. The absence of Earth-like tectonic features on Mars indicates that, for the time period represented by

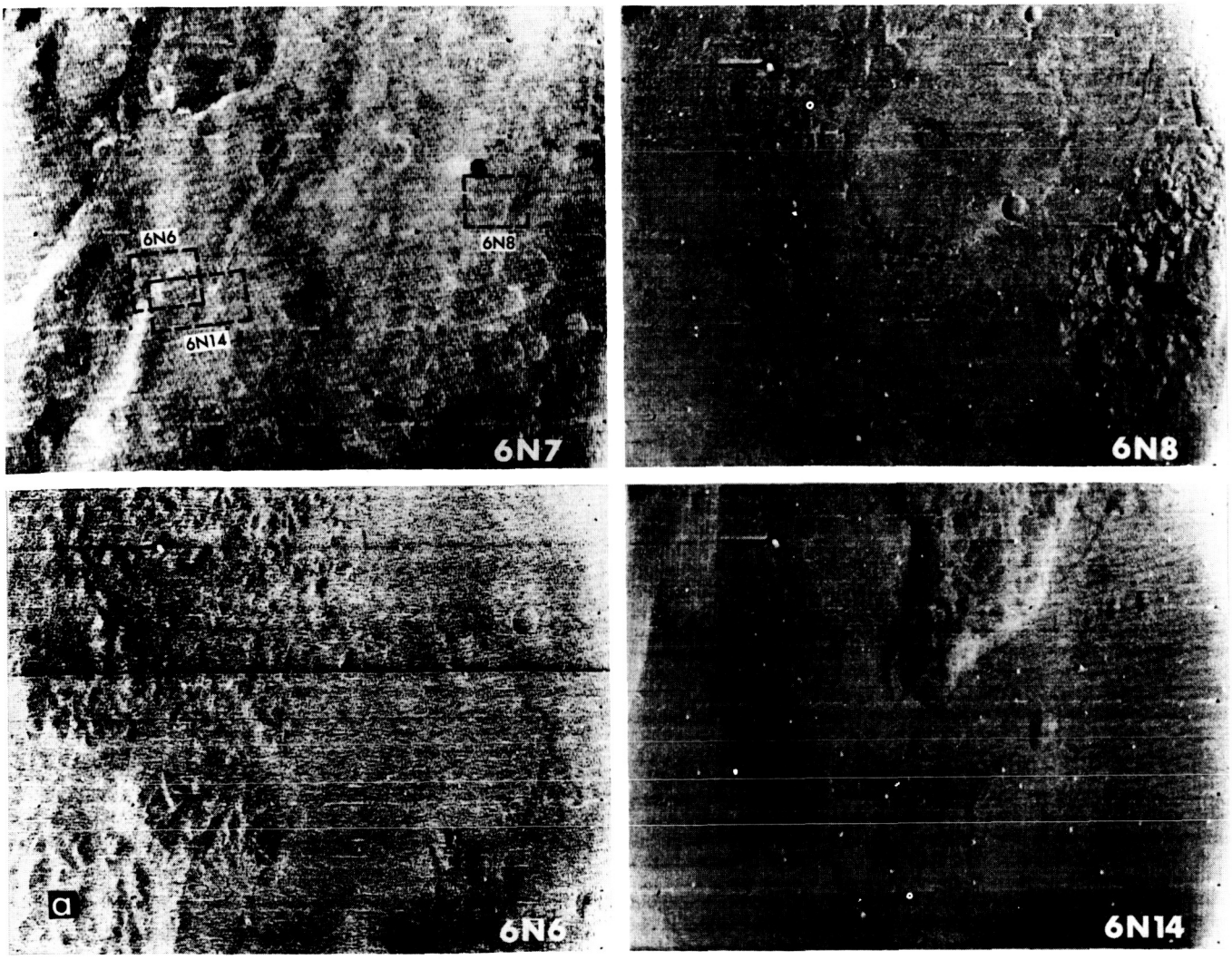

Fig. 10. (a) Examples of chaotic terrain. The approximate locations of the camera-B views inside camera-A frame 6N7 are shown by the dashed rectangles. North is approximately at the top. (b) Example of possible chaotic terrain. The lighter color and the absence of craters suggest that large parts of the right-hand half of this camera-A view may consist of chaotic terrain. (c) Example of chaotic terrain. The location of frame 6N14 inside frame 6N15 is shown by the solid rectangle.

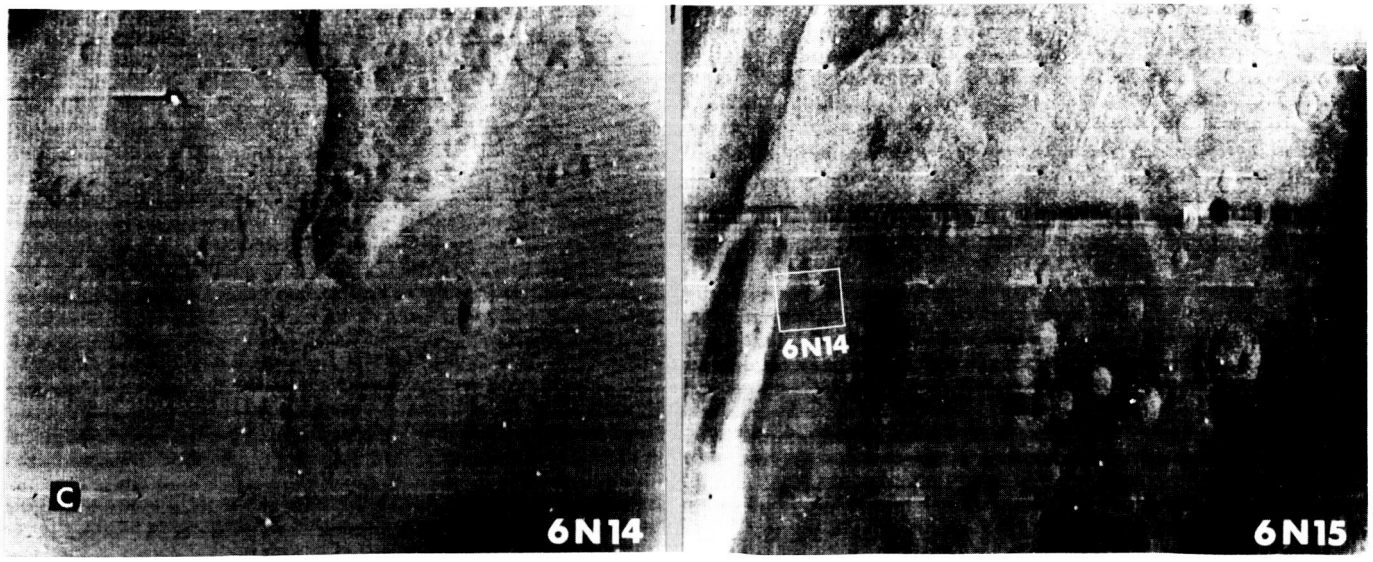

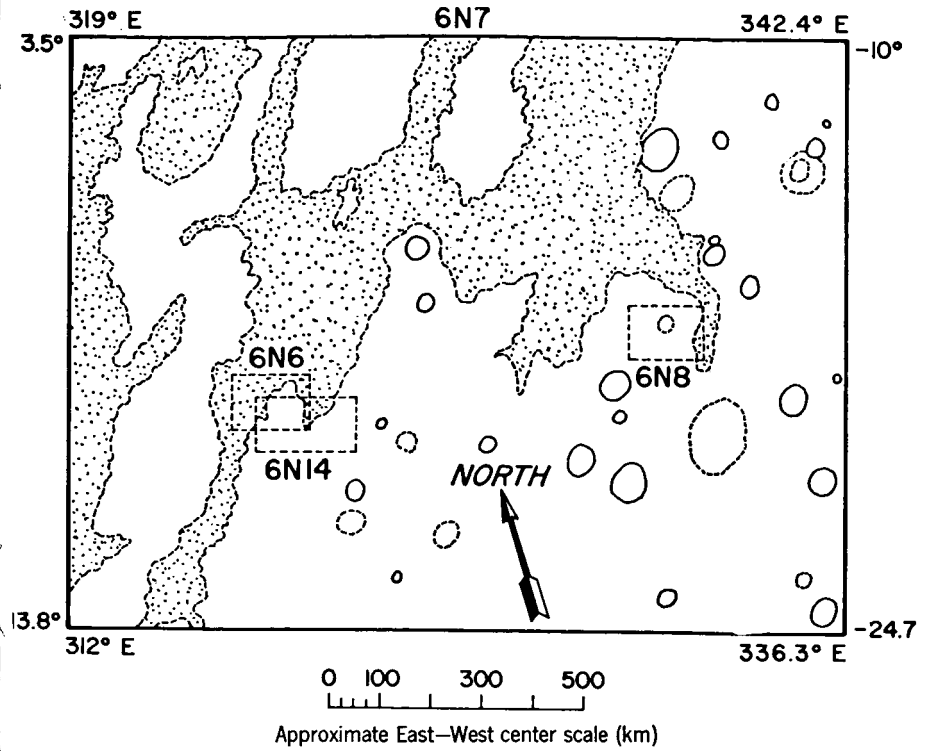

Fig. 11. Interpretive drawing showing the possible extent of chaotic terrain in frame 6N7.

the present large martian topographic forms, the crust of Mars has not been subjected to the kinds of internal forces that have modified, and continue to modify, the surface of the earth.

Inasmuch as the larger craters probably have survived from a very early time in the planet's history, it is inferred that Mars's interior is, and probably has always been, much less active than the earth's (*19*). Furthermore, a currently held view (*20*) is that the earth's dense, aqueous atmosphere may have formed early, in a singular event associated with planetary differentiation and the origin of the core. To the extent, therefore, that surface tectonic features may be related in origin to the formation of a dense atmosphere, their absence on Mars independently suggests that Mars never had an Earth-like atmosphere.

Age implications of cratered terrains. At present, the ages of martian topographic forms can be discussed only by comparison with the moon. Both the moon and Mars exhibit heavily cratered and lightly cratered areas, which evidently reflect in each case regional differences in the history of, or the response to, meteoroidal bombardment over the total life-span of the surfaces. The existence of a thin atmosphere on Mars may have produced recognizable secondary effects in the form and size distribution of craters, by contrast with the moon, where a significant atmosphere has presumably never been present. To the extent that relative fluxes of large objects impinging upon the two bodies can be determined, or a common episodic history established, a valid age comparison may be hoped for, except in the extreme case of a saturated cratered surface, where only a lower limit to an age can be found.

It is a generally accepted view that the present crater density on the lunar uplands could not have been produced within the 4.5-billion-year age of the solar system had the bombardment rate been no greater than the estimated present rate; that is, the inferred minimum age is already much greater than is considered possible. Indeed, it is found that even the sparsely cratered lunar maria would have required about a billion years to attain their present crater density. Unless this discrepancy is somehow removed by direct measurements of the crystallization ages of returned samples of lunar upland and mare materials, the previously accepted implication of an early era of high bombardment followed by a long period of bombardment at a drastically reduced rate will presumably stand.

In the case of Mars, a bombardment rate per unit area as much as 25 times that on the moon has been estimated (*21*). However, even this would still seem to require at least several billion years to produce the density of large craters that is seen on Mars in the more heavily cratered areas (*19*). Thus these areas *could also be primordial.* Further, were these areas to have actually been bombarded at a constant rate for such a time, at least a few very recent, large craters should be visible, including secondary craters and other local effects. Instead, the most heavily cratered areas seem relatively uniform with respect to the degree of preservation of large craters, with no martian Tycho or Copernicus standing out from the rest. This again suggests an early episodic history rather than a continuous history for cratered martian terrain, and increases the likelihood that cratered terrain is primordial.

If areas of primordial terrain do exist on Mars, an important conclusion follows: these areas have never been subject to erosion by water. This in turn reduces the likelihood that a dense, Earth-like atmosphere and large, open bodies of water were ever present on the planet, because these would almost surely have produced high rates of planet-wide erosion. On the earth, no topographic form survives as long as 10^8 years unless it is renewed by uplift or other tectonic activity.

Implications of modification of terrain. Although erosional and blanketing processes on Mars have not been strong enough to obliterate large craters within the cratered terrains, their effects are easily seen. On frames 6N19 and 6N21 (Fig. 6), even craters as large as 20 to 50 kilometers in diameter appear scarce by comparison with the lunar uplands [a feature originally noted by Hartmann (*19*) on the basis of the Mariner 4 data], and the scarcity of smaller craters is marked. The latter have a relatively fresh appearance, however, which suggests an episodic history of formation, modification, or both. Such a history seems particularly indicated by the apparently bimodal crater frequency distribution of Fig. 9.

Marked erosion, blanketing, and other surface processes must have been operating almost up to the present in the areas of featureless and chaotic terrains; only this could account for the absence of even small craters there. These processes may not be the same as those at work on the cratered terrains, because large craters have also been erased. The cratered terrains obviously have *never been* affected by such

processes; this indicates an enduring geographic dependence of these extraordinary surface processes.

The chaotic terrain gives a general impression of collapse structures, suggesting the possibility of large-scale withdrawal of substances from the underlying layers. The possibility of permafrost some kilometers thick, and of its localized withdrawal, may deserve further consideration. Magmatic withdrawal or other near-surface disturbance associated with regional volcanism might be another possibility, but the apparent absence of extensive volcanic terrains on the surface would seem to be a serious obstacle to such an interpretation. It may also be that chaotic terrain is the product either of some unknown intense and localized erosional process or of unsuspected local sensitivity to a widespread process.

Carbon dioxide condensation effects. The Mariner 7 NE pictures of the polar cap give no direct information concerning the material or the thickness of the polar snow deposit, since the observed brightness could be produced by a very few milligrams per square centimeter of any white, powdery material. However, they do provide important indirect evidence as to the thickness of the deposit and, together with other known factors, may help to establish its composition.

The relatively normal appearance of craters on the polar cap in the high-resolution frames, and the existence on these same frames of topographic relief unlike that so far recognized elsewhere on the planet, suggest that some of the apparent relief may be due to variable thicknesses of snow, perhaps drifted by wind. If it is, local thicknesses of at least several meters are indicated.

The structure of the polar cap edge shows that evaporation of the snow is strongly influenced by local slopes—that is, by insolation effects rather than by wind. On the assumption that the evaporation is entirely determined by the midday radiation balance, when the absorbed solar power exceeds the radiation loss at the appropriate frost-point temperature, one may estimate the daily evaporation loss from the cap. We find the net daily loss to be about 0.8 gram per square centimeter in the case of CO_2, although the loss is reduced by overnight recondensation. In the case of H_2O, the loss would be about 0.08 gram per square centimeter, and it would be essentially irreversible because H_2O is a minor constituent whose deposition is limited by diffusion.

Since the complete evaporation of the cap at a given latitude requires many days, we may multiply the above rates by a factor between 10 and 100, obtaining estimates for total cap thickness of tens of grams per square centimeter for CO_2 and several grams per square centimeter for H_2O, on the assumption that the cap is composed of one or the other of these materials. The estimate for CO_2 is quite acceptable, but that for H_2O is unacceptable because of the problem of transporting such quantities annually from one pole to the other at the observed vapor density (*22*). For the remainder of this discussion we assume the polar cap to be composed of CO_2, with a few milligrams of H_2O per square centimeter deposited throughout the layer.

Several formations have been observed which suggest a tendency for snow to be preferentially removed from low areas and deposited on high areas, contrary to what might be expected under quiescent conditions (*23*). These formations include craters with dark floors and bright rims, prominent central peaks in some craters, and irregular depressed areas (frames 7N14, 15, and 17). While such effects might result simply from wind transport of solid material, it is also possible that interchange of solid and vapor plays a role.

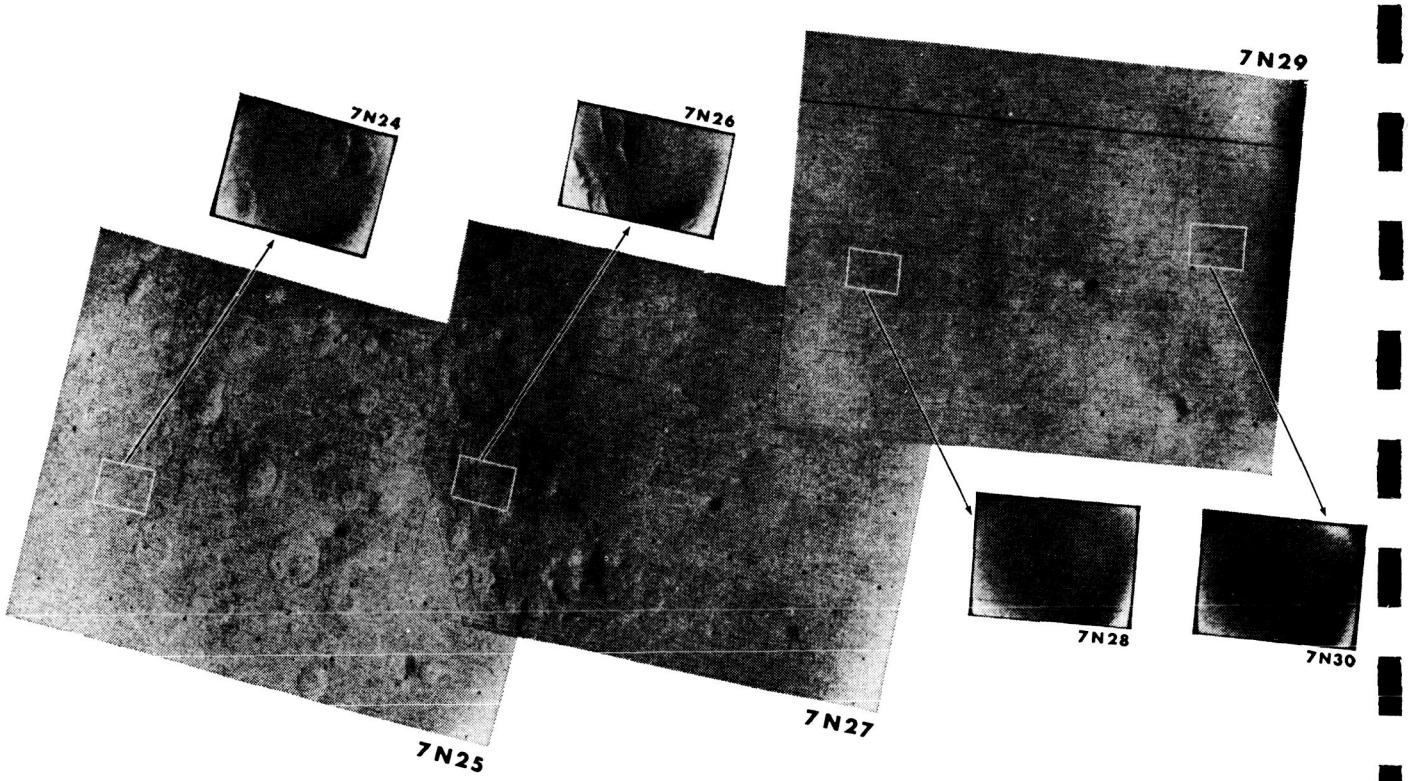

Fig. 12. Composite of seven Mariner 7 frames, showing the cratered dark area Hellespontus, the ridged, broken boundary between Hellespontus and Hellas, and the featureless terrain of the bright, circular "desert" Hellas. Large-scale variations in contrast are suppressed by AGC. Lighting conditions are similar to those of Fig. 6, frames 7N17 to 7N21. North is approximately toward the top.

The adiabatic lapse rate of the polar atmosphere is about 6°K per kilometer, as compared to a frost-point lapse rate of about 1°K per kilometer. Therefore, adiabatic heating or cooling of martian air blowing across sloping terrain may result in evaporation of low-lying solid and precipitation over high areas. The rate is determined by atmospheric density, latent heat, difference in elevation, lateral scale of relief, wind speed, turbulent-layer thickness, interfacial heat transfer, and net adiabatic gradient. For example, a wind of 20 meters per second blowing across a crater 20 kilometers in diameter and 0.5 kilometer deep, with a turbulent layer only 100 meters thick, could differentially deposit about 0.1 gram per square centimeter per day. Since this process would be effective during the entire time that snow is on the ground, several tens of grams per square centimeter could become systematically redistributed in the course of a few hundred days. A speculative possibility is that such a process, or perhaps merely a sustained accumulation of snow in a particular topographic "trap," occasionally results in sufficient accumulation during the winter to survive summer evaporation. The increased albedo might then lead to a permanent accumulation of CO_2 snow within that topographic feature—that is, to formation of a martian "ice field." The very prominent snow-covered central peaks of some of the small craters located at high latitude might conceivably be the sites of such permanent deposits of solid CO_2. The permanent part of the north polar cap is presumably such a structure (*22*).

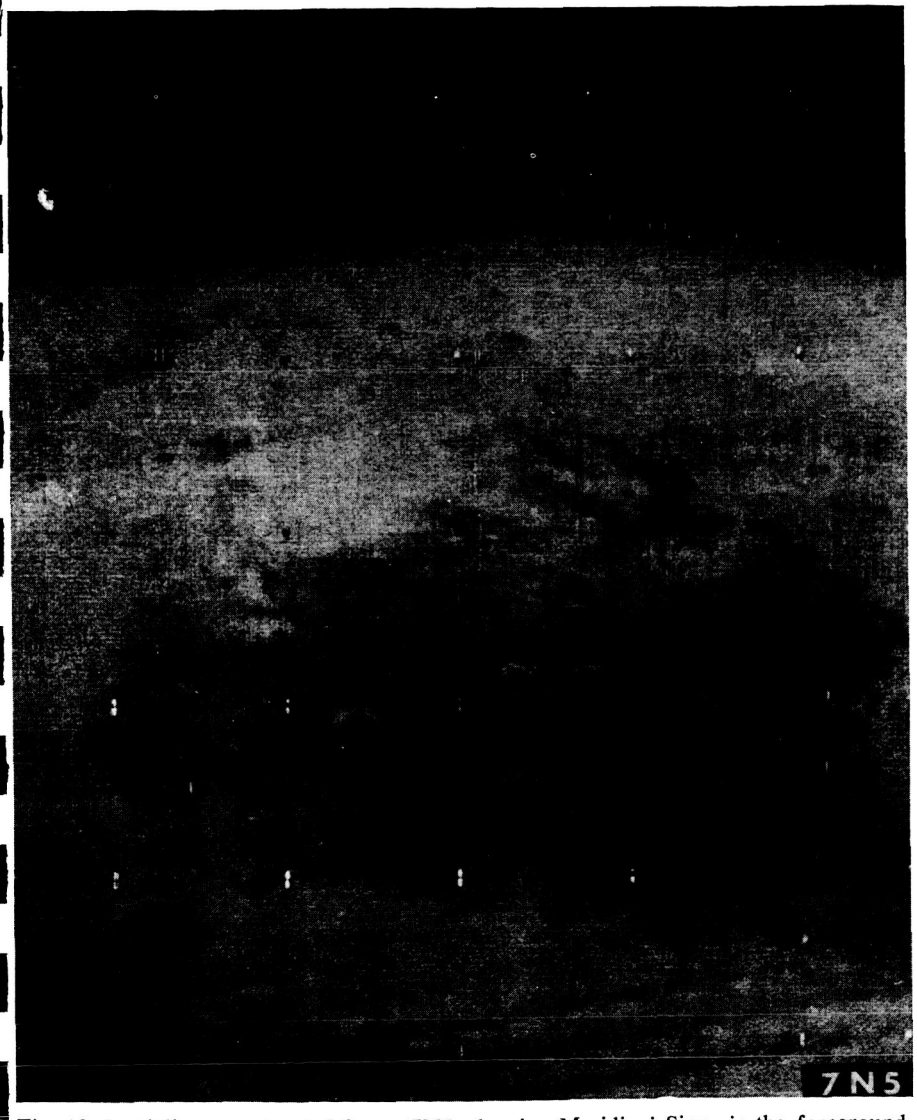

Fig. 13. Partially reconstructed frame 7N5, showing Meridiani Sinus in the foreground. The "oasis" Oxia Palus projects into the picture from the left edge, near the limb. Note the asymmetric shading in several craters in Meridiani Sinus; the isolated, dark-floored craters in surrounding bright areas; and the crater complex in Oxia Palus. The view is approximately toward N 20°W. The banded appearance of the sky area is an artifact of the picture processing.

Water: processes suggested by brightening phenomena. Several of the brightening and haze phenomena described above could be related either to formation of H_2O frost on the surface or to formation of H_2O ice clouds in the atmosphere. In most of these instances, however, the phenomena could equally well be explained by condensation of CO_2. This is true of the bright tongues and polar hood in the north polar region, of the cloud-like features observed over and near the south polar cap, and of the limb hazes observed in tropical latitudes and over the Mare Hadriaticum and Ausonia regions.

On the other hand, the brightenings in the Nix Olympica, Tharsis, Candor, and Tractus Albus regions cannot be explained by CO_2 condensation because their complete topographic control requires that they be on or near the surfaces where temperatures are well above the CO_2 frost point. An explanation of these phenomena in terms of H_2O condensation processes also faces serious difficulties, however. Most of the region is observed to brighten during the forenoon, when the surface is hotter than either the material below or the atmosphere above, so that water vapor could not diffuse toward the surface and condense on it, either from above or below. Thus a surface ice-frost is very unlikely. A few features in the area, parts of the "W-cloud," for example, are observed to brighten markedly during the late afternoon, where H_2O frost could form on the surface if the air were sufficiently saturated. These features are not observed, from the earth, to be bright in the early morning, but a thin layer of H_2O frost persisting through the night would evaporate almost immediately when illuminated by the early morning sun, provided the air were then sufficiently dry. Under these conditions, the behavior of the "W-cloud" could be due to frost.

The diurnal behavior of the bright regions throughout this part of Mars is consistent with a theory of convective H_2O ice clouds, but the absence of any cloud-like morphology and the clear topographic detail observed at the highest resolution available (frame 7F76) render this explanation questionable. Even very light winds of 5 meters per second would produce easily observable displacements of the order of 100 kilometers in the course of the more than one-fourth of the Mars day during

which these regions were continuously observed by each spacecraft. Since condensation and evaporation processes are slow at Mars temperatures and pressures, some observable distortion and streakiness due to these displacements should be seen in clouds, even if they are orographically produced. No such distortions or streakiness are observed.

An additional difficulty with an explanation of these phenomena in terms of H_2O condensation lies in the relatively rapid removal of water from the local surface. Water vapor evolved from the surface during the daytime would quickly be transported upward through a deep atmospheric layer by thermal convection, and most of it would be removed from the source region. Local permafrost sources should be effectively exhausted by this mechanism within a few hundred years at most, unless somehow replenished. Since most of this region lies near the equator, where seasonal temperature variations are small, it is difficult to see how any significant seasonal replenishment from the atmosphere could take place. The possibility of replenishment from a subsurface source of liquid water is not considered here.

In summary, in our examination of the data thus far, we see no strong indications of H_2O processes involving vapor and ice. The brightenings seen in the tropics and subtropics at far-encounter are not easily explained by a mechanism involving H_2O. On the other hand, we have no satisfactory alternative explanation for these phenomena. Perhaps detailed exploration of these regions by the Mariner '71 orbiters will provide the answer.

Biological inferences. No direct evidence suggesting the presence of life on Mars has been found in the pictures. This is not surprising, since martian life, if any, would probably be microbial and undetectable at a resolution of 300 meters. Although inconclusive on the question of martian life, the photographs are informative on at least three subjects of biological interest: the general nature of the martian maria, the present availability of water, and the availability of water in the past.

One of the most surprising results so far of the TV experiment is that nothing in the pictures suggests that the dark areas, the sites of the seasonal darkening wave, are more favorable for life than other parts of the planet. On the contrary, it would now appear that the large-scale surface processes implied by the chaotic and featureless terrains may be of greater biological interest than the wave of darkening. We reiterate that these are preliminary conclusions; it may be that subtle physiographic differences between dark and bright regions will become evident when photometrically corrected pictures are examined.

With regard to the availability of water, the pictures so far have not revealed any evidence of geothermal areas. We would expect such areas to be permanently covered with clouds and frost, and these ought to be visible on the morning terminator; no such areas have been seen. A classically described feature of the polar cap which has been interpreted as wet ground—the dark collar—has likewise not been found. Other locales which have been considered to be sites of higher-than-average moisture content are those which show diurnal brightening. A number of such places have been observed in the pictures, but on close inspection the brightening appears not to be readily interpretable in terms of water frosts or clouds. Pending their definite identification, however, the brightenings should be considered possible indications of water.

The results thus reinforce the conclusion, drawn from Mariner 4 and ground-based observations, that scarcity of water is the most serious limiting factor for life on Mars. No terrestrial species known to us could live in the dry martian environment. If there is a permafrost layer near the surface, or if the small amount of atmospheric water vapor condenses as frost in favorable sites, it is conceivable that, by evolutionary adaptation, life as we know it could use this water and survive on the planet. In any case, the continued search for regions of water condensation on Mars will be an important task for the 1971 orbiter.

The past history of water on Mars is a matter of much biological interest. According to current views, the chemical reactions which led to the origin of life on the earth were initiated in the reducing atmosphere of the primitive earth. These reactions produced simple organic compounds which were precipitated into the ocean, where they underwent further reactions that eventually yielded living matter. The pictorial evidence raises the question of whether Mars ever had enough water to sustain an origin of life. If the proportion of water outgassed relative to CO_2 is the same for Mars as for the earth, then, from the mass of CO_2 now in the martian atmosphere, it can be estimated that Mars has produced sufficient water to cover the planet to a depth of a few meters. The question is whether anything approaching this quantity of water was ever present on Mars in the liquid state.

The existence of cratered terrains and the absence of Earth-like tectonic forms on Mars clearly implies that the planet has not had oceans of terrestrial magnitude for a very long time, possibly never. However, we have only very rough ideas of how much ocean is required for an origin of life, and of how long such an ocean must last. An upper limit on the required time, based on terrestrial experience, can be derived from the age of the oldest fossils. $>3.2 \times 10^9$ years (*24*). Since these fossils are the remains of what were apparently highly evolved microorganisms, the origin of life must have taken place at a much earlier time, probably during the first few hundred million years of the earth's history. While one cannot rule out, on the basis of the TV data, the possibility that a comparably brief, aqueous epoch occurred during the early history of the planet, it must be said that the effect of the TV results so far is to diminish the a priori likelihood of finding life on Mars. However, it should be noted that if Mars is to be a testing ground for our notions about the origin of life, we must avoid using these same notions to disprove in advance the possibility of life on that planet.

Potentialities of the Data

Careful computer restoration of the pictures, starting with data recovered from six sequential playbacks of the near-encounter analog tapes, will be carried out over the next several months. This further processing will greatly enhance the completeness, appearance, and quantitative usefulness of the pictures. While it is not yet certain whether the desired 8-bit relative photometric accuracy can be attained, there are reasonable grounds for thinking that much new information bearing on the physiography, meteorology, geography, and other aspects of Mars will ultimately be obtained from the pictures. Some of the planned uses of the processed data are as follows.

Stereoscopy. Most of the NE wide-

angle pictures contain regions of two-picture overlap, and a few contain regions of three-picture overlap. These areas can be viewed in stereoscopic vision in the conventional manner of aerial photography. Preliminary tests on pictures of the south polar cap (frames 7N17 and 7N19) indicate that measurement of crater depth, central-peak height, and crater-rim height is possible. However, accuracy can be estimated for the elevation determinations at this time.

Planetary radii. Geometric correction of the FE photographs should make it possible to determine the radius of Mars as a function of latitude, and possibly of longitude. The geometric figure of Mars has been historically troublesome because of inconsistencies between the optical and the dynamical oblateness, a discrepancy amounting to some 18 kilometers in the value for the difference of the equatorial and polar radii. It is possible that the darkening of the polar limb observed by Mariners 6 and 7, if it is a persistent phenomenon, might have systematically affected the earlier telescopic measurements of the polar diameter more than irradiation has, giving too large a value for the optical flattening. However, this cannot explain the large flattening obtained from surface-feature geodesy (*25*). Although a fairly reliable figure for the polar flattening may be obtained from the Mariner data, it is unlikely that the actual radii will be determined with an accuracy greater than several kilometers because of the relatively low picture-element resolution in these frames and the difficulty in locating the limb.

Cartography. The large number of craters found on the surface of Mars makes it feasible to establish a control net which uses topographic features as control points, instead of surface markings based on albedo differences. This net should provide the basic locations for compiling a new series of Mars charts. The NE pictures, which cover 10 to 20 percent of the area of the planet, will constitute the basic material for detailed maps of these areas.

Satellites. We hope to detect the larger of Mars's satellites, Phobos, in two of the Mariner 6 FE pictures taken when Phobos was just beyond the limb of the planet. The satellite should have moved between the two frames by about ten picture elements, and should appear as a "defect" that has moved by this amount between the two pictures. If Phobos itself is not visible, its shadow (again detectable by its motion) should be. The shadow will be some five picture elements across and will have a photometric depth of about 10 percent. If the photometric depth of the shadow can be measured accurately, we can determine the projected area (and hence the diameter) of the satellite. A similar method has been used to measure the diameter of Mercury during solar transits.

Photometric studies. We expect to derive the photometric function for each color, combining data from the two spacecraft. Observations by the current Mariners were made near 25°, 35°, 45°, and 80° phase. Since data obtained from the earth can be used to establish the absolute calibration at the smaller phase angles, we will also be able to relate the 80°-phase data to Earth-based observations, thus doubling the range over which the phase function is determined. This information should then make possible the determination of crater slopes. Agreement for areas of overlap between different filters and between A-camera and B-camera frames can be used to check the validity of the results and possibly to measure and correct for atmospheric scattering.

The reciprocity principle may be useful in testing quantitatively for diurnal changes in the FE pictures. Such changes might include dissipation of frost or haze near the morning terminator and formation of afternoon clouds near the limb.

Overlap areas in NE pictures can be used to obtain approximate colors, even though these areas are seen at different phase angles in each color. In addition, color-difference or color-ratio pictures may be useful in identifying local areas of anomalous photometric or colorimetric behavior. Camera-A digital pictures obtained by Mariner 7 in late far-encounter will be very useful for making color measurements.

Comparison of pictures with radar-scattering and height data. The reflection coefficient of the martian surface for radar waves of decimeter wavelength shows marked variations at a given latitude as a function of longitude. Even though few of the areas of Mars so far observed by radar are visible at close range, some correlation of topography with radar reflectivity may become apparent upon careful study. Clearly, the Mariner pictures will become steadily more valuable in this connection as more radar results and other height data become available.

Effects on Mariner '71

The distinctive new terrains revealed in the Mariner 6 and 7 pictures, the relatively small fraction (10 to 20 percent) of the surface so far viewed even at moderate (A-camera) resolution, and the tantalizing new evidence of afternoon-brightening phenomena all emphasize the importance of an exploratory, adaptive strategy in 1971 as opposed to a routine mapping of geographic features. The fact that each of three successive Mariner spacecraft has revealed a new and unexpected topography strongly suggests that more surprises (perhaps the most important ones) are still to appear.

A primary objective should be to view nearly all of the visible surface at A-camera resolution (1-kilometer pixel spacing), and to inspect selected typical areas at higher resolution, very early in the 90-day orbiting period. The true extent and character of cratered, chaotic, and featureless terrains, and of any new kinds of terrain, can thus be determined and correlated with classical light and dark areas, with regional height data, and so on.

A second objective should be to search for and examine, in both spatial and temporal detail, those areas which suggest the local presence of water, through the afternoon-brightening phenomena, morning frosts or fogs, or other behavior not now recognized. Certainly the known "W-cloud" areas, Nix Olympica, and other, similar areas known from Earth observation take on a new interest by virtue of the Mariner 6 and 7 results.

The complex structure found in the south polar cap calls for further examination, particularly with respect to separation of its more permanent features from diurnally or seasonally varying ones. The sublimation of the cap should be carefully followed, so as to detect evidence of variations in thickness of the deposit and especially evidence of the possible existence of permanent deposits. Study of the north polar cap at close range should also be exceedingly interesting.

Effects on Viking '73

If the effects of the Mariner 6 and 7 results on Mariner '71 are substantial, they at least do not require a change of instrumentation, only one of mission strategy. This may not be true of the

effects on Viking '73. The discovery of so many new, unexpected properties of the martian surface and atmosphere adds a new dimension to the problem of selecting the most suitable landing site and may make Viking even more dependent on the success of Mariner '71 than has been supposed. Furthermore, since so much new information is revealed through the tenfold step in resolution afforded by the B-camera frames, a further substantial increase in resolution, not available to Mariner '71, may have to be incorporated in Viking in order to examine even more closely the fine-scale characteristics of various terrain types before a landing site is chosen.

Summary and Conclusions

Even in relatively unprocessed form, the Mariner 6 and 7 pictures provide fundamental new insights concerning the surface and atmosphere of Mars. Several unexpected results emphasize the importance of versatility in instrument design, flexibility in mission design, and use of an adaptive strategy in exploring planetary surfaces at high resolution.

The surface is clearly visible in all wavelengths used, including the blue. No blue-absorbing haze is found.

Thin, patchy, aerosol-scattering layers are present in the atmosphere at heights of from 15 to 40 kilometers, at several latitudes.

Diurnal brightening in the "W-cloud" area is seen repeatedly and is associated with specific topographic features. No fully satisfactory explanation for the effect is found.

Darkening of the polar cap in a band near the limb is clearly seen in FE pictures and is less distinctly visible in one or two NE frames. Localized, diffuse bright patches are seen in several places on and near the polar cap; these may be small, low clouds.

Widespread cratered terrain is seen, especially in dark areas of the southern hemisphere. Details of light-dark transitions are often related to local crater forms. Asymmetric markings are characteristic of craters in many dark areas; locally, these asymmetries often appear related, as if defined by a prevailing wind direction.

Two distinct populations of primary craters are present, distinguished on the basis of size, morphology, and age. An episodic surface history is indicated.

In addition to the cratered terrain anticipated from Mariner 4 results, at least two new, distinctive topographic forms are seen: chaotic terrains and featureless terrains. The cratered terrain is indicative of extreme age; the two new terrains both seem to require the present-day operation of especially active modifying processes in these areas. When seen at closer range, the very bright, streaked complex found in the Tharsis-Candor region may reveal yet another distinctive topographic character. Because of the afternoon-brightening phenomena long known here, this area provides a fascinating prospect for further exploration in 1971.

No tectonic and topographic forms similar to terrestrial forms are observed.

Evidences of both atmosphere-surface effects and topographic effects are seen on the south polar cap. At the cap edge, where the "snow" is thinnest, strong control by solar heating, as affected by local slopes, is indicated. Crater visibility is greatly enhanced in this area.

On the cap itself, intensity variations suggestive of variable "snow" thickness are seen. These may be caused by wind-drifting of the snow or by differential exchange of solid and vapor, or by both.

Snow thicknesses here of several grams or several tens of grams per square centimeter are inferred if the snow material is H_2O or CO_2, respectively. The possibility that the material is H_2O seems strongly ruled out on several grounds.

Variable atmospheric, and atmosphere-surface, effects are seen at high northern latitudes; these effects include the polar "hood" and bright, diurnally variable circumpolar patches.

Several classical features have been successfully identified with specific topographic forms, mostly craters or crater remnants.

The findings are inconclusive on the question of life on Mars, but they are relevant in several ways. They support earlier evidence that scarcity of water, past and present, is a serious limiting factor for life on the planet. Nothing so far seen in the pictures suggests that the dark regions are more favorable for life than other parts of Mars.

References and Notes

1. R. B. Leighton, B. C. Murray, R. P. Sharp, J. D. Allen, R. K. Sloan, *Science* **149**, 627 (1965).
2. ———, "Mariner IV Pictures of Mars," *Tech. Rep. Jet Propul. Lab. Calif. Inst. Technol. No. 32-884* (1967), pt. 1.
3. R. B. Leighton, N. H. Horowitz, B. C. Murray, R. P. Sharp, A. G. Herriman, A. T. Young, B. A. Smith, M. E. Davies, C. B. Leovy, *Science* **165**, 684 (1969).
4. ———, *ibid.*, p. 787.
5. The 1/7 digital TV data for the central 20 percent of each line were replaced by encoded data from other on-board experiments. In this region, coarser, 1/28 digital data (6-bit-encoded for every 28th pixel), stored on the analog tape recorder, were available (see Fig. 2).
6. D. G. Montgomery, in preparation.
7. This procedure is semiautomatic, subject to hand correction by the computer operator as necessary.
8. G. E. Danielson, in preparation.
9. For each spacecraft, this must be done for each filter of each camera and for all calibration temperatures, and the results must be corrected to the observed flight temperature.
10. Most of the real-time FE A-camera digital pictures were of no value because little or none of the image projected outside the central 20 percent blank area.
11. E. C. Slipher, *Pubi. Astron. Soc. Pacific* **49**, 137 (1937).
12. J. B. Pollack and C. Sagan, *Space Sci. Rev.* **9**, 243 (1969).
13. A. J. Kliore, G. Fjeldbo, B. Seidel, in preparation.
14. M. J. Trask, *Tech. Rep. Jet Propul. Lab. Calif. Inst. Technol. No. 32-800* (1966), p. 252.
15. G. E. Fischbacher, L. J. Martin, W. A. Baum, "Martian Polar Cap Boundaries," final report under Jet Propulsion Laboratory contract 951547, Lowell Observatory, May 1969.
16. E. Burgess, private communication.
17. R. M. Goldstein, private communication; C. C. Councilman, private communication.
18. M. J. S. Belton and D. M. Hunten, *Science*, in press.
19. W. K. Hartmann, *Icarus* **5**, 565 (1966).
20. D. L. Anderson and R. A. Phinney, in *Mantles of the Earth and Terrestrial Planets*, S. K. Runcorn, Ed. (Interscience, New York, 1967), pp. 113–126.
21. E. Anders and J. R. Arnold, *Science* **149**, 1494 (1965).
22. R. B. Leighton and B. C. Murray, *ibid.* **153**, 136 (1966).
23. B. T. O'Leary and D. G. Rea, *ibid.* **155**, 317 (1967).
24. A. E. J. Engel, B. Nagy, L. A. Nagy, C. G. Engel, G. O. W. Kremp, C. M. Drew, *ibid.* **161**, 1005 (1968); J. W. Schopf and E. S. Barghoorn, *ibid.* **156**, 508 (1967).
25. R. J. Trumpler, *Lick Obs. Bull.* **13**, 19 (1927).

26. We gratefully acknowledge the support and encouragement of the National Aeronautics and Space Administration. An undertaking as complex as that of Mariners 6 and 7 rests upon a broad base of facilities, technical staff, experience, and management, and requires not only money but much individual and team effort to be brought to a successful conclusion. It is impossible to know, much less to acknowledge, the important roles played by hundreds of individuals. We are deeply appreciative of the support and efforts of H. M. Schurmeier and the entire Mariner 1969 project staff. With respect to the television system, responsibility for the design, assembly, testing, calibration, flight operation, and picture data processing lay with the Jet Propulsion Laboratory. We gratefully acknowledge the contributions of G. M. Smith, D. G. Montgomery, M. C. Clary, L. A. Adams, F. P. Landauer, C. C. LaBaw, T. C. Rindfleisch, and J. A. Dunne in these areas. L. Malling, J. D. Allen, and R. K. Sloan made important early contributions. We are indebted to V. C. Clarke, C. E. Kohlhase, R. Miles, and E. Greenberg for their help in exploiting the flexibility of the spacecraft to achieve maximum return of pictorial data. We are especially appreciative of the broad and creative efforts of G. E. Danielson as Experiment Representative. The able collaborative contributions of J. C. Robinson in comparing Mariner pictures with Earth-based photographs and of L. A. Soderblom and J. A. Cutts in measuring craters are gratefully acknowledged.

Reprinted from
3 October 1969, Volume 166, pp. 98-99

SCIENCE

Mariner 1969: Preliminary Results of the Infrared Radiometer Experiment

G. Neugebauer, G. Münch, S. C. Chase, Jr., H. Hatzenbeler, E. Miner, and D. Schofield

Mariner 1969: Preliminary Results of the Infrared Radiometer Experiment

Abstract. *The thermal energy emitted by Mars was measured in the 8- to 12- and 18- to 25-micrometer bands. The minimum temperature derived for the southern polar cap is 150°K, an indication that the cap is formed by frozen carbon dioxide. No significant temperature fluctuations were detected with a 100-kilometer scale.*

The complement of scientific instruments of the Mariner 6 and 7 spacecrafts included a radiometer specifically designed to measure the energy emitted in two wide wavelength bands of the thermal spectrum of Mars.

A description of the radiometer has been given earlier (*1*). Essentially it consisted of two 1-inch (2.5-cm) refracting telescopes, each with an uncooled bimetallic thermopile detector. The radiometers were mounted on the pointable instrument platform of the spacecraft and were bore-sighted with the narrow-angle television camera (*2*, *3*). The fields of view of both infrared channels were coincident and subtended 0.7 degree at half-peak responsivity. The passbands of channel 1 (8.2 to 12.4 μm) and channel 2 (18 to 25 μm) were defined by interference filters to exclude atmospheric gaseous absorption; consequently, radiation from the surface was measured. The optical train of the radiometer included a rotatable plane mirror which reflected the incident energy into the detector telescopes. Once every 63 seconds the mirror was rotated to view empty space and thus provide a zero energy reference. The planet was viewed by rotating the mirror 90 degrees, observations being taken for 56.7 seconds at intervals of 2.1 seconds. In a third orthogonal mirror position, the instrument measured the thermal energy of a plate, whose temperature was monitored directly by a thermistor every 63 seconds. The radiometer had a dynamic range from approximately 120° to 330°K; channel 1 was selected to emphasize the upper end of this range, while channel 2 was selected to emphasize the lower temperatures. The output over this temperature range was linear in energy and was digitized into 1024 levels. In practice, the detector noise was dominated by the size of the digitization steps.

Data were obtained both in the far-encounter mode, when the spacecraft was at distances exceeding 100,000 km, and during near encounter. The radiometric sensitivity of the units during the flight remained essentially the same as that established in the laboratory calibrations. However, the radiometers were affected by stray light to an extent greater than anticipated.

The energies measured in the near-encounter mode are displayed in Figs. 1 and 2; the corresponding brightness temperatures have been derived on the assumption of unit emissivity of the planetary surface. We now report the data relating to the temperature of the southern polar cap and to the scale of the temperature variations over the surface.

The track of Mariner 7 was chosen to sweep over the south polar cap (*2*). As shown in Fig. 2, the temperature decreased to 225°K when the platform was slewed to latitudes near to, but definitely off, the polar cap. As the track continued southward, the temperature decreased slowly, but around latitude —61 degrees, when the radiometer crossed the boundary of the polar cap, the temperature suddenly dropped below 160°K. As the field of view swept over the cap, the temperature decreased to a minimum of 153°K near the terminator just before the platform was slewed north.

The frost temperature of CO_2 at a vapor pressure of 6.5 mb is 148°K. We interpret the agreement between this value and the observed temperatures, as well as the large change in temperature at the onset of the cap, to provide strong evidence for the polar cap being composed of frozen CO_2. This hypothesis has been discussed by Leighton and Murray (*4*).

The temperatures obtained under the assumption of unit emissivity need not be equal to the actual surface temperature of the polar cap. The TV pictures of Leighton *et al.* (*2*) show bare ground which is not covered by frost within the cap. If only 5 percent of the field of view in the polar cap were filled by sources with a brightness temperature of 200°K, the resultant measured brightness temperatures would be raised by 4°K. A discussion of possible instrumental systematic errors in the measurements is beyond the scope of this report.

It is nevertheless important to point out that the radiometers had a

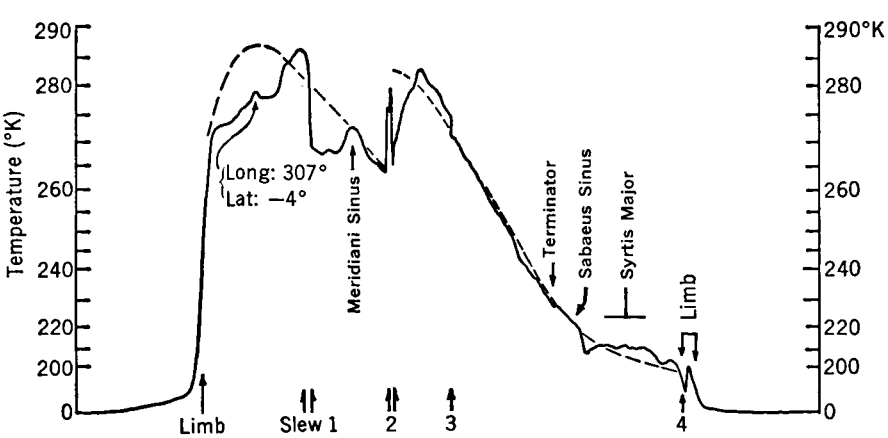

Fig. 1. Temperatures measured in channel 1 (8.5 to 12.4 μm) of the infrared radiometer in Mariner 6 during near encounter (solid curve). The times when the platform was slewed and when prominent planetary features were crossed are indicated. The dashed line represents the cooling curve of a homogeneous solid, with thermal inertia $(K\rho c)^{1/2} = 4 \times 10^{-3}$ cal/cm^2 sec$^{1/2}$ per degree Kelvin, and albedo of 0.85, for local times corresponding to the measured points.

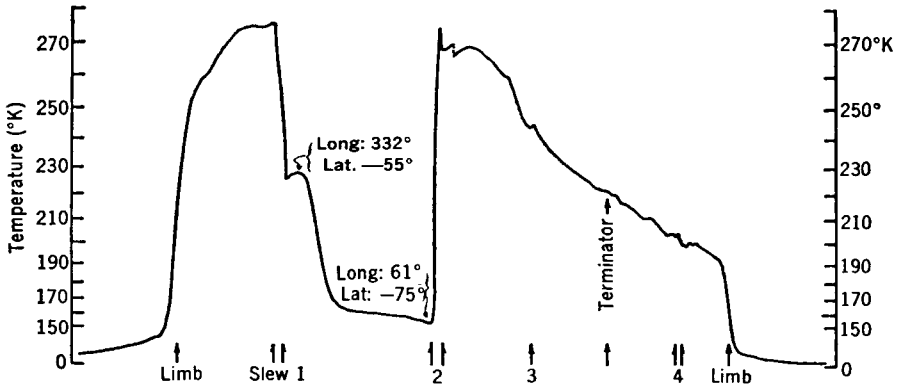

Fig. 2. Temperatures measured in channel 2 (18 to 25 μm) of the infrared radiometer in Mariner 7 during near encounter, in a scale proportional to energy. The times when the platform was slewed and the crossing of prominent planetary features are indicated. The extreme planetocentric coordinates of the swath through the polar cap are also shown.

significant response to off-axis sources. For example, the response of channel 2 of the radiometer aboard Mariner 7 to a point source at a distance of 12 degrees from axis was only 0.3 percent of that for the same source on axis. Because of the large solid angles subtended, however, the extended wings beyond a central area 1 degree in diameter contributed 27 percent of the total response of a measurement of the energy radiated by an isothermal source filling the entire object space. The correction to the minimum temperature measured in Mariner 7, due to the extended response of channel 2 and based on a model temperature distribution over the planetary surface, amounts to about —3°K. At low temperatures, the correction for off-axis radiation was greater for channel 1 than for channel 2. A more refined analysis of the systematic effects, based on data obtained before near encounter and during passage across the limb, is in process. All systematic errors that have been thought of, however, have the effect that the observed temperatures are higher than the true value.

The Mariner flights provided the opportunity to measure temperatures with an areal resolution approximately ten times that obtainable from the earth. Although transitions between dark (maria) and light (desert) areas appear well defined in the data, there were no sharp changes in temperature exceeding 1°K in contiguous fields of view (50 km at closest approach). The only sharp temperature fluctuation which does not seem to be associated with any feature in the "classical" maps of Mars was recorded in both channels of Mariner 6 at longitude 307.0° and latitude —3.5°, identified in Fig. 1. The TV pictures of this area show a complex terrain structure that may be related to this temperature anomaly (*5*).

Because the track of Mariner 6 was nearly equatorial (*3*) and extended well beyond the terminator, it is particularly suited for a determination of the parameters characterizing the gross thermophysical properties of the martian ground. The cooling curve of a homogeneous solid with $(K\rho c)^{1/2} = 4 \times 10^{-3}$ cal/cm^2 sec$^{1/2}$ per degree Kelvin, where K is heat conductivity, ρ is density, c is specific heat, and albedo of 0.85, fits the measurements quite well, although obvious departures are noticeable in Fig. 1. This result agrees with the general conclusions of Sinton and Strong (*6*). Our results should be considered tentative, although we believe that a more detailed analysis of the data will not change the conclusions significantly. A thorough analysis of the systematic effects present in the data is underway; a correlation with the results of the television and infrared spectrometer experiments is planned.

G. NEUGEBAUER
G. MÜNCH
California Institute of Technology, Pasadena 91109
S. C. CHASE, JR.
H. HATZENBELER
Santa Barbara Research Center, Goleta, California 93183
E. MINER
D. SCHOFIELD
Jet Propulsion Laboratory, Pasadena, California 91103

References and Notes

1. S. C. Chase, Jr., *Appl. Optics* **8**, 639 (1969).
2. R. B. Leighton, N. H. Horowitz, B. C. Murray, R. P. Sharp, A. G. Herriman, A. T. Young, B. A. Smith, M. E. Davies, C. B. Leovy, *Science* **165**, 787 (1969).
3. ———, *ibid.*, p. 684.
4. R. B. Leighton and B. C. Murray, *ibid.* **153**, 136 (1966).
5. We thank R. B. Leighton and the entire Mariner 69 TV team for allowing us to see their pictures before publication and for their valuable comments.
6. W. M. Sinton and J. Strong, *Astrophys J.* **131**, 459 (1960).
7. Many persons within the Mariner 1969 Project contributed to the success of this experiment, but our special thanks are due to H. Schurmeier, J. Stallkamp, and C. Kohlhase for their efforts on our behalf. We also thank J. Bennett and D. Griffith for help in the acquisition and reduction of the data.

9 September 1969

Reprinted from
5 September 1969, volume 165, pages 1004–1005

SCIENCE

Mariner 6: Ultraviolet Spectrum of Mars Upper Atmosphere

Abstract. *Emission features from ionized carbon dioxide and carbon monoxide were measured in the 1900- to 4300-angstrom spectral region. The Lyman alpha 1216-angstrom line of atomic hydrogen and the 1304-, 1356-, and 2972-angstrom lines of atomic oxygen were observed.*

The flight of Mariner 6 past Mars on 31 July 1969 presented the first opportunity to measure the ultraviolet dayglow of that planet. The technique of using ultraviolet spectroscopy to study planetary atmospheres has been developed both theoretically and experimentally over the past 9 years (*1*). Rocket experiments have shown that the ultraviolet dayglow of the earth consists of the following emission features: the Lyman alpha 1216-Å line of atomic hydrogen; the 1304-, 1356-, and 2972-Å lines of atomic oxygen; the 1200-, 1493-, 1744-, and 3466-Å lines of atomic nitrogen; the Lyman-Birge-Hopfield, Vegard-Kaplan, and second-positive bands of molecular nitrogen; the gamma bands of nitric oxide; and the first-negative bands of ionized molecular nitrogen (*2*). These emissions are produced in the earth's upper atmosphere by resonance and fluorescence scattering of ultraviolet solar radiation and by photoelectron impact excitation.

The Mariner ultraviolet spectrometer was specifically designed to measure emissions from the sunlit atmosphere above the limb of Mars. Extensive baffling in front of the telescope suppressed off-axis light from entering the 250-mm Ebert-Fastie spectrometer (*1*). Two photomultiplier tubes simultaneously recorded the spectral scans which occurred repetitively every 3 seconds. The wavelength band at 1100 to 1900 Å was measured at a resolution of 10 Å by a cesium iodide tube, and the 1900- to 4300-Å band was measured at a resolution of 20 Å with a bialkali tube.

The first observation of the sunlit atmosphere of Mars occurred when Mariner 6 was 8300 km from the planet's center, the slant range to the limb was 7600 km, and the solar zenith angle at the limb was 27°. The telescope baffling rejected the off-axis light from the disc sufficiently well so that a spectrum rich in emission features was obtained. In the spectral interval from 1900 to 4300 Å, the bialkali photomultiplier tube recorded the spectrum shown in Fig. 1.

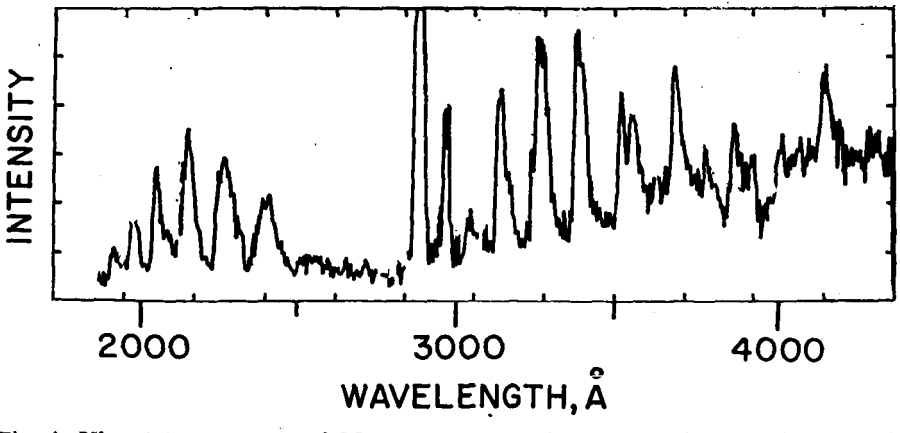

Fig. 1. Ultraviolet spectrum of Mars upper atmosphere. A nominal wavelength scale is shown on the abscissa. The ordinate is an arbitrary intensity scale uncorrected for the spectral response of the instrument. A number of spurious noise pulses have been edited out of this spectrogram.

An initial spectroscopic analysis has been performed with the use of laboratory and theoretical data prepared before the Mars encounter. A comparison spectrum synthesized from three separate sources is shown in Fig. 2 together with the individual spectra. Figure 2a was obtained from a spectrum of the Martian disc measured later in the flight by the Mariner spectrometer. This spectrum is the result of Rayleigh scattering and ground reflection of solar radiation. The spectrum in Fig. 2b was produced in the laboratory by the bombardment of carbon dioxide at 10^{-3} torr by electrons with an energy of 20 ev. This spectrum contains the prominent ionized carbon dioxide emission feature at 2890 Å and the Fox-Duffendack-Barker bands. The spectrum in Fig. 2c was composed theoretically from calculations of how the Cameron bands of carbon monoxide appear in the fluorescence scattering of sunlight (*2*), and it has been adjusted for the response of the instrument. The three spectra were normalized individually and summed to form the composite spectrum in Fig. 2d. In view of the way in which we put together the synthetic spectrum in Fig. 2d, the similarity between it and the Mars spectrum in Fig. 1 is remarkable. However, the excitation mechanisms which occur in the upper atmosphere of Mars may or may not be the ones we used to produce the synthetic spectrum.

We have identified an additional feature which appears in the Mars spectrum as the 2972-Å line of atomic oxygen. There may be further unidentified features in this spectrum.

The limb spectrum in the 1100- to 1900-Å region was recorded by the cesium iodide photomultiplier tube. The principal emission features that were observed were: the Lyman alpha 1216-Å line of atomic hydrogen, the 1304- and 1356-Å lines of atomic

oxygen, and the fourth-positive bands of carbon monoxide.

One particularly important objective of the ultraviolet spectrometer experiment was to search for nitrogen in the atmosphere of Mars. This first analysis shows no evidence of nitrogen emissions in the ultraviolet spectrum of the upper atmosphere. The following emissions were searched for and found missing: second-positive and Lyman-Birge-Hopfield bands of molecular nitrogen, first-negative bands of ionized molecular nitrogen, gamma bands of nitric oxide, and 1200- and 1493-Å lines of atomic nitrogen. The final analysis of these data will allow an upper limit to be placed on the amount of nitrogen in the upper atmosphere of Mars.

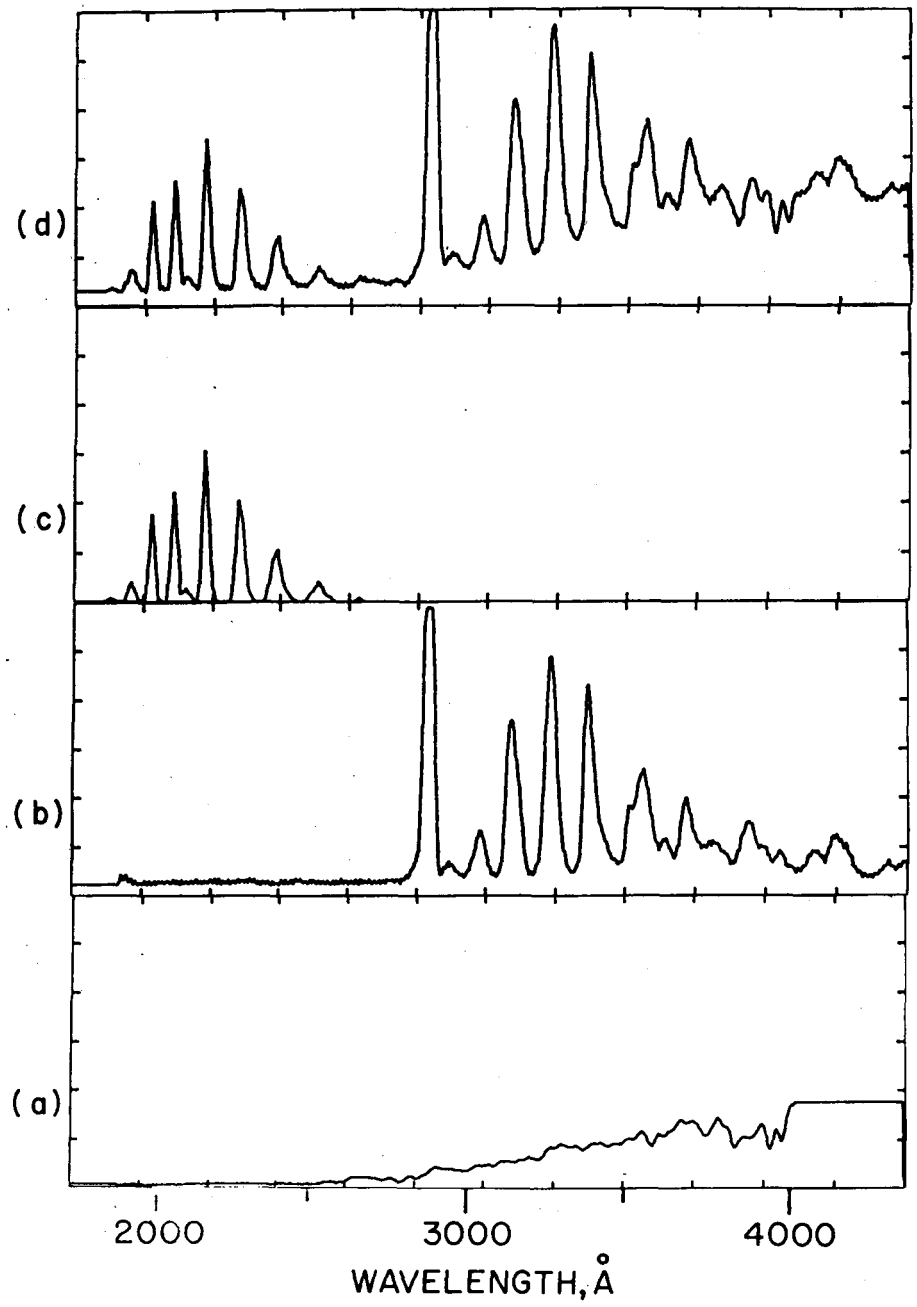

Fig. 2. Synthesis of comparison spectrum. (a) Off-axis light component from Mars disc. (b) Carbon dioxide spectrum from laboratory electron impact experiment. (c) Carbon monoxide spectrum from theoretical calculation of fluorescence scattering. (d) Composite spectrum synthesized by adding a, b, and c.

Repetitive spectra were taken as the Mariner spectrometer crossed the limb of Mars. These data, which contain information about the scale height of individual spectral emissions will be used to construct a model of the Mars upper atmosphere. This first report is simply a record of our identifications in the ultraviolet spectrum of the upper atmosphere. The instrument also obtained spectra of the bright and dark parts of the disc, the terminator, and the atomic hydrogen corona.

C. A. BARTH
Department of Astro-Geophysics and *Laboratory for Atmospheric and Space Physics, University of Colorado, Boulder 80302*

W. G. FASTIE
Department of Physics, Johns Hopkins University, Baltimore, Maryland 21218

C. W. HORD, J. B. PEARCE
K. K. KELLY, A. I. STEWART
G. E. THOMAS, G. P. ANDERSON
Department of Astro-Geophysics and *Laboratory for Atmospheric and Space Physics, University of Colorado*

O. F. RAPER
Space Sciences Division, Jet Propulsion Laboratory, Pasadena, California 91103

References and Notes

1. C. A. Barth, *Appl. Optics* **8**, 1295 (1969).
2. ———, in *The Middle Ultraviolet—Its Science and Technology*, A. E. S. Green, Ed. (Wiley, New York, 1966); W. G. Fastie, H. M. Crosswhite, D. F. Heath, *J. Geophys. Res.* **69**, 4129 (1964); C. A. Barth, *ibid.*, p. 3301; C. A. Barth and J. B. Pearce, *Space Res.* **6**, 381 (1966); unpublished results from a rocket flight, 13 June 1969.
3. The success of this experiment, which has been under preparation for 9 years, is the result of the efforts of a large number of people at NASA headquarters, the Jet Propulsion Laboratory, the University of Colorado, Johns Hopkins University, and elsewhere in the scientific community. The large scientific return from the Mariner 1969 mission is due to the technical and managerial skills of H. M. Schurmeier and the Mariner project staff at JPL and NASA headquarters. Supported by NASA under JPL contract 951790 and NASA grant NGL 06-003-052.

15 August 1969

Reprinted from
24 October 1969, volume 166, pages 496–499

SCIENCE

Infrared Absorptions near Three Microns Recorded over the Polar Cap of Mars

Kenneth C. Herr and George C. Pimentel

Infrared Absorptions near Three Microns Recorded over the Polar Cap of Mars

Abstract. *During the Mariner 7 flyby of Mars, the infrared spectrometer recorded distinct, sharp absorptions near 3020 and 3300 reciprocal centimeters between 61°S and 80°S, at the edge of the southern polar cap, with maximum optical density near 68°S and 341°E. These bands, which match in frequency the ν_3 bands of methane and ammonia, can be associated with previously unreported spectral features of solid carbon dioxide exceeding 1 millimeter in thickness. Possible reasons for the geographic localization are discussed.*

The Mariner 6 and 7 spacecraft (*1*) each carried an infrared spectrometer (*2*) that scans the spectral region from 1.9 to 14.3 μ every 10 seconds. The instrument telescope has a field of view of 2 degrees; thus at closest approach (~ 3100 km), the geographical area sampled is about 120 km square. A circular variable-transmission interference filter (*3*) provided a spectral resolution of 0.5 to 1 percent. Every 12th spectrum was recorded through a polystyrene film to provide frequency and photometry calibration *in situ*. We present here spectral observations in the spectral region near 3 μ during the Mariner 7 flyby on 4 August 1969.

Figure 1 shows a spectrum typical of those recorded at latitudes near the martian equator. Most of the spectral features are attributable to CO_2, the predominant atmospheric constituent. Also visible are two features near 2150 cm^{-1} attributable to the P and R branches of carbon monoxide and a broad absorption near 3250 cm^{-1} attributable to solid H_2O or, perhaps, to surface hydrates. A portion of the 3-μ region is recorded twice on either side of the radiometer spike, as shown by the instrumental background absorption at 2980 cm^{-1}. Spectral resolution is slightly higher in the low-frequency recording of the 3-μ overlap region.

The infrared spectrometer first viewed the planet on 4 August at 04 hours 48 minutes 54 seconds G.M.T. [all times are G.M.T. data receipt times (*4*), 5 minutes and 32 seconds after the data were recorded at Mars] at 20°N and 345°E. The instrument view swept south to 13°S and 5°E. During this period, 18 spectra were recorded, and none showed any evidence for atmospheric absorptions between 2900 and 3100 cm^{-1}.

At 04 : 51 : 41 G.M.T. the Mariner 7 scan platform was pointed so that the spectrometer viewed an area at 45°S and 315°E, 15 degrees north of the edge of the polar cap. Figure 2 shows a sampling of spectra recorded as the scan track passed onto the polar cap, moving toward the martian south pole. At 62°S and 330°E (04 : 54 : 51 G.M.T.) there were two distinctive spectral changes which indicated that the field of view of the spectrometer was directed toward the polar cap. Near 2.7 μ the brightness increased by 60 percent, and at 2.0 μ the triplet structure of the gaseous CO_2 absorption was lost and the peak intensity of

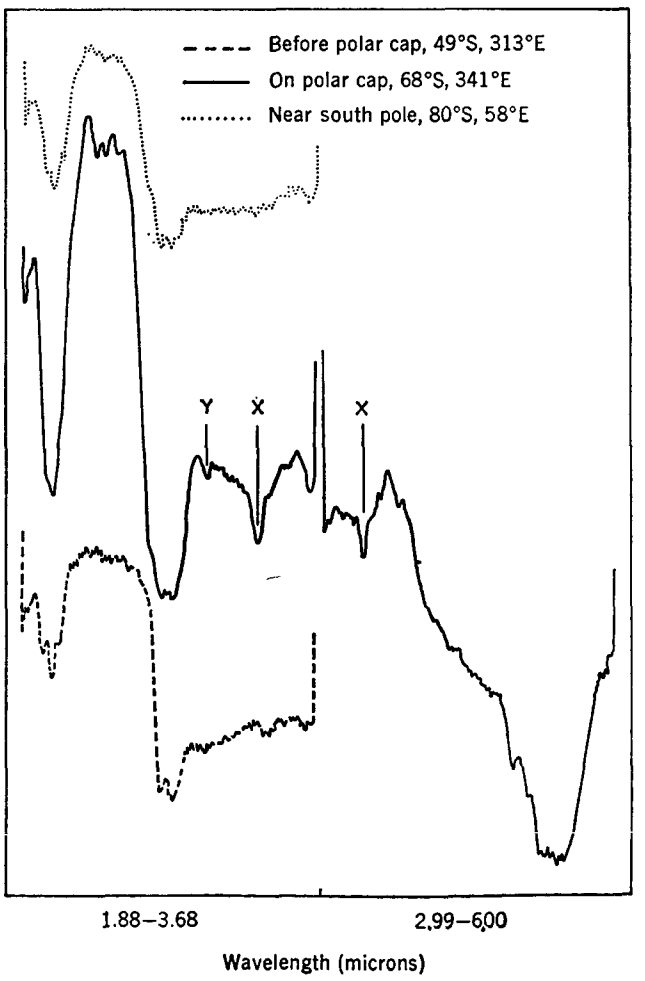

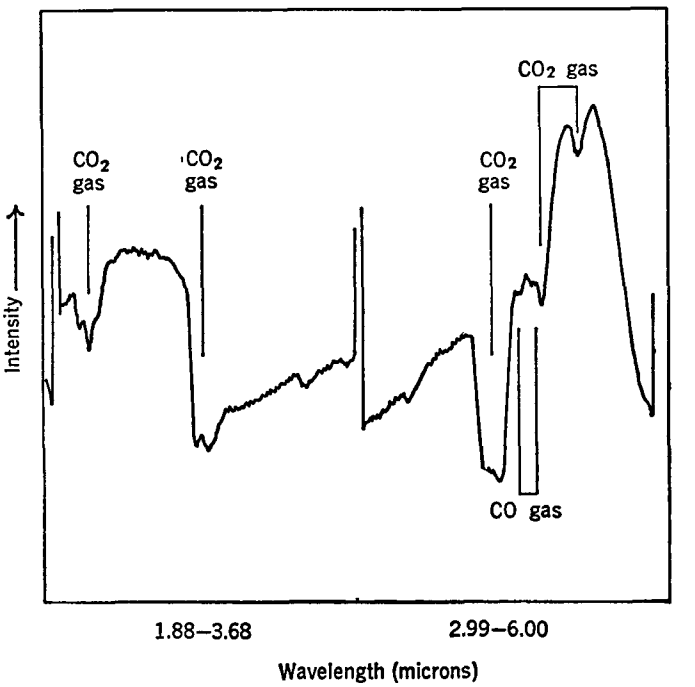

Fig. 1 (left). Near-infrared spectrum recorded at 0°N, 359°E.

Fig. 2 (right). Near-infrared spectrum recorded over the southern polar cap.

the feature more than doubled. In this same spectrum, two new absorptions are clearly recorded, X and Y (the X feature is recorded twice on either side of the radiometer spike). These features are recorded in every one of the subsequent 18 spectra. Both intensities grow, reaching maxima near 68°S and 341°E (4 : 56 : 05 G.M.T.) and then steadily decreasing, becoming almost indiscernible at 78°S, 20°E (4 : 58 : 11 G.M.T.). These two absorptions were detected again as the scan platform slewed back to northerly latitudes at a time approximately corresponding to that at which the spectrometer view would pass over the edge of the polar cap, but in none of the 120 spectra recorded at latitudes more northerly than the edge of the polar cap. Plainly, the X and Y absorptions are geographically concentrated near 68°S and localized over the edge of the polar cap, 61° to 80°S (*5*). The edge of the martian polar cap at the date of encounter was near 60° to 61°S.

An on-board measurement of the frequency is provided by the polystyrene calibration spectrum. Laboratory spectra measured before the launch of the Mariner 7 spectrometer indicated that this particular polystyrene film has absorption features centered at 2940 and 3050 cm^{-1}. Linear interpolation gives two independent measurements of the X frequency, 3020 and 3027 cm^{-1}. A less accurate estimate of the Y frequency obtained by extrapolation is 3294 cm^{-1}.

The most accurate determination of X and Y frequencies is based upon laboratory reference spectra recorded with the Mariner 7 spectrometer before launch. Figure 3 shows the superposition of a laboratory spectrum of a gas sample containing about 0.2 m-atm each of methane and ammonia pressure-broadened by 1 atm of air. The Q-branch frequency of the laboratory methane ν_3 band at 3020.3 cm^{-1} matches the X frequency in both left and right spectra within the possible accuracy, which we estimate to be ± 15 cm^{-1}. Similarly, the Q-branch frequency of the laboratory ammonia ν_1 band at 3336.7 cm^{-1} matches the Y frequency. The bandwidths at half height are estimated to be about 30 cm^{-1}, to be compared with an expected resolution of 24 cm^{-1}.

The identification of these features is of particular interest because of the close frequency match to bands of methane and ammonia, molecules that might have biological origin. These bands were not initially associated with the spectrum of solid CO_2 for a number of reasons:

1) The intensities of the X and Y features do not correlate uniformly with each other or with the intensity of the rather intense solid CO_2 absorption near 4900 cm^{-1}. For example, the ratio of optical density at 4900 cm^{-1} to that at 3020 cm^{-1} varies by as much as a factor of 2, sometimes in successive spectra.

2) No features have been attributed to solid CO_2 at these frequencies in the spectra reported in the literature (*6, 7*).

3) No features were detected at these frequencies in our laboratory spectra of solid CO_2 recorded before launch with the Mariner instruments or with conventional infrared spectrometers.

4) These features became quite indistinct during the Mariner 7 scan period while the spectrometer was still viewing the polar cap between 79° and 80°S.

Nevertheless, we felt it necessary to prove that these features could not be due to solid CO_2 since the spectra recorded near 68°S are so heavily dominated by spectral features obviously attributable to solid CO_2. Accordingly, two kinds of experiments were performed to test this possibility.

A flight model spectrometer identical to the Mariner instruments was placed in an evacuated environmental chamber with wall temperatures of 77°K. The spectrometer telescope viewed at normal incidence a stainless steel plate that filled the field of view. The steel plate, which has an emissivity of 0.3 at 3 μ, was cooled to 77°K. Gaseous CO_2 (Matheson) was allowed to condense upon this plate at a thickness rate of 0.7 mm per hour. The spectrum of the solid was then periodically recorded in the 2- to 4-μ region under illumination by a concentric ring of tungsten filaments heated to about 2800°K. At the center of the sample, the angle between the optical path and the direction of illumination could be selected to be 73, 55, or 33 degrees. Figure 4 shows a typical "reflection-absorption" spectrum recorded with a sample thickness near 2 to 3 mm. Absorption features corresponding to the X and Y features are clearly visible in the thickest samples. A mass spectrometric analysis of the carbon dioxide used showed that less than 10 parts per million CH_4 or NH_3 were present as an impurity.

In addition, using a conventional cold cell (*8*) and a Beckman IR-7 spectrophotometer, we recorded transmission spectra of thick solid CO_2 samples. Gaseous CO_2 (Matheson) was deposited at a rate of 0.005 mole per hour onto a CsI salt window held at 77°K [the temperature was measured with a thermocouple (Au-Co versus Cu) embedded in the window]. The transmission spectrum was recorded with a solid sample 1.5 mm thick. A distinct absorption at 3013 cm^{-1} was observed, and absorption near 3350 cm^{-1} was discernible, though not distinct. This same sample displayed no absorption at 1305 cm^{-1} that could be attributed to methane suspended in solid CO_2 (*9*).

At first consideration, it seems surprising that these absorptions have not been reported earlier. Herzberg (*10*), for example, does not list them among the 43 transitions observed in the infrared and Raman spectra of gaseous CO_2. Nevertheless, there are possible transitions that correspond to these frequencies. The transitions $(0,0,0) \rightarrow (0,1,1)$ and $(0,0,0) \rightarrow (1,3,0)$ are calculated to be near 3016 and 3320 cm^{-1}, respectively. The first transition is harmonic oscillator–forbidden (as a binary combination), and it is also selection rule–forbidden ($g \not\longleftrightarrow g$). The second transition is harmonic oscillator–forbidden (as a quaternary combination). Among the 43 transitions listed by Herzberg, none involve odd changes of both quantum numbers ν_2 and ν_3 as required for the transition at 3016 cm^{-1}.

Solid CO_2 has crystal symmetry T_h, and the CO_2 molecules occupy sites of symmetry C_{3i} with four molecules per unit cell (*6*). The combination of ν_2 (symmetry Π_u) and ν_3 (symmetry Σ_u^+) gives a state of symmetry Π_g which does not lead to an infrared-active component either in the site group or in the factor group analysis. These facts are sufficient to explain the *absence* of the band—we must explain its appearance.

There is, perhaps, an analog in the spectrum of solid oxygen (*11*). Despite a completely forbidden selection rule for this homonuclear diatomic molecule, the fundamental transition at 1549 cm^{-1} can be observed in very thick samples comparable to those used

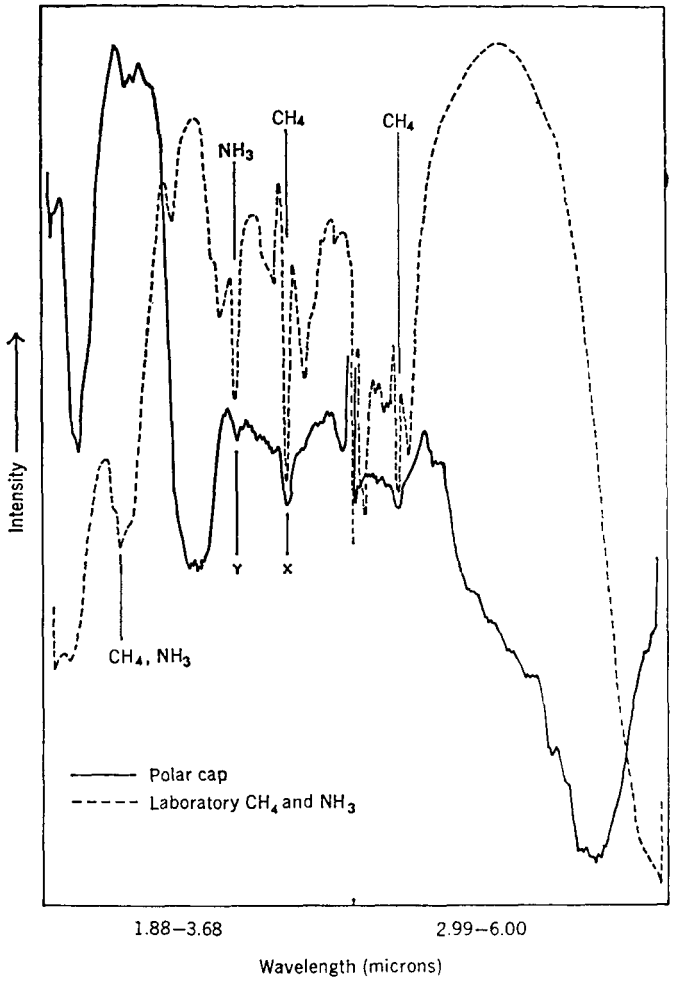

Fig. 3 (left). Calibration with the laboratory spectrum of gaseous methane and ammonia.

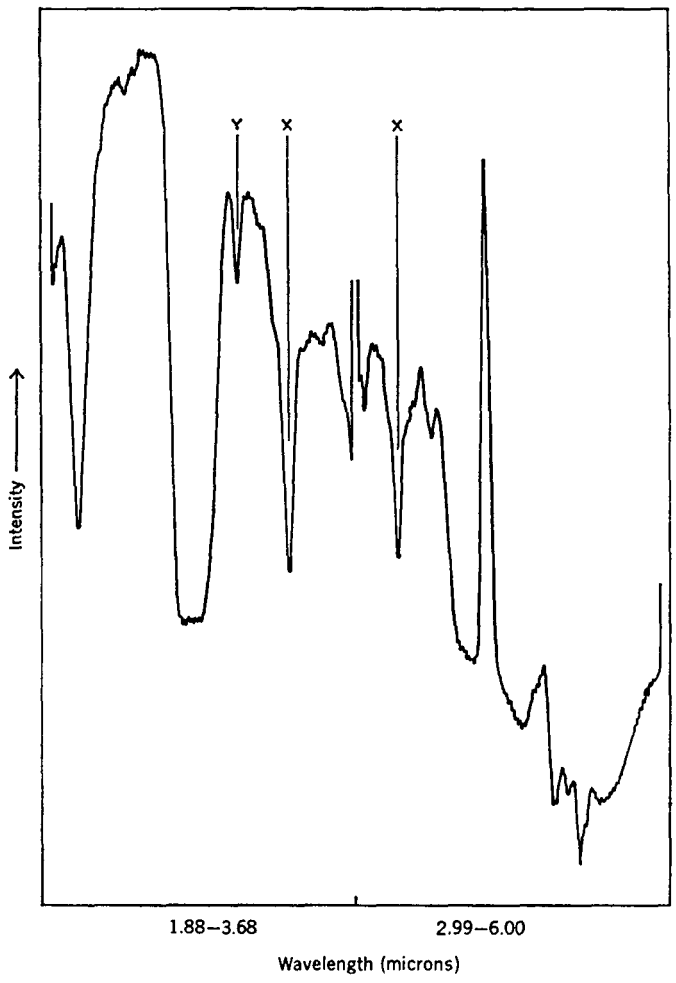

Fig. 4 (right). Laboratory near-infrared "reflection-absorption" spectrum of solid CO_2 (77°K).

in the present work. In the case of oxygen, the intensity of the forbidden band is sensitively dependent upon deposition conditions; it becomes about four times more intense if the deposition is carried out at 4°K. All of the evidence indicates that the feature appears because of lattice imperfections, a thesis strongly supported by the enhancement of the band after the deliberate addition of inert-gas impurities (*12*). The evidence suggests that the band at 3013 cm^{-1} observed in the laboratory spectra is due to the forbidden (0,0,0) → (0,1,1) transition of solid CO_2, appearing because of lattice imperfections (surface sites, impurity sites, vacancies, stacking faults, or grain boundaries). We believe that the same explanation is probably applicable to the martian spectral feature at 3020 cm^{-1}. The appearance and frequency of the feature are also consistent with the spectrum of gaseous methane, but the more mundane explanation seems more likely (*13*). Though the band near 3300 cm^{-1} was difficult to obtain in transmission spectra, its presence in the "reflection-absorption" spectra suggests that this band, too, should be attributed to solid CO_2.

There remains the need to explain the lack of intensity correlation between the bands at 3020, 3300, and 4900 cm^{-1}, if they are all to be attributed to solid CO_2. Furthermore, we must rationalize the disappearance of these features at the more southerly latitudes if the polar cap near the pole is attributed to solid CO_2. Several possibilities are under investigation. The edge of the polar cap could be shrouded by a solid CO_2 cloud (or fog) which the spectra suggest clears at the more southerly latitudes and more easterly longitudes. This would explain both discrepancies since cloud height, thickness, and coverage could vary during the 10-second period needed to obtain a spectral record. Such a cloud should, however, be detectable through poorer definition in the television pictures near the edge of the polar cap, an observation that has not been reported. If the solid CO_2 we observe is on the ground, then its spectrum at the edge of the polar cap must differ quite significantly from that nearer the pole. The difference may be due to the thickness of the layer, particle size, the inclusion of impurities (such as water), or different growth conditions. It may be significant that the southern polar cap may recede only to latitudes near 80°S.

It is clear that our continuing studies, directed at laboratory reproduction of the spectra of the martian polar cap, will settle more definitely the proper assignment of the two 3-μ features. For the present, the interpretation that they are due to solid CO_2 must be preferred, despite the fact that other questions remain that must be considered further.

KENNETH C. HERR
GEORGE C. PIMENTEL
Chemistry Department and *Space Sciences Laboratory, University of California, Berkeley 94720*

References and Notes

1. Mariner 6 and 7 were NASA missions managed by the Jet Propulsion Laboratory (JPL) and directed by Project Manager H. M. Schurmeier.
2. The spectrometers were designed and constructed by the authors in the Chemistry Department and Space Sciences Laboratory at the University of California at Berkeley. This instrument will be described in detail in a later publication.
3. Provided by Optical Coating Laboratories, Inc., Santa Rosa, California.
4. All times, latitudes, and longitudes are based upon JPL Pegasis calculations made on 8 August 1969 after the encounter. Because the Mariner 7 spacecraft experienced an orbit anomaly before the encounter, these latitudes and longitudes are subject to change as post-encounter tracking refines the actual orbit.
5. There was no trace of either of these absorptions in any of the 150 spectra recorded during the Mariner 6 flyby, which viewed an equatorial region between 13°N and 16°S and between 280°E and 95°E.
6. W. E. Osberg and D. F. Hornig, *J. Chem. Phys.* **20**, 1345 (1952).
7. D. A. Dows, *Spectrochim. Acta* **13**, 308 (1959).
8. E. D. Becker and G. C. Pimentel, *J. Chem. Phys.* **25**, 224 (1956).
9. In a separate experiment, conducted with Y. M. Huang, CH_4 was trapped in solid CO_2 at 20°K. When the sample was warmed to 77°K, the spectrum of CH_4 became more diffuse and somewhat weaker, but plainly most of the methane remained. After the solid was warmed to 100°K and recooled to 77°K, the amount of methane was reduced by approximately half. The experiment shows that methane can be trapped in solid CO_2 even at temperatures as high as 100°K and that near 3020 cm^{-1} the spectrum of methane suspended in solid CO_2 is not readily distinguishable from the Mars absorption.
10. G. Herzberg, *Infrared and Raman Spectra of Polyatomic Molecules* (Van Nostrand, Princeton, N.J., 1945).
11. B. R. Cairns and G. C. Pimentel, *J. Chem. Phys.* **43**, 3432 (1965).
12. B. R. Cairns, thesis, University of California, Berkeley (1964).
13. No methane absorption was observed at 1305 cm^{-1} in the martian spectra, but this does not constitute sufficient evidence to eliminate the methane interpretation. Spectra recorded in this spectral region depend upon the temperature difference between the planetary surface, which furnishes the spectral source, and the gaseous absorber. This provides a "thermal attenuation factor" that approaches zero as these temperatures approach each other. Thus a gas near the ground could not be observed at all. Furthermore, the feature at 1305 cm^{-1} is weaker than the band at 3020 cm^{-1} (under our resolution) and the path length is less than half as great (because the solar light at 3020 cm^{-1} passes through the atmosphere twice).

14. We acknowledge generous support by NASA for the development of the 1969 Mariner infrared spectrometers, as well as the endurance of the JPL Project staff and their courage as they turned on our instrument when it was thought to be the cause of the flight anomalies of the Mariner 7 spacecraft and a threat to the mission. We thank the personnel of the Chemistry Department Machine Shop and the staff of the Space Sciences Laboratory Electronic Shop for their enormous contribution to the fabrication of this instrument. We express our indebtedness to the Berkeley Group, led by P. B. Forney, J. L. Hughes, D. A. Waston, R. H. Weitzmann, and M. A. Carlson, for their dedicated efforts throughout the project.

29 September 1969

Reprinted from
2 January 1970, Volume 167, pp. 47-49

SCIENCE

Evidence for Solid Carbon Dioxide in the Upper Atmosphere of Mars

Kenneth C. Herr, George C. Pimentel

Evidence for Solid Carbon Dioxide in the Upper Atmosphere of Mars

Abstract. *The infrared spectra recorded by Mariner 6 and 7 show reflections at 4.3 microns, which suggest the presence of solid carbon dioxide in the upper atmosphere of Mars.*

In each of the Mariner 6 and 7 missions to Mars (*1*), the infrared spectrometer (*2*) recorded spectra in the 4-μ region as the field of view passed through the atmosphere on the bright limb of the planet. This occurred three times and each time a reflection spike was recorded at 2346 ± 10 cm^{-1}, at the center of the ν_3 absorption band of CO_2. No such reflection was observed in either of two dark limb crossings. Figure 1 shows the three bright limb observations. Figure 2 shows again the second Mariner 7 limb crossing in addition to the spectrum recorded 20 seconds earlier (off the limb) and that recorded 10 seconds later (over the planet). Figure 3 shows a laboratory "reflection-absorption" spectrum of 15 μ of annealed solid CO_2 (Matheson) condensed at 77°K on a stainless steel plate that filled the field of view of a flight model spectrometer identical to the Mariner instruments (*3*). With thicknesses exceeding a few microns, a reflection spike is observed due to the index of refraction variation (*4*) through the 4.3-μ absorption band of CO_2.

It is clear that the reflection spikes displayed in Fig. 1 are highly characteristic and are attributable to solid CO_2. They are surely not due to solid CO_2 on the planetary surface viewed with stray light from outside the principal field of view of the spectrometer. Local surface temperatures at these latitudes exceed 250°K, much too high to permit condensation on the surface. Furthermore, reflection at 2346 cm^{-1} from the surface would not be observed because the atmosphere is opaque at this frequency. The reflection must be associated with solid CO_2 at such high altitudes that the atmosphere is no longer optically thick.

Trajectory calculations (*5*) provide geometrical parameters that help to interpret these observations. Table 1 lists the slant range to the point above which the center of the field of view passes closest to the planet, the latitude and longitude of this point, and the aperture width at this slant range. For the second Mariner 7 limb crossing, it is possible to deduce the time between the reflection spike observation and the limb crossing as 5.5 ± 1.5 seconds. This corresponds to an altitude of the optical path at closest approach of 25 ± 7 km.

If it is assumed that this reflection originates over the field of view's closest approach point, the condensation of CO_2 gives an indication of the temperature at this altitude (T_h). The value of T_h so derived, based on an assumed scale height of 8 km, is 130°K.

There are other infrared absorptions that may also be connected with solid CO_2 in the atmosphere—solid CO_2 ab-

Table 1. Conditions under which reflection at 2346 cm^{-1} was observed by Mariner 6 and 7 in 1969.

	Mariner 6	Mariner 7	Mariner 7
Date	30 July	4 August	4 August
Time	5:19:07	4:43:23	4:54:55
Latitude	2.5°S	22°N	3°S
Longitude	300°E	343°E	355°E
Local time	Noon	Late morning	Noon
Surface temperature		~250°K	~275°K
Slant range	8180 km	9830 km	6500 km
Aperture width	11 km	17 km	11 km

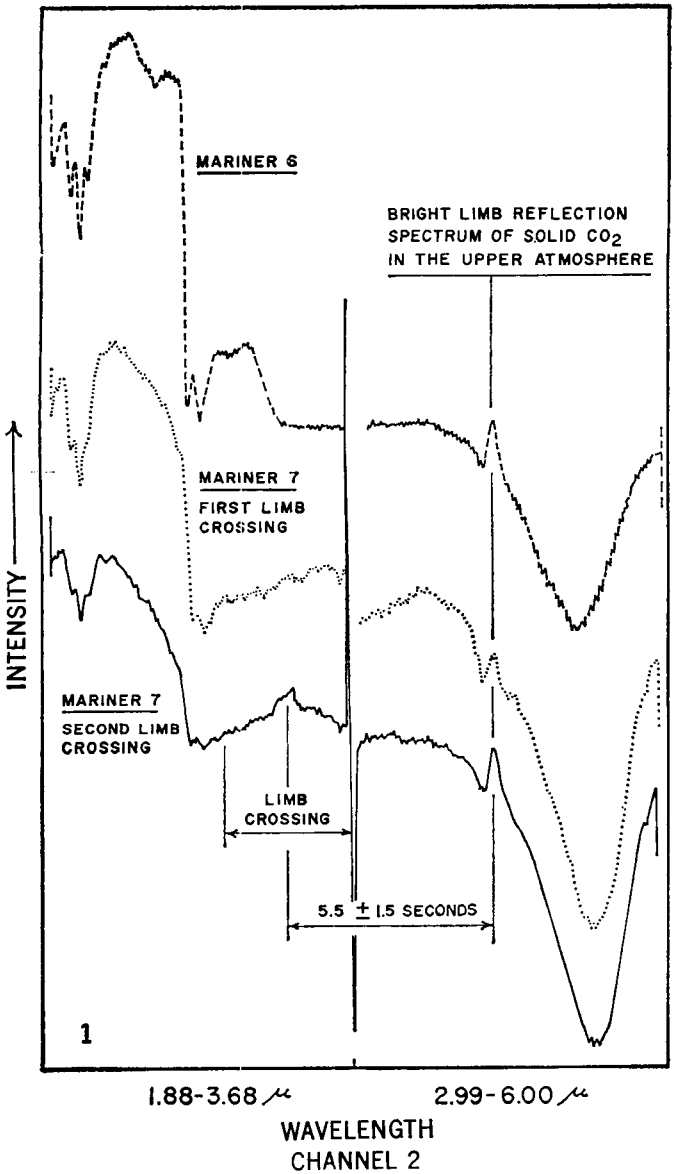

Fig. 1. Near infrared spectra recorded through the martian atmosphere on the bright limb. Fig. 2. Near infrared spectra recorded just before and after the bright limb crossing.

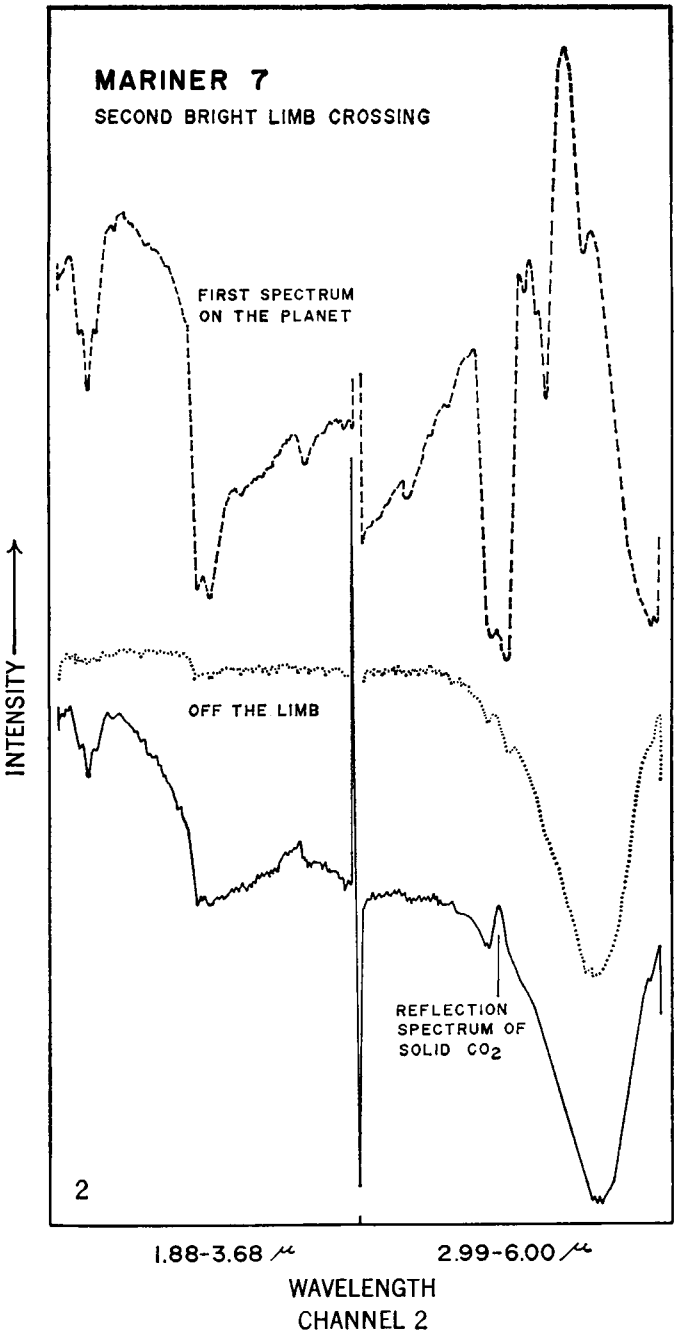

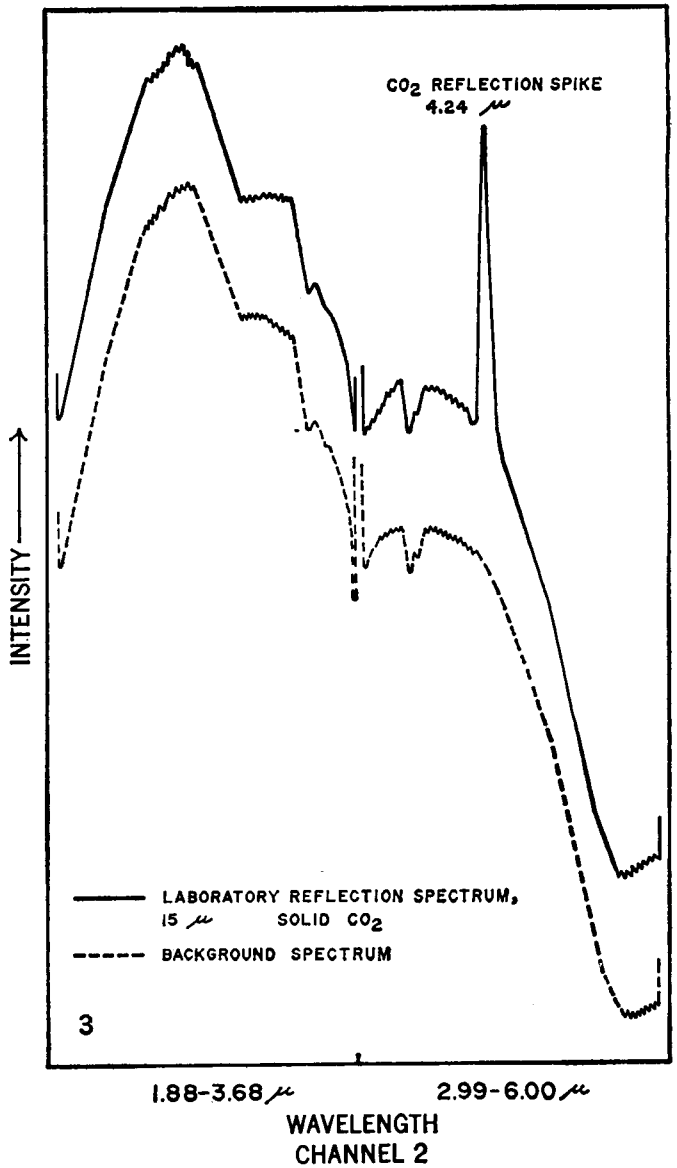

Fig. 3. Laboratory infrared "reflection-absorption" spectrum of solid carbon dioxide.

sorptions at 3 μ observed over the polar cap edge (*3*) and dark limb absorptions near 12 μ. The possible relations among these observations are under study.

KENNETH C. HERR
GEORGE C. PIMENTEL
Department of Chemistry and
Space Sciences Laboratory,
University of California, Berkeley

References and Notes

1. Mariner 6 and 7 were NASA missions managed by the Jet Propulsion Laboratory (JPL) and directed by Project Manager H. M. Schurmeier.
2. The spectrometers were designed and constructed by the authors in the chemistry department and Space Sciences Laboratory at the University of California, at Berkeley.
3. The manner of illumination and rate of deposition have been described [K. C. Herr and G. C. Pimentel, *Science* **166**, 496 (1969)].
4. Analogous transmission spikes are observed in transmission spectra of molecular solids. They have been observed, for example, for solid carbon monoxide by G. E. Ewing and G. C. Pimentel [*J. Chem. Phys.* **35**, 925 (1961)]; see also G. E. Ewing, thesis, University of California, Berkeley (1960).
5. These trajectory calculations are based on JPL Pegasis calculations made for Mariner 6 after encounter and for Mariner 7 on 8 August 1969. Because the Mariner 7 spacecraft experienced a pre-encounter orbit anomaly, altitudes were inferred from the spectra themselves. All times are Greenwich mean times at the moment of observation of Mars.

10 October 1969

Radio Science, Volume 5, Number 2, pages 381–386, February 1970

The Mariner 1969 occultation measurements of the upper atmosphere of Mars

Gunnar Fjeldbo, Arvydas Kliore, and Boris Seidel
Jet Propulsion Laboratory, California Institute of Technology, Pasadena, California 91103

(Received October 10, 1969.)

Data from the Mariner 1969 radio occultation measurements are utilized to derive altitude profiles for the refractivity, the free electron number density, and the plasma temperature above the occultation points. Initial results indicate that the ionosphere was denser and warmer in 1969 than during the quiet solar conditions prevailing at the time of the Mariner 4 encounter with Mars in 1965. The dayside ionosphere consists of two layers with peak densities of the order of 7×10^4 and 1.7×10^5 electrons/cm^3 at 110- and 135-km altitude, respectively. Assuming that CO_2^+ is the principal ion in the main layer yields a topside plasma temperature of 400°–500°K. A marked change in the scale height near 250 km may reflect the transition to a lighter ion such as CO^+. No clear signature of nighttime ionosphere was observed.

The Mariner 1969 flyby mission to Mars has yielded new data on the atmosphere of that planet. This latest mission consisted of the two spacecraft Mariner 6 and 7. Both spacecraft were utilized to conduct occultation experiments. The purpose of this report is to present the initial results of these latest measurements of the upper atmosphere of Mars. A companion paper [*Kliore et al.*, 1970] outlines the preliminary results for the lower neutral atmosphere.

Mariner 6 encountered Mars on July 31 at 0519 GMT. During immersion into occultation, the *S*-band tracking and telemetry link was utilized to probe the dayside atmosphere near the boundary between Meridiani Sinus and Thymiamata at 5°W and 4°N. Emersion on the dark side of the planet occurred near 82°E and 79°N.

The second spacecraft, Mariner 7, encountered Mars on August 5 at 0501 GMT. Immersion on the sunlit side of Mars occurred near Hellespontus at 30°E and 58°S. The nightside atmosphere was probed during emersion that took place between Nix Olympica and Propontis at 149°W and 38°N.

The data to be discussed here were obtained from radio Doppler measurements conducted with the *S*-band radio links to the two Mariner probes. (The instrumentation was similar to that employed during the first Mariner mission to Mars [*Kliore et al.*, 1965; *Levy et al.*, 1967].) Both radio links were operated in the two-way mode during the immersion measurements; i.e., signals generated from rubidium standards on the ground were transmitted to the space probes, where they were coherently retransmitted to earth. Thus the signals received at the tracking stations had completed a round trip through the Martian atmosphere, and the refractive Doppler perturbations could be determined by comparing the received signals with the frequency of rubidium standards stable to few parts in 10^{12}. Owing to anticipated difficulties in acquiring two-way tracking instantly upon exit from occultation, it was decided to conduct the emersion measurements in the one-way mode. In this configuration, the on-board crystal oscillators, stable to about one part in 10^{10}, provided the reference signals.

Figure 1 shows the atmospheric Doppler shift observed with the *S*-band link during the immersion of Mariner 6. The atmospheric Doppler effect was obtained by taking the observed carrier frequency and subtracting from it the radio frequency computed from changes in the geometrical distance between the spacecraft and the tracking station. A small correction for trajectory imperfections, oscillator drift, and refractive index changes in the terrestrial atmosphere and the interplanetary medium was approximated by subtracting a linear frequency term. This last correction was required to make the residual Doppler equal to zero just prior to immersion behind the Martian ionosphere.

Integral inversion of the Doppler perturbation

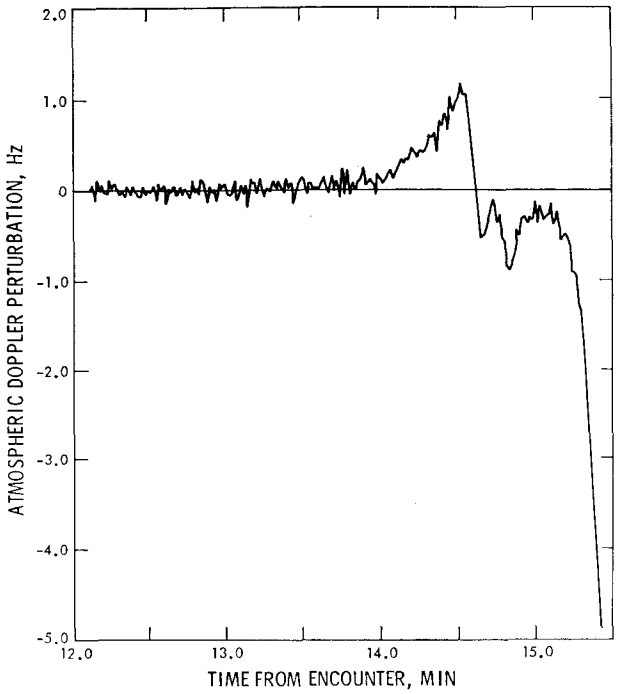

Fig. 1. Atmospheric Doppler perturbation observed during two-way tracking of the Mariner 6 immersion. Data from phase-locked receiver at tracking station DSS 14.

illustrated in Figure 1 yields the refractivity profile shown in Figure 2. In deriving this profile, it was assumed that the atmospheric refractivity distribution was spherically symmetric in the region probed by the signal. Vacuum is seen to prevail above approximately 400 km; i.e., the ionosphere above this level is too tenuous to be detected with the *S*-band link. Two ionospheric layers appear between 80 and 400 km. The refractivity in this region is negative and proportional to the electron number density. Below 60 km altitude we see the signature of the neutral atmosphere.

In order not to modify or suppress any structure that may have been present in the atmosphere, the refractivity profile shown in Figure 2 was derived without any filtering of the data. Consequently, the Doppler quantization noise present in Figure 1 appears in Figure 2 as refractivity fluctuations with a spatial period, or height interval, of about 5 km.

Another dayside refractivity profile was obtained with Mariner 7. The result is shown in Figure 3. Nighttime profiles were also obtained with both space probes, and these are shown in Figures 4 and 5. The most apparent difference between the day and nightside measurements is the absence of a clear ionospheric signature on the dark side of the planet. Note also that the nightside profiles are less precise than those obtained on the dayside. A close inspection of Figures 4 and 5 shows refractivity variations with an amplitude of about 0.1 and a spatial period of 100 to 300 km. These variations were apparently caused by frequency changes in the on-board crystal oscillators.

Converting the dayside refractivity measurements in the upper atmosphere into electron number density yields the ionization profiles shown in Figures 6 and 7. A peak density of 1.6 to 1.7 $\times$ 10^5 electrons/cm^3 was observed near 135 km. A minor layer with a maximum density of 6 to 8 $\times$ 10^4 electrons/cm^3 was detected near the 110-km level. Solar extreme ultraviolet rays and X rays are probably the principal agents producing the upper and lower layer, respectively.

Between 140 and 250 km, the plasma scale height appears to be constant and approximately equal to 45 km. Above 250 km, the topside scale height is 70 $\pm$ 25% greater than at lower levels. This marked

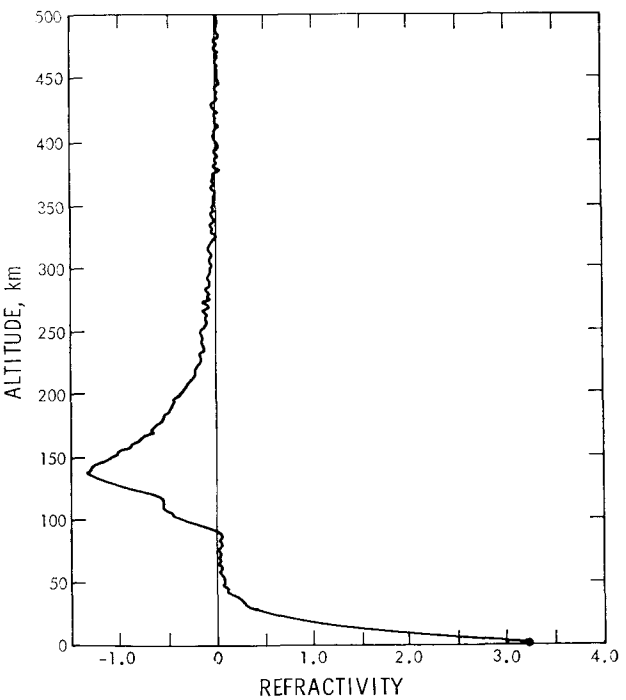

Fig. 2. Atmospheric refractivity profile obtained near Meridiani Sinus at 5°W, 4°N, at 1544 local time in early fall. Data were obtained from two-way tracking during the Mariner 6 immersion. No filtering was employed in the data analysis.

increase in the scale height with altitude may be due to a transition from a heavy ion, probably CO_2^+, to a lighter ion such as CO^+.

Using as a basis the assumption that the ionospheric topside is in ambipolar diffusive equlibrium and that CO_2^+ is the principal ion in the main layer, we have computed the plasma temperature distributions shown in Figures 8 and 9. The calculations were performed for two different boundary temperatures near 200 km. The results indicate a topside temperature of 400° to 500°K.

The general shape of the new ionization profiles presented here is similar to that observed with Mariner 4 in 1965 [*Fjeldbo and Eshleman,* 1968]. However, the peak density is greater by 60 to 70%, and the topside scales height (and temperature) is 50 to 60% higher than the earlier measurements. As evidenced by the increased altitude of the peak, the atmosphere was also warmer below the main layer. Increased solar activity and a 10% reduction in the distance to the sun are probably the principal reasons for the higher plasma density and temperature. The provisional sunspot number at the time of the Mariner 4 measurements was 11 [*Lincoln,* 1965]. The preliminary sunspot numbers for July 31 and August 5, 1969, were 128 and 158, respectively (J. V. Lincoln, personal communication, 1969).

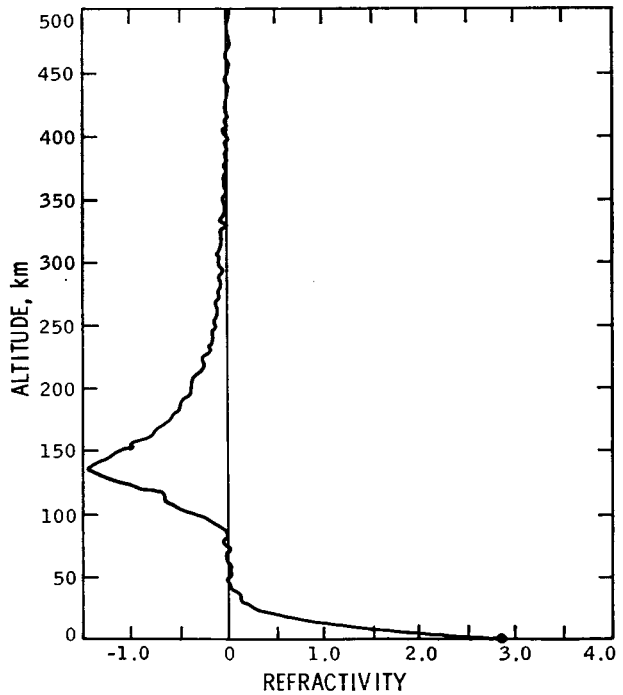

Fig. 3. Atmospheric refractivity profile obtained near Hellespontus at 58°S, 30°E, at 1432 local time in early spring. Data were obtained from two-way tracking during the Mariner 7 immersion. No filtering was employed in the data analysis.

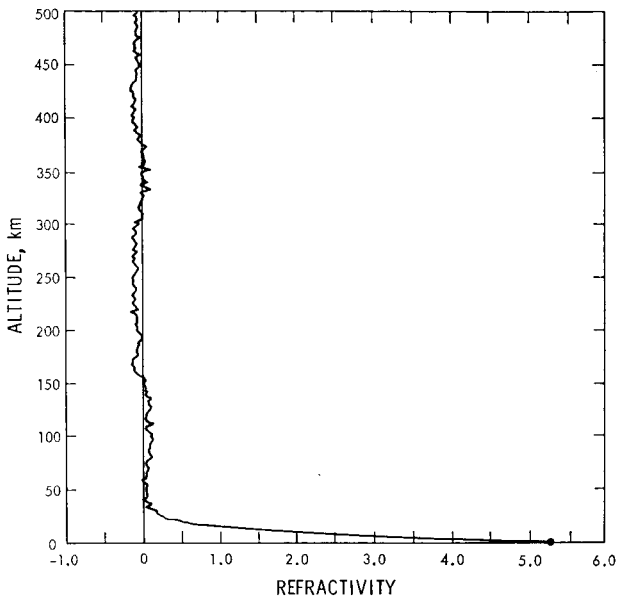

Fig. 4. Atmospheric refractivity profile obtained near 82°E, 79°N, at 2150 local time in early fall. The solar zenith angle was 107°. Data were obtained from one-way tracking of the Mariner 6 emersion. No filtering was employed in the data analysis.

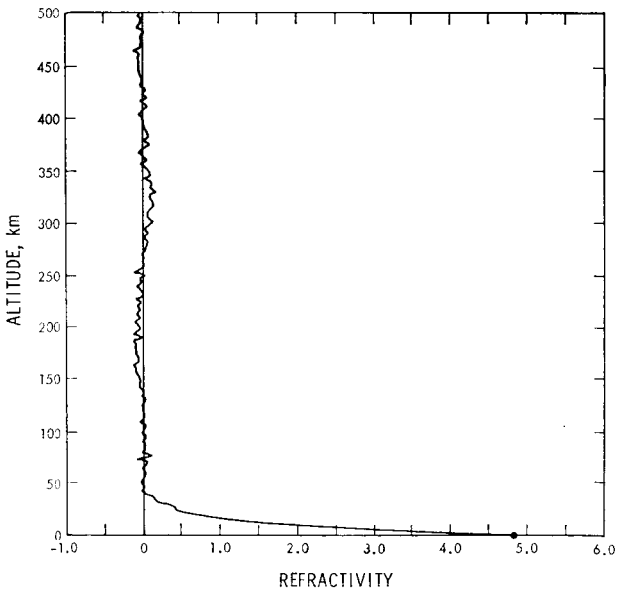

Fig. 5. Atmospheric refractivity profile obtained in the vicinity of Nix Olympica near 149°W, 38°N, at 0304 local time in early fall. The solar zenith angle was 130°. Data were obtained from one-way tracking of the Mariner 7 emersion. No filtering was employed in the data analysis.

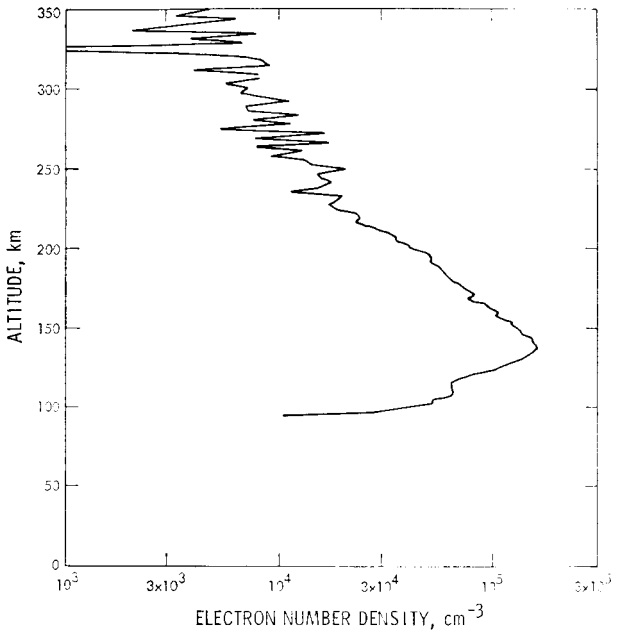

Fig. 6. Ionospheric electron number density distribution derived from Figure 2. The measurements were made near 5°W, 4°N, at 1544 local time in early fall. The solar zenith angle was approximately 57°.

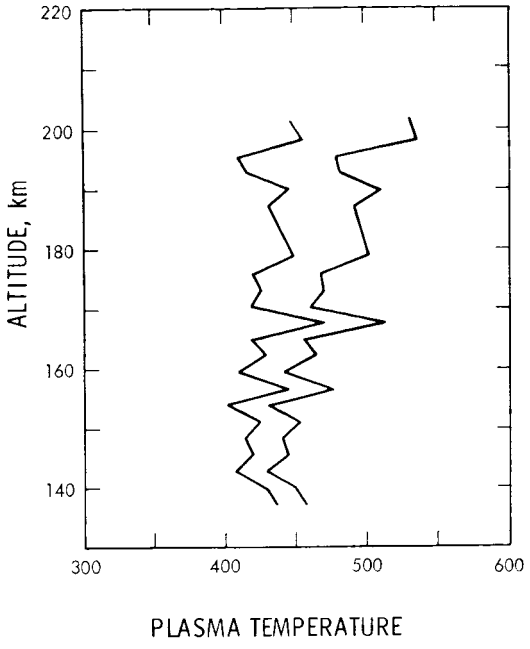

Fig. 8. Plasma temperature on the topside of the profile shown in Figure 6. The principal ion is assumed to be CO_2^+. Plasma temperature is in degrees Kelvin.

The topside plasma temperatures derived in Figures 8 and 9 may be roughly equal to the temperature of the neutral gas in these regions of the atmosphere. Theoretical estimates made by *Stewart and Hogan* [1969], for example, predict exospheric temperatures of 480° ± 50°K and 495° ± 55°K

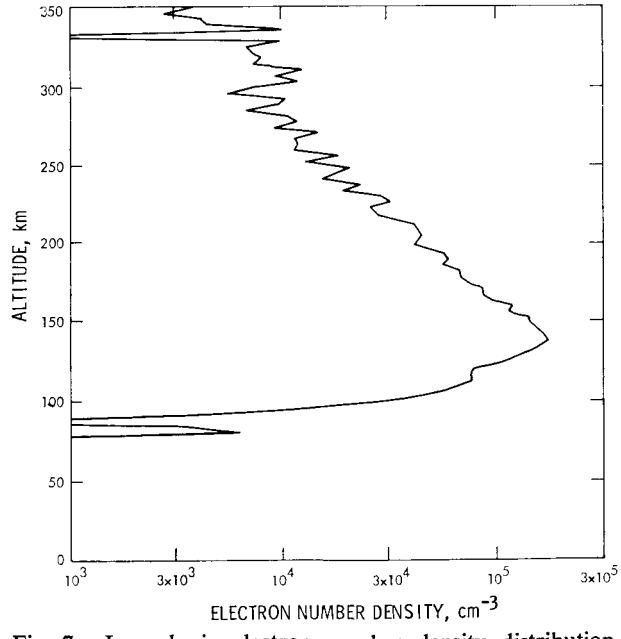

Fig. 7. Ionospheric electron number density distribution derived from Figure 3. The measurements were made near 58°S, 30°E, at 1432 local time in early spring. The solar zenith angle was about 56°.

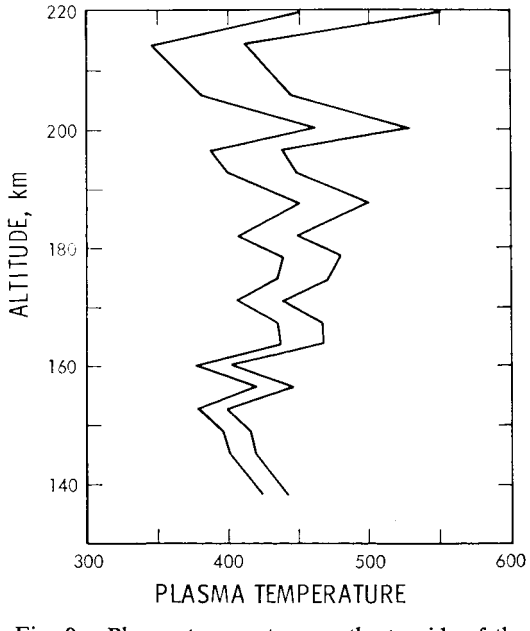

Fig. 9. Plasma temperature on the topside of the profile shown in Figure 7. The principal ion is assumed to be CO_2^+. Plasma temperature is in degrees Kelvin.

at the Mariner 6 and 7 immersion points, respectively. For other discussions of the thermal properties of the Martian ionosphere the reader is referred to *Johnson* [1965], *Chamberlain and McElroy* [1966], *Fjeldbo and Eshleman* [1968], and *McElroy* [1969].

A dual spacecraft mission, such as this latest Mariner mission, provides a unique opportunity whereby the Doppler effects caused by the planetary atmosphere may be separated from the Doppler effects produced by refractive index changes along the rest of the propagation path. This calibration may be accomplished by tracking both spacecraft simultaneously. While one radio link is being used to probe the planetary atmosphere, the other can monitor variations in the terrestrial atmosphere and the interplanetary medium. Such an experiment was successfully conducted during the Mariner 7 encounter with Mars (see Figure 10); however, the calibration data obtained with the Mariner 6 link were not available in time for inclusion in the analysis discussed here.

During the next decade, the rubidium frequency standards currently in use at the Deep Space Net will be replaced by hydrogen masers, which are expected to provide an order of magnitude improvement in the frequency stability of the radio system. With this increased system stability, the noise level in the two-way occultation refractivity measurements may be set primarily by scintillations in the terrestrial atmosphere and the interplanetary medium. Dual spacecraft tracking of the type discussed here is expected to become a valuable technique for reducing this refractivity noise.

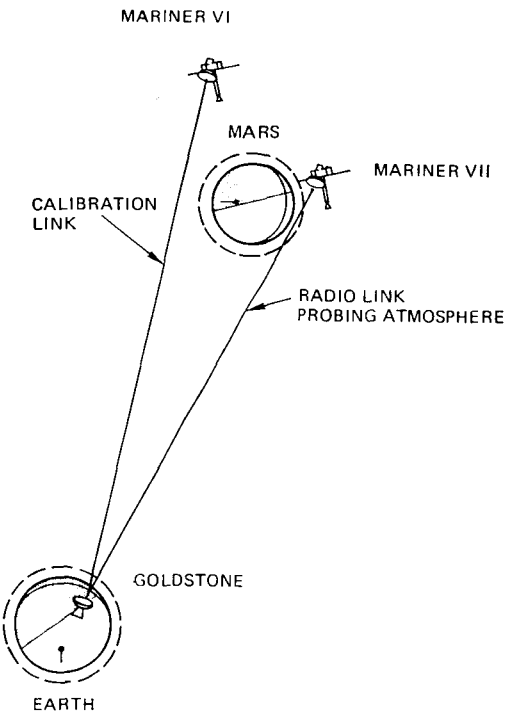

Fig. 10. Dual spacecraft tracking for planetary occultation measurements.

Acknowledgments. The assistance of the Mariner 1969 Project Office and the NASA Deep Space Net is gratefully acknowledged. We thank Nancy Hamata, Joan E. Jordan, David L. Nixon, and Joseph W. Witt for providing invaluable support in the analysis of the data.

This work was supported by the National Aeronautics and Space Administration under contract NAS-7-100.

REFERENCES

Chamberlain, J. W., and M. B. McElroy (1966), The Martian atmosphere: An interpretation of the Mariner occultation experiment, *Science, 152,* 21.

Fjeldbo, G., and V. R. Eshleman (1968), The atmosphere of Mars analyzed by integral inversion of the Mariner 4 occultation data, *Planetary Space Sci., 16,* 1035–1059.

Johnson, F. S. (1965), Atmosphere of Mars, *Science, 150,* 1445–1448.

Kliore, A., D. L. Cain, G. S. Levy, V. R. Eshleman, G. Fjeldbo, and F. D. Drake (1965), Occultation experiment: Results of the first direct measurement of Mars' atmosphere and ionosphere, *Science, 149,* 1243–1248.

Kliore, A., G. Fjeldbo, and B. Seidel (1970), First results of the Mariner 6 radio occultation measurement of the lower atmosphere of Mars, *Radio Sci.*, this issue.

Levy, G. S., T. Y. Ostoshi, and B. L. Seidel (1967), Ground instrumentation for Mariner 4 occultation experiment, *IEEE Trans. Instrum. Meas.*, IM-6,2.

Lincoln, J. V. (1965), Geomagnetic and solar data, *J. Geophys. Res., 70*(23), 5953.

McElroy, M. B. (1969), Structure of the Venus and Mars atmospheres, *J. Geophys. Res., 74*(1), 29.

Stewart, R. W., and J. S. Hogan (1969), Solar cycle variation of exospheric temperatures on Mars and Venus: A prediction for Mariner 6 and 7, *Science, 165,* 386–388.

DISCUSSION

J. V. Evans: Have any calculations been made for the ionosphere of Mars to determine the expected temperature ratio of ions and electrons? This will influence the scale height you expect in the topside of the layer.

G. Fjeldbo: No, not to my knowledge. What we measure is, of course, the average of the electron and ion temperatures.

P. Cloutier: It was stated in the presentation that

the observed temperature profiles of Mars are in agreement with the theory of R. W. Stewart and others. I would like to point out, however, that the density profiles are not in agreement with this theory. The observed height of maximum electron density is 130 km, whereas the calculated height is 148 km.

G. Fjeldbo: It was stated that the topside plasma temperature obtained from the preliminary analysis of the occultation data was comparable with the exospheric temperature computed by Stewart and Hogan. The difference in altitude between the observed and the computed ionization peaks is not relevant. This difference may only imply that the occultations occurred over elevated regions, i.e., elevated relative to Stewart and Hogan's surface level, or it might mean that the actual temperature below the ionization peak was on the average 10% lower than the theoretical estimate.

Reprinted from
12 December 1969, volume 166, pages 1393–1397

SCIENCE

Mariners 6 and 7: Radio Occultation Measurements of the Atmosphere of Mars

Arvydas Kliore, Gunnar Fjeldbo

Boris L. Seidel, S. I. Rasool

Mariners 6 and 7: Radio Occultation Measurements of the Atmosphere of Mars

Abstract. *Radio occultation measurements with Mariners 6 and 7 provided refractivity data in the atmosphere of Mars at four points above its surface. For an atmosphere consisting predominantly of carbon dioxide, surface pressures between 6 and 7 millibars are obtained at three of the points of measurement, and 3.8 at the fourth, indicating an elevation of 5 to 6 kilometers. The temperature profile measured by Mariner 6 near the equator in the daytime indicates temperatures in the stratosphere about 100°K warmer than those predicted by theory. The measurements of Mariner 6 taken at 79°N at the beginning of polar night indicate that conditions are favorable for the condensation of carbon dioxide at almost all altitudes. Mariner 7 measurements taken at 58°S in daytime and 38°N at night also show that carbon dioxide condensation is possible at altitudes above about 25 kilometers. Measurements of the electron density in the ionosphere show that the upper atmosphere is substantially warmer than it was in 1965, possibly because of increased solar activity and closer proximity to the sun.*

The successful flights of Mariners 6 and 7 provided opportunities for four more occultation measurements of the atmosphere, ionosphere, and surface configuration of Mars, thus increasing the amount of data obtained at Mars with the radio occultation method by more than 200 percent. Mariner 6 made its closest approach to Mars at 05 : 19 : 06 U.T. on 31 July. Approximately 20 minutes later it disappeared from the view of the earth and its radio beam was interrupted by the surface of Mars at a point near Maridiani Sinus (latitude 4°N, longitude 355°E). The local time at this point was 15:40, and the solar zenith angle was approximately 57 degrees. At the moment of occultation the spacecraft was about 9800 km from the limb. After remaining in occultation for about 20 minutes, the spacecraft emerged in the vicinity of the north polar region of Mars, at a latitude of 79°N and a longitude of 84°E. The local time at that point was 21 : 40, and the solar zenith angle was about 107 degrees. At this time the spacecraft was approximately 17,400 km from the limb.

Mariner 7 arrived in the vicinity of Mars approximately 5 days later, making its closest approach at 05 : 00 : 49 U.T. on 5 August. Some 19 minutes later its S-band radio beam was cut by the surface of Mars in the area of Hellespontus at a latitude of 58°S and a longitude of about 30°E. The local time there was approximately 14 : 20, and the solar zenith angle was approximately 56 degrees. At that time the Mariner 7 spacecraft was about 9050 km from the limb. About 30 minutes later the spacecraft's radio signal emerged from behind Mars in the vicinity of Amazonis and Arcadia at a latitude of 38°N and a longitude of 211°E. The local time there was 03 : 00 and the solar zenith angle about 130 degrees. At that time the spacecraft was about 20,180 km from the limb.

During each entry and exit of the radio beam through the atmosphere of Mars, the frequency and amplitude of the signal received afterward at the earth were changed by the effects of refraction upon the propagation of the radio signal. These effects are treated in more detail in descriptions of previous radio occultation experiments (*1*, *2*). The methods of obtaining and analyzing the data have been described (*3*), and the following is only an abbreviated description of the procedures used during the present experiment. For both Mariner 6 and Mariner 7, the entry into occultation was performed in a two-way mode of operation, in which a frequency referenced to a rubidium standard at the Deep Space Net (DSN) station is transmitted to the spacecraft, where it is coherently retransmitted. The exit data, however, were obtained in the one-way mode of operation, in which the spacecraft's transmitter is referenced to its on-board crystal oscillator. The received signal was passed through the standard phase-locked-loop receiver, and the record of nondestructively counted Doppler was recorded by the Tracking Data Handling System. This constituted the closed-loop data, on which the results described in the present paper are based. Simultaneously, the signal was passed through a special open-loop receiver, having an audio passband of approximately 5 khz. It produced a frequency-translated version of the received signal which was recorded on an analog tape recorder, as well as being digitized in real time and recorded on digital magnetic tape. These data are referred to as the open-loop data, which have not yet been thoroughly analyzed.

For the Mariners 6 and 7 occultation experiments, Deep Space Station (DSS) 14 (Mars) and 12 (Echo) at the Goldstone, California, complex were instrumented with open-loop receivers, and the open-loop data from DSS 14 were transmitted over a microwave link to DSS 13 (Venus) where they were digitized in real time and recorded. Closed-loop Doppler data were also taken at DSS 14 and DSS 12, as well as DSS 41 in Woomera, Australia. The open-loop receiver is necessary to insure instantaneous reception of the data as the spacecraft reemerges from behind the planet. This is difficult to accomplish with the phase-locked-loop receiver because of its finite lockup time. Another purpose of the open-loop receiver is the obtaining of amplitude data that cannot be obtained from the locked-loop receiver because of the long time constant of its AGC circuit. The bandwidth of the open-loop receiver was selected on the basis of the projected Doppler frequency rates due to the motion of the spacecraft. These rates, together with the fact that it was undesirable to retune the receiver within 3 minutes of occultation, led to an open-loop passband selection of approximately 5 khz. In order to insure precise tuning of the open-loop receivers, as well as to preserve their frequency-translation integrity, all the local oscillator frequencies were synthesized from a rubidium standard. An audio phase-locked-loop receiver as well as a spectrum analyzer and other test equipment were provided in the open-loop system to give a real time indication of the signal being received and recorded. This test equipment could be switched between the

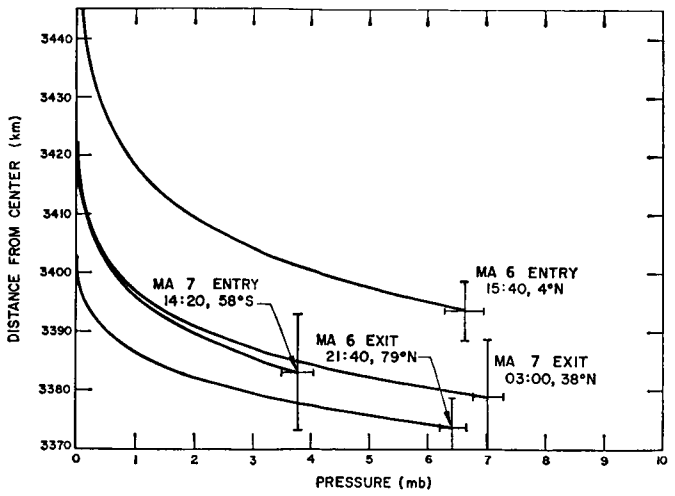

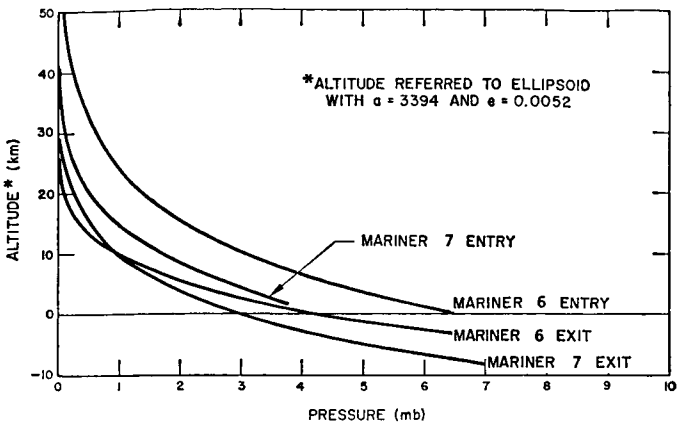

Fig. 1 (left). Pressure as a function of distance of the radio beam from the center of Mars from the Mariner 6 and 7 measurements. Fig. 2 (right). Pressure as a function of altitude with respect to a reference ellipsoid with $a = 3394$ km and $e = 0.0052$.

output of the open-loop receiver and the various reproducing units of the analog tape recorders. A 20 khz test-tone referenced to a rubidium standard was added to the data channel prior to recording to insure that the frequency recorded by the analog recorders was not distorted by more than a fraction of a hertz. Later this test tone was used as a time base for keying the digitizers sampling the data. The analog recordings were used primarily as backups to the real-time digital recordings which, because of system constraints, had to be obtained over a microwave link.

The digital open-loop data are passed through the Decimation and Spectral Analysis programs and the Digital Phase-Lock Receiver program which produces a record of the frequency and amplitude of the received signal sampled at arbitrary intervals of time. The frequency is then compared with predictions based on the orbit of the spacecraft, and the differences in frequency constitute the open-loop residuals. The closed-loop data, consisting of the biased Doppler counts, are processed by the Orbit Determination program, which compares the counts to predictions based on an orbit, and the differences constitute the closed-loop residuals. Because of system limitations, the maximum sampling frequency is one sample per second. The residuals are then passed through a Data Preparation program, which removes any bias or drift that might be present and integrates to obtain a record of the total phase path change due to refraction effects in the ionosphere and atmosphere. From there, the data go to the Inversion program which makes use of trajectory data provided by the Double Precision Trajectory program and performs integral inversion (*4*) of the data to obtain the refractivity profile. This profile is then used to compute the electron density in the ionosphere and the pressure, temperature, and other parameters of the lower atmosphere.

The profile of refractivity, as obtained by inversion, can be directly interpreted in terms of the electron density in the upper atmosphere; however, in order to obtain profiles of density, pressure, and temperature in the lower atmosphere, an assumption of the composition must be made. In deriving the results presented here, we assumed that CO_2 is the predominant constituent in the Martian atmosphere. This assumption is based on the results of ground-based spectroscopy, as well as on the results of other experiments aboard Mariners 6 and 7 (*5*). The temperature and pressure profiles shown in Figs. 1 through 4 were obtained for a composition of 90 percent CO_2 and

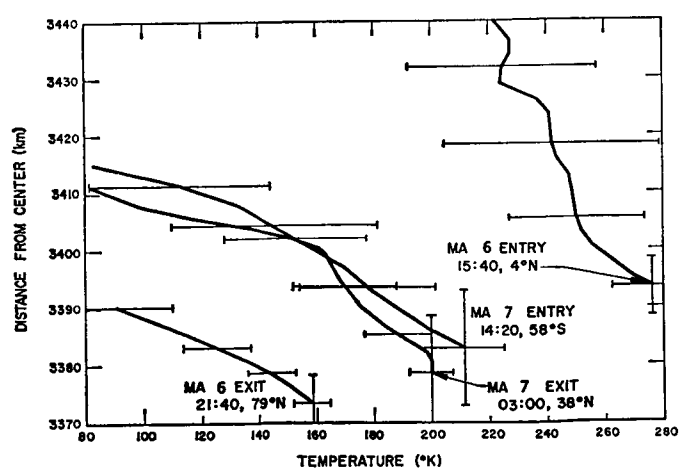

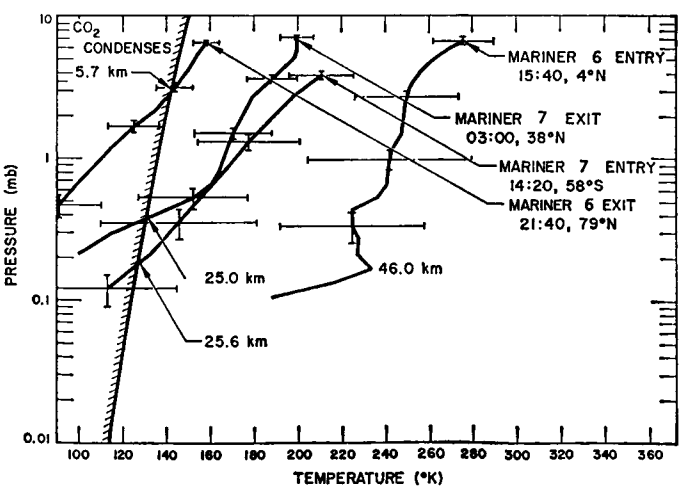

Fig. 3 (left). Temperature as a function of distance from the center of Mars. The uncertainty boundaries include only the effect of estimated uncertainty in the determination of refractivity. Fig. 4 (right). Pressure as a function of temperature for all profiles derived from Mariner 6 and Mariner 7 measurements. The region to the left of the shaded boundary is favorable for the condensation of CO_2. The numbers referred to in the boundary denote altitude at which the boundary is reached.

10 percent argon. They are valid as long as the composition remains predominately CO_2. Should it, however, be necessary to revise the estimate of CO_2 downward and to fill the remaining portion with some less refractive gas, the results would have to be substantially changed. For instance, if the composition should change to 80 percent CO_2 and 20 percent neon, the temperatures at all altitudes would decrease by approximately 10 percent. A more reliable composition will emerge when the data from the Mariners 6 and 7 spectrometer experiments are completely analyzed.

Figure 1 shows the profiles of pressure as a function of the distance of the radio beam from the center of Mars for all four of the occultation measurements. The error limits on the pressure measurements are based on an assumption of a 0.05 N-unit uncertainty in the refractivity. It should be pointed out that these error limits do not include the possible effects of an incorrectly assumed composition. The uncertainties in the vertical scales depend on the accuracy of the knowledge of the orbital paths of Mariners 6 and 7. At the time these results were computed, the uncertainties in the orbits produced an uncertainty in the knowledge of the position of the radio beam with respect to the center of Mars of ±10 km for Mariner 7, and about ±5 km for Mariner 6. It is expected that these uncertainties will be reduced to about ±1 km when the orbit becomes more precisely known. For an atmosphere in hydrostatic equilibrium, the pressure should be approximately equal on a gravitational equipotential surface. Figure 2 shows the derived pressure profiles plotted as a function of altitude above a mean reference ellipsoid having an equatorial radius of 3394 km and an ellipticity of 0.0052. This corresponds to a figure of Mars inferred from dynamical measurements of oblateness. If the reference ellipsoid were correct, and if the radial distance scales of the original pressure profiles were correct, then one would expect the profiles to lie very close to one another. The evident disagreement between the profiles in Fig. 2 indicates that this is not yet the case. However, when the radial distance coordinates are established to a greater degree of precision, it will be possible to use these measurements to compute the reference equipotential gravitational surface of Mars.

It is evident from Figs. 1 and 2 that three of the four measurements of pressure at the surface fall between 6.4 and 7 mb. Thus it seems that these measurements taken over widely different latitudes and longitudes on Mars appear to lie close to a common equipotential surface. The fourth measurement, however, taken in the area of Hellespontus (58°S) yields a pressure of only 3.8 mb, an indication that the surface feature which interupted the radio signal at that point lies at some 5 to 6 km above the mean ellipsoid in the vicinity of which the other three occultation observations were taken. For Mariner 6, the radius measured at 4°N differs from that measured at 79°N by approximately 20 km. Since the pressures measured at these two points are very nearly equal, one can assume that one is measuring the shape of the gravitational equipotential surface, and thus one may conclude that the physical surface of Mars has a shape similar to the shape of the gravitational equipotential surface predicted by the dynamical oblateness of Mars as opposed to the optically observed flattening.

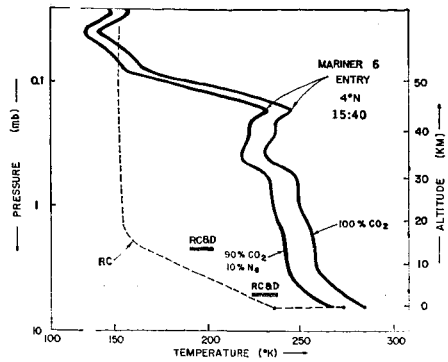

Fig. 5. Temperature as a function of pressure in the atmosphere of Mars at the entry point of Mariner 6 (thick line) for two assumed compositions. The broken line represents temperature distribution calculated for radiative convective equilibrium (RC) by Gierasch and Goody (*7*), also for the entry point of Mariner 6. The horizontal bars marked RC&D are the temperature values estimated for two pressure levels when atmospheric dynamics is also taken into account; adapted from Leovy and Mintz (*9*).

The profiles of temperature as a function of distance from the center of Mars for all four measurements are shown in Fig. 3. The uncertainty boundaries again have been established if we assume an uncertainty of .05 N units in the refractivity, and they do not reflect possible errors due to uncertainties in composition. The pressure and temperature profiles are crossplotted in Fig. 4.

The vertical distributions of temperature in the atmosphere of Mars, as shown in Figs. 3 and 4, have been deduced on the assumptions that the atmosphere is in hydrostatic equilibrium and that the ideal gas law is valid. The thermodynamics of atmospheric condensation has not been taken into account. For this reason, in three of the four cases shown in Fig. 4, especially that of Mariner 6 exit, the atmospheric temperatures are substantially lower than the condensation temperatures of CO_2, implying that the atmosphere at these levels is supersaturated. In reality, if suitable condensation nuclei are present, condensation should occur, releasing latent heat, and thereby raising the atmospheric temperatures. If it is assumed that radiational cooling is balanced by transport of energy by circulation, then the atmospheric temperatures should closely follow the saturation temperature curve shown in Fig. 4. As this may well be the case, particularly in the polar night on Mars, it seems more appropriate that, when the derived temperatures fall below the condensation temperature of CO_2, the "saturation" law, rather than the ideal gas relation, be used to deduce the temperature and pressure profiles. When the refractivity data are reduced in this manner, the atmospheric temperatures are never lower than the saturation temperatures of CO_2 and have the effect of raising the surface pressure by a few percent. The results of this analysis are shown in Figs. 5, 6, 7, and 8.

Each of these figures shows two profiles, one for 100 percent CO_2, and the other for 90 percent CO_2 and 10 percent Ne. Though it is generally accepted that CO_2 is the major constituent of the martian atmosphere, its exact concentration has not yet been established. Estimates range from 60 to 100 percent. This poses an interesting question regarding the identity of the

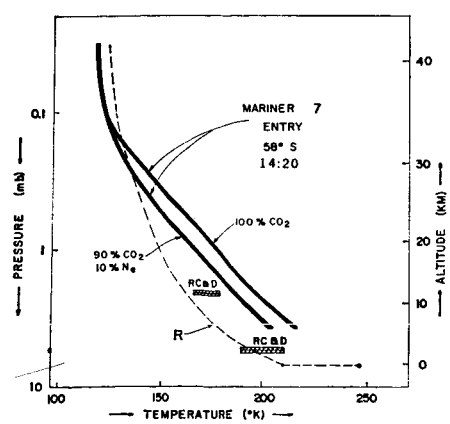

Fig. 6. Same as Fig. 1 but for Mariner 7 entry. The radiative curve (R) is adapted from Ohring and Mariano (*12*).

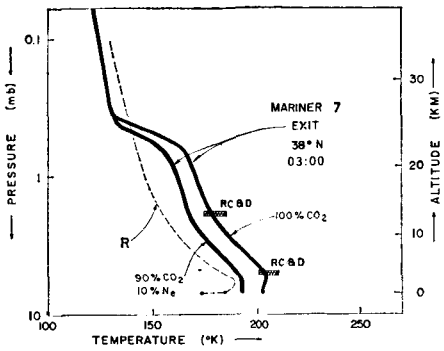

Fig. 7. Same as Fig. 1 but for Mariner 6 exit. The radiative curve is after Gierasch and Goody (*7*).

other constituents in the atmosphere of Mars. The problem has bearings on the origin of the martian atmosphere. It has been argued that if the present atmosphere of Mars is a remnant of a primordial atmosphere, which once had the solar composition, then after the escape of H_2 and He the atmosphere should contain 60 percent CO_2, 25 percent Ne, and about 15 percent N_2 (*6*).

However, if the present atmosphere of Mars is the result of outgassing from the interior, as with the earth, then by analogy with the earth Ne should be completely absent and the atmosphere should contain about 95 percent CO_2, 2 to 3 percent N_2, and traces of Ar, depending upon the extent of outgassing. The presence or absence of Ne in the atmosphere of Mars is therefore an important datum for the understanding of the problem of the origin of the martian atmosphere. Interestingly, in the interpretation of the refractivity data in terms of atmospheric number density, it is also the presence of Ne which makes a substantial difference in the resulting temperature

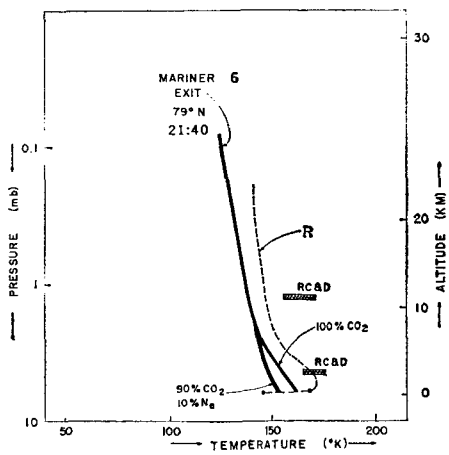

Fig. 8. Same as Fig. 1 but for Mariner 7 exit. The radiative curve (R) is adapted from Ohring and Mariano (*12*).

profiles. The addition of only 10 percent Ne in the atmosphere makes the derived temperatures substantially lower than those for 100 percent CO_2 because the refractivity of Ne is about six times smaller than that of CO_2.

The variety and range of the temperature profiles shown in Figs. 5, 6, 7, and 8 reveal several important and unexpected aspects of martian meteorology. In the following discussion, the salient features of these results are emphasized by comparing each of the observed temperature profiles with the atmospheric temperatures predicted by existing theoretical models of the martian atmosphere.

The thermal structure of the atmosphere of Mars has been the object of several comprehensive studies during the last few years. Notably, it has been argued that because CO_2 is the major constituent of the atmosphere and the total surface pressure is only about 10 mb, radiative heat exchange should dominate over convective and advective energy transport (*7, 8*). Consequently, the martian atmosphere should be coupled radiatively to the surface much more strongly than is the terrestrial atmosphere, and the temperature distribution in the atmosphere above a given point on the martian surface should be determined essentially by local radiative-convective balance. Furthermore, because the atmosphere is optically thin, one might expect a sharp temperature discontinuity between the atmosphere near the surface and the surface itself of as much as $+70°K$ at midday and $-50°K$ at night (*7, 8*).

In reality, however, atmospheric circulation on a planetary scale would modify such a thermal structure to some extent. Detailed numerical computations by Leovy and Mintz (*9*) indicate that the net effect of advection is to decrease the magnitude of the temperature discontinuity at the ground and to raise the atmospheric temperatures so that the lapse rate becomes subadiabatic at the equator and close to zero at the poles.

In Figs. 5, 6, 7, and 8 the measured temperature distributions are compared with temperature profiles calculated for similar conditions, taking into account radiative transfer alone (R), and both radiative and convective exchange (RC). Also indicated are the temperatures anticipated at two different levels in the atmosphere if all three processes—radiation, convection, and dynamics (RC &D)—are considered.

Figures 5 and 6 correspond to daytime, while Figs. 7 and 8 correspond to nighttime on Mars. Comparison of the observed temperature structures with the theoretical models for the four different locations indicates the following important features.

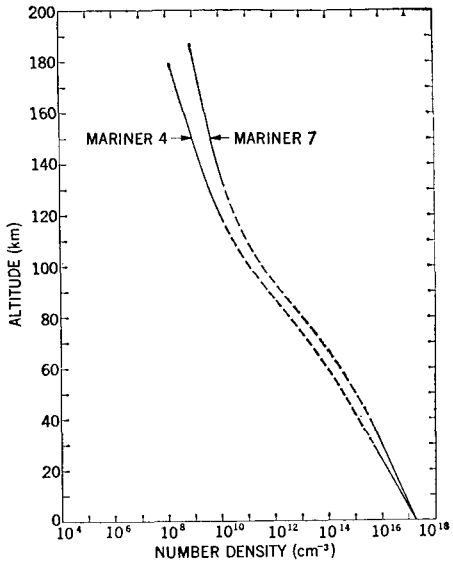

Fig. 9. Number density versus altitude. The Mariner 4 (1965) data were obtained near 50°S, at 13:00 local time in late winter. The solar zenith angle was 67 degrees. The Mariner 7 (1969) data were obtained near 58°S at 14:30 local time in early spring. The solar zenith angle was approximately 56 degrees.

1) The atmospheric temperatures observed at the equator in midafternoon are significantly higher than the predicted temperatures up to an altitude of 40 km. The observed gradient in the lower atmosphere is subadiabatic and this suggests the presence of a tropopause at an altitude of 9 km. The temperature found in the equatorial strato-

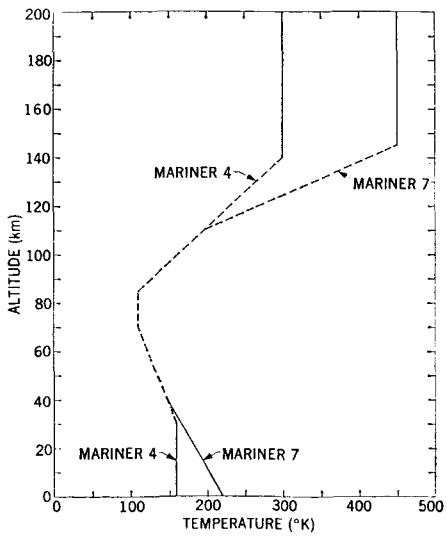

Fig. 10. Temperature versus altitude.

sphere is 100°K higher than that predicted from radiative transfer alone. The observations also indicate a sudden decrease of temperature at 0.2 mb, with the temperature gradient becoming superadiabatic. However, this is the least certain feature of the temperature profile.

2) The temperature distributions in midafternoon near the southern polar cap (Fig. 6) and in the subtropics in the early morning hours (Fig. 7) appear to be quite close to the profiles predicted when atmospheric dynamics were taken into account.

3) At 79°N, where the polar night is just beginning, the observed temperature profile, if interpreted with the assumption of saturation and condensation of CO_2 in the atmosphere, suggests that condensation of CO_2 is occurring at practically all heights in the atmosphere.

The case of the tropical atmosphere in daytime (Fig. 5) is the most interesting. At the equator, the atmosphere is much warmer than expected. For the 100 percent CO_2 case, the atmospheric temperature near the surface is about 283°K. However, the actual surface temperature measured by the infrared radiometer near the point of occultation is about 275°K (*10*), indicating an inconsistent negative temperature discontinuity of 8°K. For the case with 10 percent Ne, the atmospheric temperature near the ground is 268°K and the temperature discontinuity is only 7°K, differing markedly from the predicted value of Gierasch and Goody. In addition, the problem still remaining is that the atmosphere is substantially warmer than that suggested from the theoretical calculations. Either the opacity of the atmosphere is much higher than that estimated from the various CO_2 band models, or a significant amount of solar radiation is deposited in the middle atmosphere by absorption in the near-infrared bands of CO_2, or a combination of both.

The Mariner 1969 refractivity measurements in the upper atmosphere of Mars yielded results similar to those obtained with the Mariner 4 in 1965 (*1*). On the dayside, the main layer was now located near 135 km altitude, and it had a peak density of approximately 1.7×10^5 electron/cm^3. The minor layer was observed near an altitude of 110 km. The topside plasma temperature was 400° to 500°K on the assumption that CO_2^+ is the principal ion. No ionization was detected on the dark side of the planet (*11*).

Figures 9 and 10 show the density and temperature profiles deduced from the high latitude dayside measurements made with Mariners 4 and 7. The atmospheric models illustrated in these figures are based on the assumption that the main ionization layer is an F_1 region produced by solar extreme ultraviolet. Solid curves represent results derived from the refractivity data. Stippled curves indicate interpolation between the measurements made in the ionosphere and the neutral atmosphere. The figures show both the upper and the lower atmosphere to be warmer now than in 1965. The temperature increases are presumably due to seasonal changes, increased solar activity, and a 10 percent reduction in the distance to the sun.

ARVYDAS KLIORE
GUNNAR FJELDBO
BORIS L. SEIDEL
Jet Propulsion Laboratory,
California Institute of Technology,
Pasadena

S. I. RASOOL
Institute for Space Studies,
Goddard Space Flight Center,
New York

References and Notes

1. A. Kliore, D. L. Cain, G. S. Levy, V. R. Eshleman, G. Fjeldbo, F. D. Drake, *Science* **149**, 1243 (1965).
2. A. Kliore, D. L. Cain, G. S. Levy, in *Space Research VI—Moon and Planets*, A. Dollfus, Ed. (North-Holland, Amsterdam, 1967), p. 226; G. Fjeldbo and V. R. Eshleman, *Planet. Space Sci.* **16**, 1035 (1968).
3. G. S. Levy, T. Otoshi, B. L. Seidel, *Inst. Elect. Electron. Eng. I.E.E.E. Trans. Instr. Meas.* **16**, 100 (1967).
4. G. Fjeldbo and V. R. Eshleman, *J. Geophys. Res.* **70** (1965).
5. C. A. Barth, W. G. Fastie, C. W. Hord, J. B. Pearce, K. K. Kelly, A. I. Stewart, G. E. Thomas, G. P. Anderson, O. F. Raper, *Science* **165**, 1004 (1969).
6. S. I. Rasool, S. Gross, W. E. McGovern, *Space Sci. Rev.* **5**, 565 (1966); S. H. Gross, W. E. McGovern, S. I. Rasool, *Science* **151**, 1216 (1966).
7. P. J. Gierasch and R. M. Goody, *Planet. Space Sci.* **16**, 615 (1968).
8. R. Goody, *Comments Astrophys. Space Phys.* **1**, 128 (1969).
9. C. Leovy and Y. Mintz, *Rand Corporation Memorandum RM-5110-NASA*, December 1966; *J. Atmos. Sci.*, in press.
10. G. Neugebauer, G. Munch, S. C. Chase, Jr., H. Hatzenbeler, E. Miner D. Schofield, *Science* **166**, 98 (1969).
11. G. Fjeldbo, A. Kliore, B. Seidel, *Radio Sci.*, in press.
12. G. Ohring and J. Mariano, *J. Atmos. Sci.* **25**, 673 (1968).
13. We thank the Mariner Project and DSN personnel at Jet Propulsion Laboratory who, through their competence, guaranteed the flawless acquisition of our data. In particular we thank D. Nixon for help in the acquisition and M. P. Milane, Joan Jordan, and Nancy Hamata for help in the reduction of the data. Special thanks are due to P. J. Gierasch and C. Leovy as well as R. Stewart for discussions helpful to the interpretation of our results. This work presents the results of one phase of research carried out at JPL, California Institute of Technology, under NASA contract NAS 7-100.

Radio Science, Volume 5, Number 2, pages 373–379, February 1970

First results of the Mariner-6 radio occultation measurement of the lower atmosphere of Mars

Arvydas Kliore, Gunnar Fjeldbo, and Boris Seidel

Jet Propulsion Laboratory, California Institute of Technology, Pasadena, California 91103

(Received September 8, 1969; revised October 13, 1969.)

As the radio signal of Mariner 6 was intercepted by the surface of Mars near Meridiani Sinus, the presence of an atmosphere caused small changes in the frequency of the received signal. Analysis of these changes indicates that the pressure at the surface of Mars at that point is about 6.6 mb and the temperature approximately 276°K. Data taken as the radio beam emerged from behind Mars in the vicinity of the north pole indicate a surface pressure of approximately 6.4 mb and a temperature of about 158°K. Extrapolation of the 6.6-mb pressure measurement at the point of entry over the 12-km range of topological variation measured by earth-based radars indicates that the surface pressure in the near north equatorial regions of Mars may vary from about 3 to about 8 mb.

In 1965 the radio signal of Mariner 4 was used to perform the first radio occultation measurements of a planetary atmosphere [*Kliore et al.*, 1965; *Cain et al.*, 1965; *Kliore et al.*, 1968; *Fjeldbo and Eshleman*, 1968]. These measurements indicated an unexpectedly low surface pressure on Mars, ranging from about 5 mb at the point of entry into occultation to about 9 mb at the point of exit.

During the planning of the Mariner-6 mission, the trajectory was designed in such a way that occultation measurements could be obtained near the equator and near the pole. A pictorial view of this geometry is shown in Figure 1. Approximately 15 min after the closest approach, the *S*-band radio signal of Mariner 6 was intercepted by the surface of Mars in the vicinity of Meridiani Sinus, when the spacecraft was approximately 9800 km from the occulting limb. The latitude of that point was approximately 4° north, the longitude 356° east, and the local time was approximately 1540. The rate at which the radio beam moved through the atmosphere before being interrupted was about 3 km/sec. Approximately 20 min later, the radio beam emerged from behind Mars in the vicinity of the north pole, at a latitude of 79° north and a longitude of about 84° east. The local time in this region was approximately 2140, and at the time of exit the spacecraft was approximately 17,400 km from the limb. The season was early fall in the northern hemisphere of Mars.

The location on the surface of Mars of the point of entry into occultation turned out to be extremely fortuitous, for it appears in the wide-angle pictures provided by the television experiments of both Mariners 6 and 7 (see Figure 2). It will therefore be possible to obtain at least a qualitative impression of the relative small-scale topography of the occultation area. In addition, the occultation point lies within the swath of subradar points in which range measurements with earth-based planetary radars have been performed during the current opposition of Mars. Thus, the position of that point on the surface of Mars is known in relation to the large-scale topographical variations in the north equatorial region of Mars.

The basic method of obtaining radio occultation data has been described in previous publications [*Levy et al.*, 1967]. A simplified schematic diagram of the data recovery process is shown in Figure 3. In the two-way mode of operation, a frequency referenced to a rubidium frequency standard at the Deep Space Network (DSN) station at Goldstone, California, is transmitted to the spacecraft, where it is coherently retransmitted and received at the station some time later. It then passes through the standard phase-locked-loop receiver, and a record of nondestructively counted, biased Doppler is recorded by the tracking data handling system. This is referred to as closed-loop data. A special open-loop receiver having an audio pass-band of approximately 5 KHz is also used to record the oc-

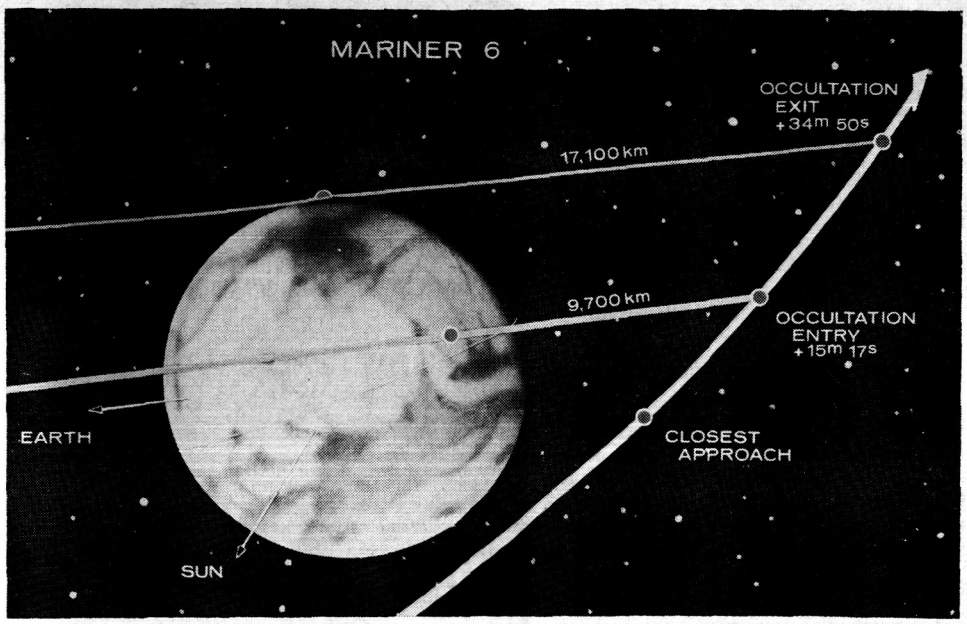

Fig. 1. Pictorial view of the Mariner-6 occultation.

cultation data. It produces a frequency-translated version of the received signal, which is recorded on an analog tape recorder as well as digitized in real time and recorded digitally. These data are referred to as the open-loop data. For the Mariner-6 occultation experiment, deep space stations (DSS) 14 (Mars) and DSS 12 (Echo) at the Goldstone, California, complex were instrumented with open-loop receivers, and the open-loop data from DSS 14 were transmitted to the DSS-13 (Venus) station over a microwave link, where they were digitized in real time and recorded. Closed-loop Doppler data were also taken at DSS 14 and 12 as well as DSS 41 in Woomera, Australia.

The analysis of these data is explained in Figure 4. The closed-loop data are transmitted via teletype to the Space Flight Operations Facility at the Jet Propulsion Laboratory, where they are run through the ordinary tracking data handling programs and are passed through an orbit fit generated by the single precision orbit determination program, which computes the deviations in the received Doppler from the predictions based only on the dynamical motion of the earth and the spacecraft. The resulting data are referred to as the closed-loop residuals.

The digital open-loop data are passed through the decimation and spectral analysis program and a digital phase-locked receiver program that produces a record of the frequency and amplitude of the received signal sampled at arbitrary intervals of time. The frequency is then compared with predictions based on the orbit of the spacecraft, and the differences in frequency constitute the open-loop residuals. The residuals are then passed through a data preparation program that removes any bias or drift terms that might be present in the residuals and integrates the resulting residuals to obtain a record of the total phase-path change due to the refraction effects of the ionosphere and the atmosphere. From there, the data go into the inversion program, which makes use of trajectory data provided by the double precision trajectory program and performs an integral inversion of the data to obtain a refractivity profile [*Fjeldbo and Eshleman*, 1965]. This profile is then used to compute the electron density in the ionosphere and pressure, temperature, and other parameters of the lower atmosphere.

This paper describes the results of the measurements of the lower atmosphere. The upper atmosphere is described in a companion paper [*Fjeldbo et al.*, 1970].

The results obtained during entry into occultation are described first. Figure 5 shows the Doppler residuals caused by the passage of the signal through the ionosphere and atmosphere of Mars. There is a very clear signature of two ionosphere peaks and

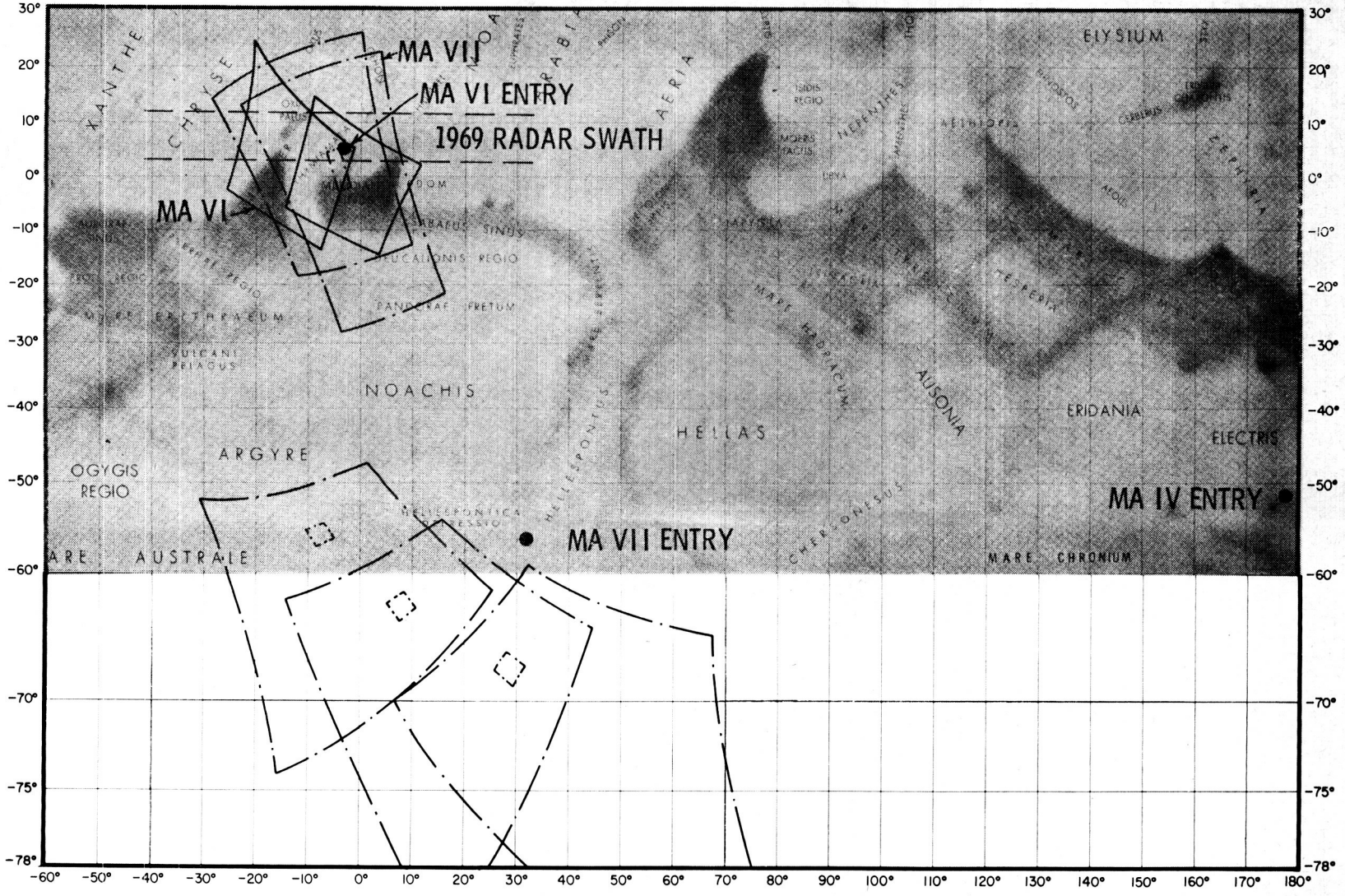

Fig. 2. Television coverage of the occultation region.

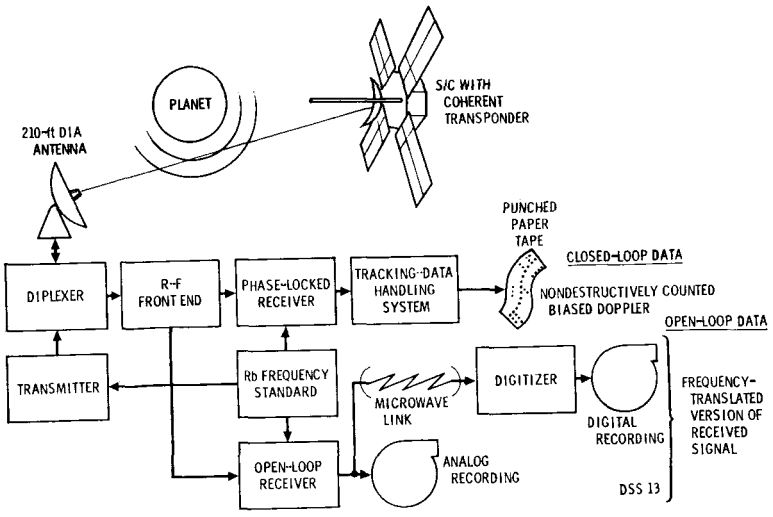

Fig. 3. Occultation data acquisition.

finally the effect of the neutral atmosphere. The refractivity profile, which is obtained by inversion of the data, is shown in Figure 6. It should be noted that in all of these figures the horizontal scale, representing the radial distance from the center of Mars, is uncertain by about 10 km because of current orbit uncertainty. The refractivity is given unambiguously by inversion of the occultation data; however, pressure and temperature depend on assumptions regarding the composition of the neutral atmosphere. For the purpose of this analysis, a composition of 90% CO_2 and 10% argon was assumed. This assumption is based on the results of Mariner 4 and partly on the unpublished results of Mariner 6. The mean molecular weight of such an atmosphere would be approximately 43.6. On the basis of these assumptions, we computed the pressure and temperature profiles for the lower atmosphere above the point of entry into occultation. These profiles are shown in Figures 7 and 8, respectively. The pressure is computed by downward integration of the hydrostatic equation, and the temperature is then determined from the ratio of pressure to refractivity. Some smoothing of data was used. The pressure at the level at which the radio signal was cut off is about 6.6 mb, and the temperature at the same level is about 276°K. Since an occultation measurement presents a probing of the

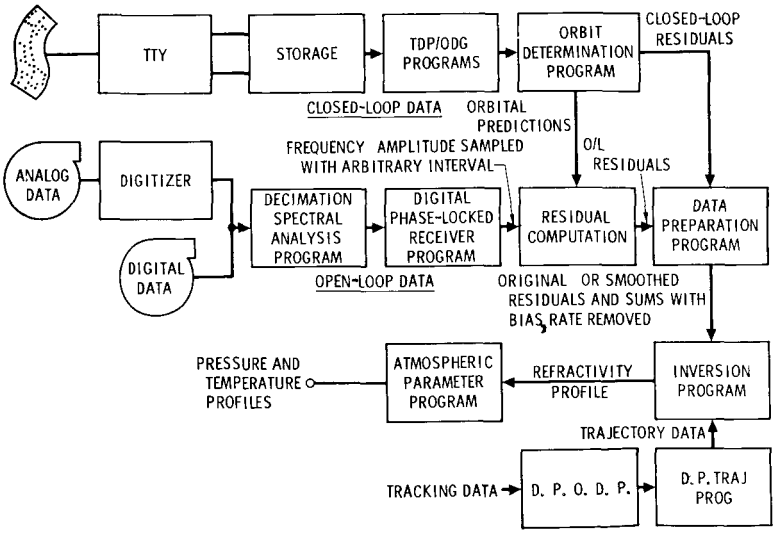

Fig. 4. Occultation data analysis.

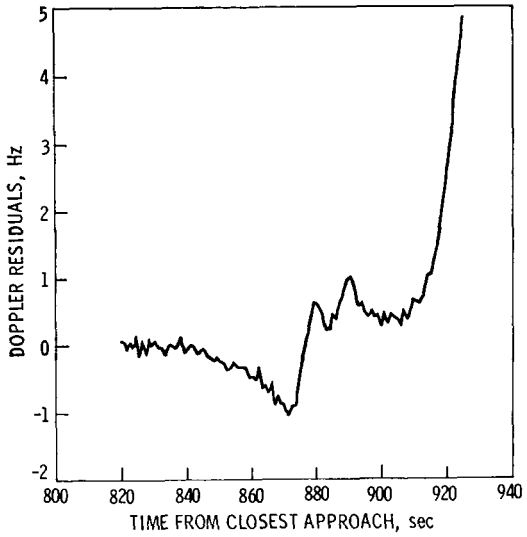

Fig. 5. Mariner-6 Doppler residuals obtained during entry.

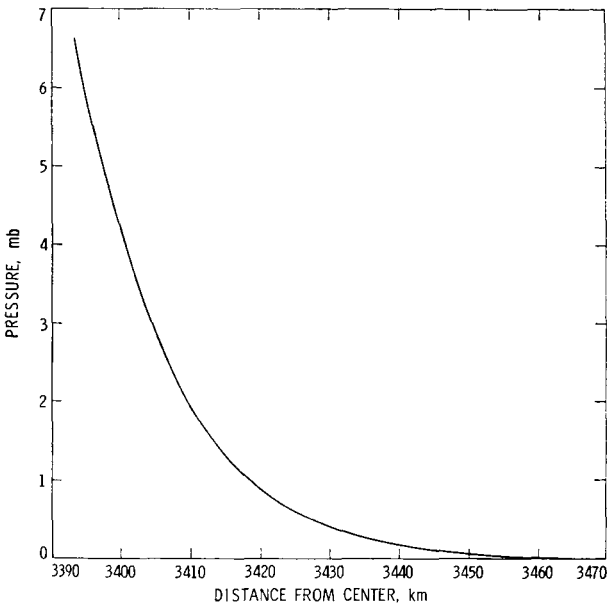

Fig. 7. Mariner-6 pressure profile obtained during entry.

atmosphere with a beam having a thickness of about one Fresnel zone (about 1 km), the measured temperature of 276°K is quite consistent with the surface temperature in that region as measured by other instruments on Mariner 6 (unpublished results).

Corresponding results for the exit measurement are shown in Figures 9 through 12. In this case, two values of initial (high-altitude) temperature were assumed, and the hydrostatic and ideal gas laws were used to obtain the temperature and pressure. No smoothing of the data was used. The pressure measured at the point at which the signal emerged from occultation is about 6.4 mb, and the temperature (as expected in the north polar region at nighttime) is approximately 158°K. Although it is premature now, it is expected that comparison of the radial distances at the entry and exit points will provide a fairly reliable measure of the oblateness of Mars.

Although much more processing and analysis lie ahead, these results allow us to make certain con-

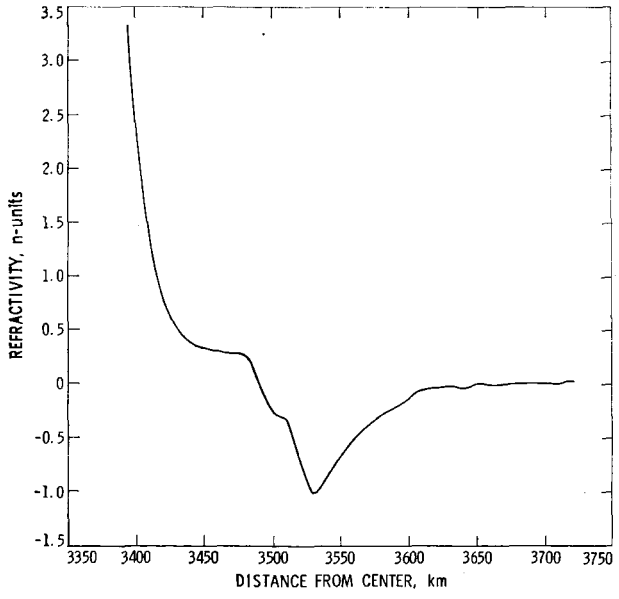

Fig. 6. Mariner-6 refractivity profile obtained during entry.

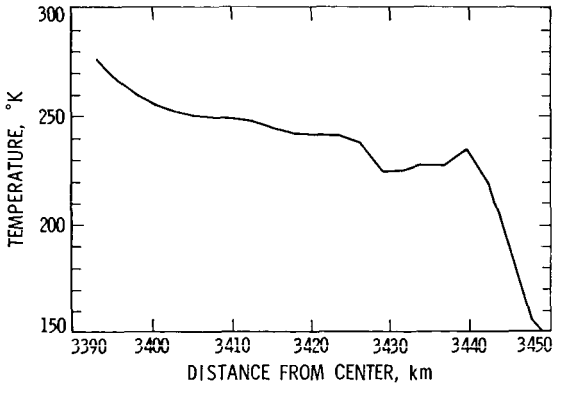

Fig. 8. Mariner-6 temperature profile obtained during entry.

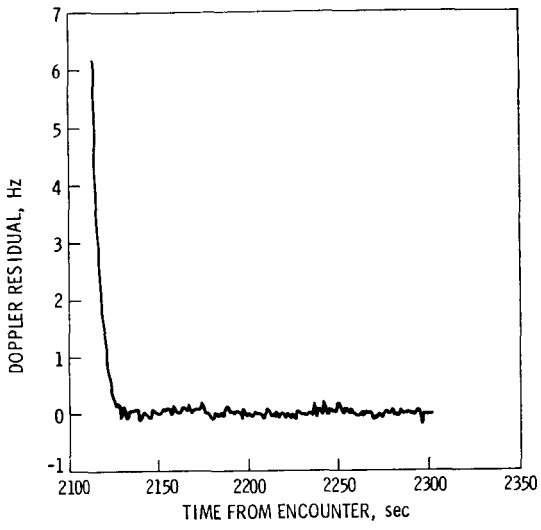

Fig. 9. Mariner-6 Doppler residuals obtained during exit.

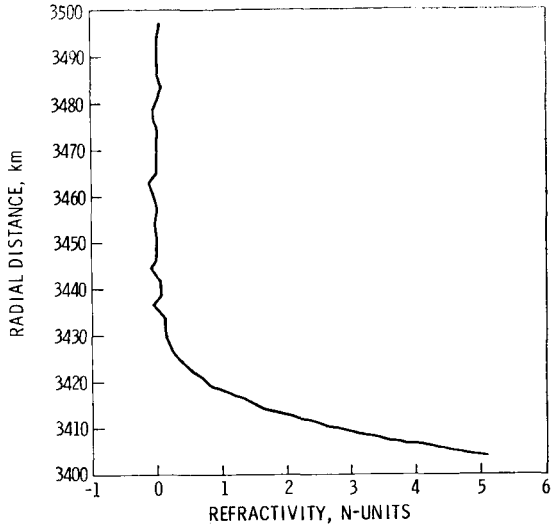

Fig. 10. Mariner-6 refractivity profile obtained during exit.

clusions regarding the atmosphere of Mars. It certainly appears that these measurements have confirmed the measurements of Mariner 4, and they indicate that the low values of surface pressure obtained with Mariner 4 were not accidental. It must be borne in mind, however, that radio occultation measurements by their very nature are biased toward higher elevations, where the signal is interrupted. It is therefore possible that small-scale features of a few kilometers in height could exist, and if so, the pressures in the valleys would be higher by an appropriate factor.

Perhaps the most interesting conclusion can be drawn with respect to the result of the earth-based radar measurements of the large-scale topographical variations on the surface of Mars. These unpublished results (R. M. Goldstein, private communication, 1969) indicate that in the north equatorial region from about a north latitude of 3° to 11° the relative elevation of the surface of Mars varies by about 11 km. At the point of occultation entry, which occurs within the swath probed by radar, the elevation measured by radar is 2.3 km above its lowest point and hence about 8.7 km below the highest point measured. A very crude extrapolation of the 6.6-mb pressure measured at the occultation point, assuming a scale height of 13 km, yields a pressure at the lowest elevation point of about 7.9 mb and at the

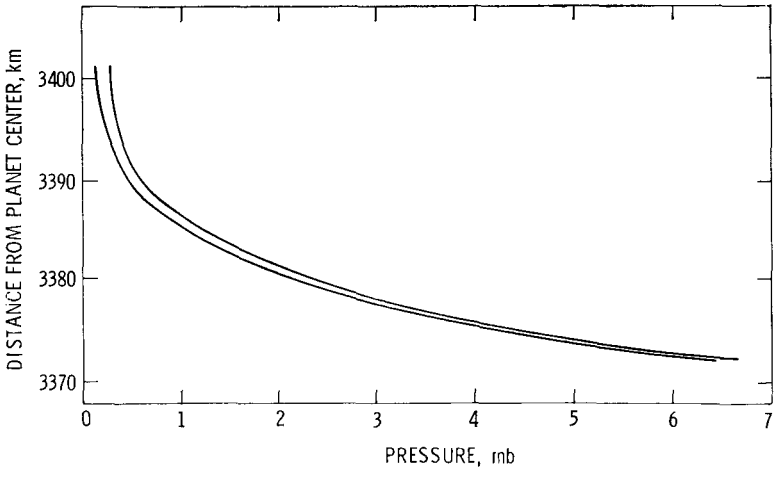

Fig. 11. Mariner-6 pressure profile obtained during exit.

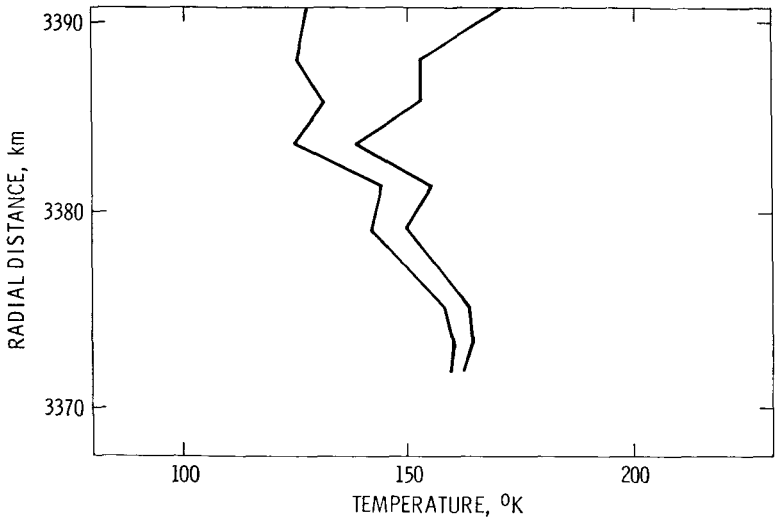

Fig. 12. Mariner-6 temperature profile obtained during exit.

highest point, about 3.4 mb. Thus it appears that on Mars it would not be unusual to expect a variation in the surface pressure of approximately 3 to 1 or greater from the deepest valley to the highest mountain top. It is expected that the measurement of CO_2 absorption by the other instruments on Mariners 6 and 7 as well as the occultation measurements of Mariner 7 will cast more light on the effect of topography on the variation of the surface pressure on Mars.

Acknowledgments. The authors wish to express their gratitude to the Mariner 1969 Project and the JPL Deep Space Net for their excellent cooperation in the acquisition of these data. In particular, we wish to thank S. I. Rasool for his enthusiastic help with the analysis; David L. Nixon for his efforts in the acquisition and analysis of the open-loop data; Joseph Witt, Michael P. Milane, Joan E. Jordan, and Nancy Hamata for their considerable help with the computations; and Richard Rackus for his help with the graphics.

This paper presents the results of one phase of research made at the Jet Propulsion Laboratory, California Institute of Technology, under contract NAS-7-100 sponsored by the National Aeronautics and Space Administration.

REFERENCES

Cain, D. L., V. R. Eshleman, G. Fjeldbo, A. Kliore, and G. S. Levy (1965), A summary of preliminary results of the Mariner 4 radio occultation experiment, *Proc. Ionos. Res. Comm. Avionics Panel,* AGARD, NATO, Rome, Italy.

Fjeldbo, G., and V. R. Eshleman (1965), The bistatic radar occultation method for the study of planetary atmospheres, *J. Geophys. Res., 70,* 3217–3226.

Fjeldbo, G., and V. R. Eshleman (1968), The atmosphere of Mars analyzed by integral inversion of the Mariner-4 occultation data, *Planet. Space Sci., 16,* 1035–1059.

Fjeldbo, G., A. Kliore, and B. Seidel (1970), The Mariner 1969 measurements of the upper atmosphere of Mars, *Radio Sci., 5,* this issue.

Kliore, A., *et al.* (1965), Occultation experiment: Results of the first direct measurement of Mars's atmosphere and ionosphere, *Science, 149,* 1243–1248.

Kliore, A., D. L. Cain, and G. S. Levy (1968), Radio occultation measurement of the Martian atmosphere over two regions by the Mariner-4 space probe, in *Space Research 7, Moon and Planets,* North-Holland, Amsterdam, 227–239.

Levy, G. S., T. Otoshi, and B. L. Seidel (1967), Ground instrumentation for the Mariner-4 occultation experiment, *IEEE Trans. Instrum. Meas., 6*(2), 110–114.

DISCUSSION

Question: Are the temperatures derived from the Mariner-7 observations in agreement with Neugebauer's infrared data?

A. J. Kliore: The value at the entry point is in agreement with Neugebauer's data, but the surprisingly low temperature of 160°K at the exit point has not yet been checked with his data.

M. Ya. Marov: What was the scale height observed?

A. J. Kliore: The scale height at the surface is 13 km, but it changes somewhat with height.

S. I. Rasool: I am surprised at the observed temperature profiles. They are in violent disagreement with those computed on the basis of radiation heat transfer. It appears as if advective activity is very important.

Reprinted from
16 January 1970, Volume 167, pp. 277-279

SCIENCE

Martian Mass and Earth-Moon Mass Ratio from Coherent S-Band Tracking of Mariners 6 and 7

John D. Anderson, Leonard Efron, and S. Kuen Wong

Martian Mass and Earth-Moon Mass Ratio from Coherent S-Band Tracking of Mariners 6 and 7

Abstract. *Range and Doppler tracking data from Mariners 6 and 7 have been used to obtain values for the ratio of the mass of the earth to that of the moon which are in substantial agreement with those determined from other Mariner and Pioneer spacecraft. There is an inconsistency of about 0.004 percent in values for the mass of the moon determined from lunar trajectories. A gravitational constant for Mars of 42,828.48 ± 1.38 cubic kilometers per second per second, obtained on the basis of data collected during the 5 days prior to the closest approach of Mariner 6 to Mars, is in excellent agreement with the result obtained by Null from tracking data of Mariner 4.*

The accurate navigation of Mariners 6 and 7 to the vicinity of Mars required the use of two-way, phase-coherent range and Doppler tracking data from the National Aeronautics and Space Administration/Jet Propulsion Laboratory (NASA/JPL) Deep Space Network. Because of the importance of these data in celestial mechanics, JPL scheduled tracking coverage of both Mariners 6 and 7 from launch to encounter with Mars, the closest approach to Mars, and beyond in such a way that new information could be obtained on the ratio of the mass of the earth to that of the moon, the gravity field of Mars (in particular, the mass of the planet), and the ephemerides of Mars and the earth. In addition, it was recognized that these data complemented Doppler data from Mariner 4; however, range measurements were not obtained from that spacecraft. Furthermore, a combination of data from the three flyby trajectories and direct radar range measurements to the planet itself during the 1969 opposition would not only result in significant improvements in values for the ephemeris of Mars, but, because of these improvements, would also permit an exploration of the size, shape, and gross topography of Mars by utilization of the radar range measurements to its surface. In this regard, it was realized that the times of immersion and emersion of the Mariner spacecraft as they were occulted by Mars would provide important calibration points for the size of the planet (*1*).

Tracking data from Mariners 6 and 7 and the radar range measurements to Mars are still being collected; meaningful analysis will require many months. Therefore, this report deals with the use of the tracking data alone to determine the earth-moon mass ratio and the mass of Mars.

As the earth revolves about the center of mass of the earth-moon system at a distance of about 4671 km and at a speed of 12.4 m/sec, it impresses a sinusoidal curve on range and Doppler tracking data with a frequency equal to the sidereal mean motion of the moon and with an amplitude inversely proportional to $(1 + \mu^{-1})$, where μ^{-1}, the ratio of the mass of the earth to that of the moon, is approximately equal to 81.3. The principle involved in the determination of μ^{-1} is that there is a value which eliminates the monthly cycle in the tracking data residuals in a least-squares sense. No other unknown parameter in the representation of the tracking data has a frequency anywhere near that of the moon's orbit; the determination of μ^{-1} is direct and reliable. The lunar ephemeris is known to an accuracy of seven or eight figures, and the use of this value does not introduce any noticeable error into μ^{-1}, which, by comparison, can be determined to the order of 10 to 20 parts in 10^6.

In our search for possible sources of systematic error in the data, it has been very difficult to think of anything important that has a monthly cycle, although a significant S-band propagation effect correlated with the rotation of the sun would be close enough to cause difficulty. However, periodic variations in the interplanetary medium, the only reasonable possibility, if present, must be very small for Mariners 6 and 7; the total delay for an inverse square distribution of electrons with a density of 6 per cubic centimeter at the earth's distance is at most only 4 m for the Mariner trajectories from the earth to Mars. Melbourne (*2*) has suggested that a 28-day sinusoidal variation of solar flux of 0.1 percent with the appropriate phase could produce an error of about 0.001 in μ^{-1} because of a similar variation in the solar radiation pressure on the spacecraft. The agreement of the several interplanetary spacecraft, however, does not seem to indicate that this sort of systematic error is present unless the phase of the flux variation is the same for each mission, which does not seem likely.

There is an instrument on both Mariners 6 and 7 which measures relative variations in solar flux to an accuracy of better than 0.1 percent. When these data are reduced, it should be possible to determine whether a variation is present that could significantly bias the solutions for μ^{-1}.

Values for the earth-moon mass ratio as determined from Mariner 6 Doppler

Table 1. Determinations of the ratio of the mass of the earth to that of the moon, μ^{-1}, from Mariner, Pioneer, and Ranger tracking data, and from radar bounce data to the planets. [Deviation $(\mu^{-1} - \bar{\mu}^{-1})$ from the arithmetic mean $\bar{\mu}^{-1}$ of the Mariner and Pioneer values is tabulated for each determination. The root-mean-square deviation from a mean of 81.3008 is 0.0008 for the Mariner and Pioneer determinations.]

Spacecraft	μ^{-1}	$\mu^{-1} - \bar{\mu}^{-1}$
Mariner 2 (Venus)	81.3001 ± 0.0013	−0.0007
Mariner 4 (Mars)	81.3015 ± 0.0017	0.0007
Mariner 5 (Venus)	81.3006 ± 0.0008	−0.0002
Mariner 6 (Mars)	81.3011 ± 0.0015	0.0003
Mariner 7 (Mars)	81.2997 ± 0.0015	−0.0011
Pioneer 6	81.3005 ± 0.0007	−0.0003
Pioneer 7	81.3021 ± 0.0004	0.0013
Combined Rangers	81.3035 ± 0.0012	0.0027
	Radar data	
	81.302 ± 0.002	0.0012

Table 2. Statistical properties of the fit to preencounter Doppler data. (Units are hertz at S-band frequency which can be converted approximately to millimeters per second if the values are multiplied by 67.)

Tracking station	Number of points	Data interval (UTC)	Mean residual (hz)	Root-mean-square residual (hz)
Australia	200	7/26, 06:49 to 7/30, 15:41	0.000006	0.0028
South Africa	26	7/27, 16:28 to 7/27, 23:02	0.000164	0.0019
Spain	80	7/26, 17:29 to 7/30, 22:31	−0.000086	0.0025
California	311	7/26, 01:23 to 7/31, 04:40	−0.000105	0.0043
California	53	7/26, 00:35 to 7/30, 06:38	−0.000098	0.0024

data measured over a period of 12 weeks (4 May to 28 July 1969) and Mariner 7 Doppler data measured over a period of 11 weeks (8 May to 22 July 1969) are shown in Table 1 along with results from Mariner 2 (*3*), Mariner 4 (*4*), Mariner 5 (*5*), Pioneers 6 and 7 (*6*), and reductions of passive radar reflection measurements to the planets (*7*).

A solution obtained by a combination of data from Rangers 6, 7, 8, and 9 (*8*) is also shown, although the selenocentric gravitational constant GM for the moon was determined directly by the Ranger impact trajectories; μ^{-1} must be computed with an assumed value for the geocentric gravitational constant GE ($\mu^{-1} = GE/GM$). The error in GE, however, is on the order of 1 part in 10^6. Therefore, the percentage error in the value of μ^{-1} determined from Ranger measurements is practically equal to the percentage error in GM. The fundamentally different method for the determination of μ^{-1} from Ranger impact trajectories, as opposed to the use of interplanetary trajectories such as those from the Mariner and Pioneer flights, is reflected in a significant difference in the values. The arithmetic mean of the seven Mariner and Pioneer values of μ^{-1} is 81.3008 with a deviation from the mean of 0.0008. On the other hand, the Ranger value differs by 0.0027 from this mean value.

We can see no reason why one should suspect that the direct determination of μ^{-1} from measurements of the Mariner and Pioneer spacecraft is subject to systematic errors of a size that would adjust the value to that given by Ranger. We have even processed the Mariner data with two computer programs, one in a single precision code (about eight figures) and the other in double precision (about 16 figures) and with both heliocentric and geocentric formulations of the equations of condition in the method of weighted least squares. The value of μ^{-1} is essentially the same in all cases. In our opinion, therefore, it is necessary to perform new reductions of data from the lunar spacecraft.

Several conditions have changed since the Ranger solution for μ^{-1} was obtained about 2½ years ago. First of all, values for the gravity field and the ephemeris of the moon have been improved significantly by analyses of Lunar Orbiter data (*9*). In addition, it is now possible to perform the necessary computations in double precision, whereas those of 2½ years ago were processed in single precision. In any case, the question of reconciling the lunar and interplanetary values of μ^{-1} is receiving increased attention because of the results of Mariners 6 and 7 which support a value of μ^{-1} closer to 81.300 or 81.301 than to 81.303 or 81.304 as suggested by the combined Ranger flights.

The determination of the mass of Mars based on measurements of both Mariners 6 and 7 is complicated by nongravitational forces that act on the spacecraft. In particular, one channel of the infrared spectrometer (IRS) operates in a cryogenic environment produced by the expulsion of hydrogen and nitrogen gas from a pressure-regulated system. This expulsion of gases imparts a force of 100 dynes or more to the spacecraft and produces a velocity change in its trajectory on the order of 0.1 m/sec. In normal operation, the system starts to expel gases about 35 minutes before encounter and continues at a constant pressure through encounter for a period of about 80 minutes. After this, the gas is allowed to escape into space without pressure regulation; about 5 hours are required before the decay reaches an insignificant level at approximately an exponential rate. On Mariner 6, the system did not operate normally, and, as a result, the force on the spacecraft acted over a period of 4 or 5 days after encounter instead of over a few hours as intended. The system operated normally on Mariner 7. This spacecraft, however, was affected 6 days before encounter by an unknown "event" which imparted a velocity increment to the trajectory of 1 m/sec or less, or a change of less than 4×10^7 g cm/sec in momentum.

Telemetry records indicate that the spacecraft attitude was disrupted by the event, whatever the source. The nature of the unknown forces acting is not yet clear. One possibility is that a meteorite struck the spacecraft. Another possibility is that the on-board battery (which gave indication of malfunction after the time of the event) was punctured, either by the meteorite impact or as a result of an internal pressure buildup, and that the leaking electrolyte imparted a low-thrust force for a day or so. Because of uncertainties over the nature of the event and the resulting forces on the spacecraft in the few days prior to the encounter, we have not been able to obtain any results for Mariner 7 at this time.

The data recorded prior to the initiation of the blowdown of the IRS cryogenic system on Mariner 6 are not influenced by unknown forces and can be used to obtain a value for the mass of Mars. However, data from about 35 minutes prior to the encounter and beyond cannot be used until, in a fashion similar to that for Mariner 7, engineering telemetry data can be combined with the tracking data in an analysis of the nature of the nongravitational forces acting on the spacecraft.

To obtain the mass of Mars, we fitted Doppler data (670 points) from 26 July, 5 days before encounter, to 31 July, 04:39:57 (Universal Time Coordinated), a time approximately 7 minutes before the start of the IRS cooling.

Table 3. Range residuals from the fit to preencounter range and Doppler data. (Units are 10^{-9} second which can be converted to residuals in meters for the topocentric distance to the spacecraft if the values are multiplied by 0.15. The mean residual is −0.30, and the root-mean-square value of the nine residuals is 26.9, or 4.0 m.)

Time of reception 27 July 1969 (UTC)	Residual
01:12:02	−42.1
01:59:02	62.7
02:29:02	5.9
02:59:02	6.2
03:29:02	2.9
03:59:02	−16.2
04:29:02	5.5
06:06:02	−8.2
06:36:02	−19.5

The parameters in the least-squares solution were the position and velocity of the spacecraft at the epoch, the gravitational constant GM_{σ} for Mars, the distance off the earth's axis of rotation, and the longitude of each of the five NASA/JPL Deep Space Network tracking stations for which data were available. The statistical properties of the fit, which were good, are summarized in Table 2. The solution for GM_{σ} is $42{,}828.22 \pm 1.83$ km^3/sec^2. A second solution was performed in which the Doppler data were fitted along with nine range measurements taken on 27 July from the NASA/JPL Deep Space Network (Mars tracking facility) at Goldstone, California, with the experimental ranging system used for Mariner 5. The statistical properties of the Doppler fit were not changed appreciably by the addition of the range data. The nine range residuals are shown in Table 3. The value of GM_{σ} for the range and Doppler fit is $42{,}828.48 \pm 1.38$ km^3/sec^2, which is not significantly different, either in size or in estimated standard error, from the value based on Doppler measurements alone. This estimate was computed with a standard error of 62×10^{-9} second on each range point and a standard error of 0.05 hz on Doppler data sampled at 1-minute intervals.

Although the introduction of range data into the fit does not appreciably affect the solution for the mass of Mars, it is of value in the determination of the orbit of the Mariner spacecraft. This has important implications for other Mariner experiments which will require good orbital data for final analysis. Precise knowledge of the orbit is important in relation to information on the ephemeris of Mars and will be significant in later analyses of the tracking data when the nongravitational forces on Mariners 6 and 7 are better understood. At present, we believe that the areocentric orbit for Mariner 6 from the fit to range and Doppler data can be used to predict events along the trajectory to better than 1 second in time or to better than 8 km along the flight path. For example, our best estimate of the time of closest approach to Mars is 31 July 1969, 05:19:06.4 ($\pm$ 1 second) (UTC).

In addition to Mariners 6 and 7, the only other source for an accurate determination of the mass of Mars is Mariner 4. A recent analysis (*10*) of Doppler data, taken over a 10-day interval during which the spacecraft was centered about a closest approach, has yielded a value for GM_{σ} of $42{,}828.32 \pm 0.13$ km^3/sec^2. Therefore, the masses determined from Mariners 4 and 6 are in agreement, and there is good reason to use the value determined from spacecraft measurements in calculations with other planetary data.

JOHN D. ANDERSON
LEONARD EFRON
S. KUEN WONG
Jet Propulsion Laboratory, California Institute of Technology, Pasadena

References and Notes

1. A. Kliore, G. Fjeldbo, B. L. Seidel, S. I. Rasool, *Science* **166**, 1393 (1969).
2. W. G. Melbourne, paper presented at the 12th plenary meeting of the Committee on Space Research, Symposium C: Space Probes–Part I, Prague, Czechoslovakia, 1969.
3. J. D. Anderson, thesis, University of California at Los Angeles (1967); *Jet Propulsion Lab. Tech. Rep. 32–816* (1 July 1967).
4. G. W. Null, H. J. Gordon, D. A. Tito, *Jet Propulsion Lab. Tech. Rep. 32–1108* (1967).
5. G. E. Pease, *Jet Propulsion Lab. Tech. Rep. 32–1363* (1969).
6. J. D. Anderson and D. E. Hilt, *AIAA (Amer. Inst. Aeronaut. Astronautics) J.* **7**, No. 6, 1048 (1969).
7. M. E. Ash, I. I. Shapiro, W. B. Smith, personal communication.
8. C. J. Vegos and D. W. Trask, *Ranger Combined Analysis Part II: Determination of the Masses of the Earth and Moon from Radio Tracking Data* [*Jet Propulsion Lab. Space Programs Sum. 37–44* (1967), vol. 3, pp. 11–28].
9. J. Lorell, *Jet Propulsion Lab. Tech. Rep. 32–1387* (1969); W. H. Michael, Jr., W. G. Blackstear, J. P. Capcynski, paper presented at the 12th plenary meeting of the Committee on Space Research, Symposium C: Space Probes–Part I, Prague, Czechoslovakia, 1969.
10. G. W. Null, paper presented at the 130th meeting of the American Astronomical Society, Albany, N.Y., 1969.
11. The authors acknowledge the assistance and support given to the Mariner Mars 1969 Celestial Mechanics Experiment by H. Gordon, D. Curkendall, B. Zielenbach, M. Sykes, S. Reinbold, N. Thomas, and others in both the Mariner Mars 1969 Flight Path Analysis and Command Team and the Precision Navigation Project at JPL. This paper presents the results of one phase of research carried out at the Jet Propulsion Laboratory, California Institute of Technology, under NASA contract No. NAS 7-100.

3 October 1969